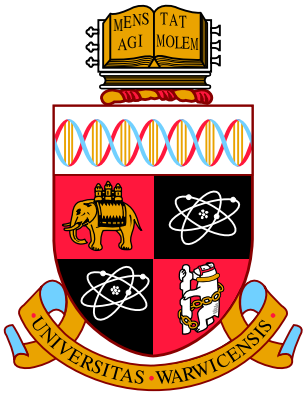

Optimising Chronotherapy for Gastrointestinal Cancers

by

Roger Hill

Thesis

Submitted to The University of Warwick

for the Degree of

Doctor of Philosophy

Centre for Complexity Science

October 2019

Table of contents

List of figures

List of tables

Acknowledgements

I would like to thank first and foremost Annabelle Ballesta, without her constant support, encouragement and passion for this field, none of this work would have been possible. You are an inspiration and I am extremely grateful for everything you have done over the past 4 years. I would also like to thank Francis Lévi for providing me with the clinical input to understand the importance of chronotherapy and the impact it could make on future treatment. Your knowledge and connections made me see that this is not only an interesting problem but one with the potential to really help people.

To everyone in Mathsys and complexity the support and camaraderie has been essential to keeping me going throughout my PhD and I hope the friends I have made will last a lifetime. In particular I want to mention my long suffering office mates: Ayman Boustati, Cameron Lack, Christopher Davis, Ellen Webborn, Joe Hilton and Sami Al-Izzi, who have listened to my complaining and helped me stay on track and together during my time at Warwick. I would also like to thank Robert Gowers for his advice and input on my work over the years and Alvaro Cabrejas Egea for our lunch strolls putting the world to rights.

I am so grateful to the support of my family, the Hills and the Cherrys. Whether they had any idea what I was doing or not, I knew they always cared and wanted me to succeed.

Finally, I want to thank Chloe Cherry. You have supported me no matter what. You have built me up and kept me going when things felt like they were far more than I could bare and your unwavering love has helped me get to the end of this journey. Thank you.

Declaration

This thesis is submitted to the University of Warwick in support of my application for the degree of Doctor of Philosophy. It has been composed by myself and has not been submitted in any previous application for any degree. Parts of the material in this thesis have been published as follows:

- Chapter 3 has been submitted to the Journal of Computational Biology and is currently under review. All code used is accessible at https://github.com/Rogerjwhill/Optimizing-circadian-drug-infusion..git
- The algorithm outlined in Chapter 3.3 is under review for a European patent.
- Chapter 4.2 is being prepared for publication with the inclusion of new experimental data which will become available shortly.

Roger Hill
October 2019

Abstract

Gastrointestinal cancers are some of the most common and deadly cancers in the world. The improvement of current treatments is of great importance to improve patients survival and quality of life and decrease the burden of these cancers. Within this thesis we will focus on two particular cancers: colorectal and pancreatic cancer, and their treatment by three cytotoxics oxaliplatin, 5-fluorouracil and irinotecan. The improvement of treatment will focus on the use of circadian rhythms. Circadian rhythms are the innate approximately 24 hour rhythms present in almost all living organisms. Treatments which take this innate rhythm into account is known as chronotherapy and has already been shown to improve patient outcomes. However, recent findings highlight the need of personalising drug timing to account for the patient's gender, chronotype and genetic background. We will firstly look at potential improvements which can be made directly to current treatment protocols by using mathematical models. A model of the drug solution dynamics from an infusion pump to the patient blood will be developed and used to improve the accuracy of chronomodulated drug delivery. Subsequently, semi-mechanistic models of individual patient drug pharmacokinetics will be connected to the pump-to-patient model and used as a method of patient stratification in order to better personalise treatments. We will then use a multiscale approach- from in vitro to mouse studies- to build a physiologically-based whole body model of oxaliplatin pharamcokinetics to look at sexual dimorphism in the drug chronoefficacy and chronotoxicity. This model can then be used to connect differences in drug dynamics to measurable biomarkers and help inform future human trials. Overall, this thesis aims to develop mathematical tools to personalize chronotherapy treatments and further the knowledge available to biologists and clinicians working in this important area of cancer research.

Nomenclature

Acronyms / Abbreviations

5-FU 5-Fluorouracil

ADME Aborsption, distribution, metabolism and excretion

CaSyM Coordinated Action for Systems Medicine

CMAES Covariance Matirx adaptation Evolution Strategy

CPT11 Irinotecan

CRC Colorectal cancer

CTS Circadian timing system

CV Coefficient of variance

DAISY Differential Algebra for Identifiability of SYstems

FAP Familial adenomatous polyposis coli

FOLFIRINOX 5-fluorouracil, leucovorin, irinotecan and oxaliplatin

FOLFOX 5-fluorouracil, leucovorin and oxaliplatin

fpc Fuzzy partition coefficient

GSH Glutathione

LOHP Oxaliplatin

ODE Ordinary differential equations

PB Physiologically Based

PD Pharmacodynamic

PDE Partial differential equations

PK Pharmacokinetic

PM Personalised medicine

SCN Suprachiasmatic nuclei

TOP1 Topoisomerase I

UGT UDP-glycosyltransferases

Chapter 1

Background

1.1 Introduction

Cancer is the largest broad class cause of death in the UK and puts a significant pressure on society [19]. The search for improved treatment is always ongoing and mathematics has been shown to help in this search. An increasingly important source of improvement is the timing of treatments to the human body clock (circadian clock). The benefits of such timing schemes have been shown in many drugs [1] but the underlying reasons are still in need of investigation. The use of predictive and explanatory mathematical models can help give new and important insights into possible improvements and what can be done to help implement them in clinical settings. This thesis will develop mathematical models to improve the treatment of gastrointestinal cancers, by deepening the understanding of how circadian rhythms influence drug pharmacokinetics and pharmacodynamics. This will be done by drawing from biological studies of the drugs in question and using this information as well as specific techniques to create realistic physiologically-based models. The accurate fitting of these models will give parameters which have biological meaning and can be used to inform new investigations into the causes of circadian differences.

1.2 Personalised Medicine

Currently most medicines are given empirically, meaning that it is assumed to work equally for almost all relevant patients and prescribed as such [20]. Personalised medicine is defined as patient care which is guided by an individual's characteristics, such as genetic profile or sex. The aim is to be able to assess each patient so they get the right drug at the right time for them [21]. There are in fact varying degrees of personalisation. The first level of personalisation would be stratified medicine, this is where the population of patients is split into subgroups by certain criteria and

then each group will be treated in specific ways. Then there is the truly personalised medicine or "individualised medicine", which is the development of a treatment programme that is designed for a single patient [22]. Each of these methods has been shown to give considerable benefit to treatments [23].

Oncology has felt the biggest impact from 'personalised medicine' [24]. The terms 'personalised medicine', 'genomic medicine', 'precision medicine' or 'precision oncology' are all interchangeable and describe the process of using an individual's molecular information (genomics and proteomics) to inform diagnosis, prognosis, treatment and prevention of cancers for patients. This is the definition that the European Society for Medical Oncology (ESMO) Personalised Medicine Task Force prefers to use [24], and the one which will be used within this thesis.

A particularly famous example of prophylactic personalised medicine, medicine intended to prevent disease, within oncology is the genetic testing of patients for the breast cancer (BRCA) genes with a strong family connection of breast cancer. The detection of these genes is associated with a high (45%) chance of developing breast cancer [25]. If a patient is found to have these genes there are then prophylactic measures that can be taken i.e. breast tissue removal or chemical oestrogen deprivation [26]. A Cochrane review showed that mastectomy helped significantly reduce the "worry" of cancer and effectively reduced incidence of death [27].

Another example of prophylactic personalised medicine is in the case of colorectal cancer (CRC) caused by familial adenomatous polyposis coli (FAP). FAP is a autosomal dominant disorder with complete penetrance, i.e. everyone with the mutation will have the clinical symptoms. The presence of FAP leads to frequent development of CRC by 40-50 year olds. Genetic screening for FAP allows for the potential for prophylactic treatment which in this case is bowel resection. Bowel resection as a prophylactic treatment has led to a 55% reduction of CRC incidence in FAP patients and improved overall survival. However, bowel resection does not guarantee complete prevention [28, 29]. Although this thesis does not focus on prophylactic therapies the use of personalised medicine is interesting and shows how these new ideas have been used already.

An example of treatment using personalised medicine is in CRC where if a patient expresses wild-type KRAS (an on-off switch in cell signalling) then treatment with Cetuximab would be able to improve quality of life and has been shown to almost double overall and progression free survival, whereas patients with a mutated KRAS did not benefit from Cetuximab treatment [30]. Predicting drug response via gene mutation has potential health economic benefits as it can reduce prohibitive treatment costs, however targeted therapies carry a cost of their own. To optimise personalisation of treatments understanding of important biomarkers, as mentioned above, and cost effective measurements of these biomarkers need to be found.The

understanding of important biomarkers and cost effective measurements need to be found in order to optimise personalisation.

Alongside personalised treatments which use these biomarkers chronotherapy can also be used in personalisation (see section 1.5). Chronotherapy has shown great potential to improve and enrich personalised medicine [3, 5, 31, 32]. The understanding of precise mechanisms, including biomarkers and timings, and their influence on treatments has a key role in improving the access and quality of personalised medicine.

1.3 Gastrointestinal Cancers and their treatments

Gastrointestinal cancers are any of the cancers that affect the digestive tract. These include cancers of the oesophagus, gallbladder, liver, pancreas, stomach, small intestine, bowel (large intestine or colon and rectum), and anus. The main focus of this thesis is gastrointestinal cancers that are currently treated with oxaliplatin, an anticancer drug. The cancers which are treated with oxaliplatin are colorectal cancer and pancreatic cancer [33].

Colorectal cancer is the is 4^{th} most common cancer in the UK, however, if the cancer incidences are split between sexes then it is 3^{rd} most common for both males and females [34]. Colorectal cancer accounts for approximately 42,000 new cases each year in the UK. 1 in 14 men and 1 in 19 women will be diagnosed with colorectal cancer within their lifetime. In Europe there are approximately 500,000 new cases of colorectal cancer estimated to have been diagnosed in 2018 [35] and approximately 1.4 million new cases were diagnosed worldwide in 2016 [36].

The mortality rates of colorectal cancer account for 10% of all cancer deaths in the UK which equates to approximately 16,000 people every year. In Europe 215,000 people were reported to have died of colorectal cancer with the worldwide mortality of almost 700,000 people every year. 57% of people with colorectal cancer will survive over 10 years and 59% of people will survive over 5 years [37].

There are multiple treatment options for colorectal cancer relating to some combination of up to three chemotherapy drugs and one folinic acid supplement. These are 5-fluorouracil (F), irinotecan (IRIN), oxaliplatin (OX) and folinic acid (FOL) (also know as leucovorin). These can be combined to make different regimes: FOLFIRINOX all of the above drugs, FOLFOX folinic acid, 5-fluorouracil and oxaliplatin, FOLFIRI folinic acid, 5-fluorouracil and irinotecan. More details on these drugs can be found in section 1.3.1. The standard treatment would be to receive the FOLFOX regime [38]. Interactions between irinotecan and oxaliplatin, and between oxaliplatin and 5-fluorouracil have not been demonstrated [39, 40] and irinotecan and

5-fluorouracil also showed no interaction if irinotecan is delivered first [41]. Folinic acid is used to enhance the antitumour effect of 5-fluorouracil by increasing binding of 5-fluorouracil to enzymes in the cells and prolonging 5-fluorouracil exposure [42]. Due to this interaction folinic acid is given before 5-fluorouracil.

As with most chemotherapy treatments each of the regimes come with toxicities and side effects. A list of common toxicities are: Myelosuppression, diarrhoea (can appear very quickly and has a treatment to reduce impact), nausea and vomiting, mucositis, neurotoxicity, allergic reactions (specifically to oxaliplatin, in which case oxaliplatin will be stopped), alopecia, fatigue, cholinergic syndrome (combination of diarrhoea, sweating, salivation and bradycardia, can be controlled with treatment), palmar-plantar erythema (PPE), coronary artery spasm (caused by 5-fluorouracil, and stops treatment), acute dysaethesia (tingling or pain in extremities, caused by oxaliplatin sensitivity, extended infusion time to reduce effect), ovarian failure/infertility and interstitial pulmonary disease (uncommon) [43].

For each drug there is also the problem of the toxicities becoming dose-limiting, meaning that the treatment may have to be reduced or even stopped due to the severity of the side effects. The main dose limiting toxicity for oxaliplatin is the neurotoxicity, specifically peripheral neuropathy [44, 45]. Peripheral neuropathy is the damage of nerves in the extremities of the body. It can vary from numbness and tingling in hands or feet to severe pain, loss of balance and muscle weakness [46]. The two main dose-limiting toxicities for irinotecan are diarrhoea and neutropenia [47]. Neutropenia is when a patient has low levels of the white blood cells, neutrophils [48]. In the early stages of irinotecan use, diarrhoea was the major dose-limiting toxicity however, better ways to deal with this side-effect have made it more manageable and reduced the magnitude of this toxicity [47]. The dose limiting toxicities for 5-fluorouracil are myelosuppression, diarrhoea, plantar-palmar and mucositis [49, 50].

Pancreatic cancer is the 11^{th} most common cancer in the UK with almost 10,000 new cases each year. Incidence rates have increased by 15% since 1990s, by 11% in the last decade and are predicted to rise by 6% by 2035 [51, 52]. There are approximately 132,600 new cases of pancreatic cancer and 128,000 deaths caused by pancreatic in 2018 in Europe [35].

Pancreatic cancer, although only being the 11^{th} most common cancer, is the 5^{th} most common cause of cancer death in the UK. There is approximately 9,000 people that die from pancreatic cancer each year. The rate of mortality has been shown to have increased over the past decade, and is predicted to increase by a further 3% by 2035 [51, 52]. Despite many clinical trials testing available pharmacotherapy strategies, the survival rates for pancreatic cancer are very low with only 3-6% surviving past five years and only 1% surviving for ten years. This 1% survival rate past ten years has not changed since the 1970s [51, 53].

1.3.1 Treatments

To improve the care and life of patients their treatments need to be understood. When gastrointestinal cancers are treated with chemotherapy drugs they are usually treated with one or a combination of the following, oxaliplatin, irinotecan and 5-fluorouracil. Understanding the biological background of these chemotherapy agents is key to making models which can give insight into the pathways and processes which are key to efficacy and toxicity.

Oxaliplatin

Oxaliplatin predecessor cisplatin was brought onto the market in the late 1970's, with a second platinum compound following in the late 1980's [54]. Oxaliplatin was originally proposed in the late 1970's but did not receive FDA approval until 2002 when four large phase III clinical trials demonstrated the potential of the combination treatment of 5-fluorouracil, leucovorin and oxaliplatin (FOLFOX). Oxaliplatin was later combined with 5-fluorouracil, leucovorin, irinotecan and oxaliplatin into FOLFIRINOX [55]. This treatment regime was then also approved for metastatic pancreatic cancer in 2015.

There is limited experimental knowledge publicly available about the pharmacokinetics (PK) of oxaliplatin. Oxaliplatin is considered to pass into the cells mainly via passive uptake, although copper transporters have been shown to also contribute to the uptake of platinum complexes [56, 57]. Copper transporters have also exhibited efflux mediation of oxaliplatin, in particular the copper transporter ATP7A (adenosine triphosphate copper transporting alpha) [58, 59]. Copper transporters have also been indicated as the sources of oxaliplatin resistance [59, 57]. Once delivered into the body oxaliplatin undergoes spontaneous non-enzymatic conversions, and forms several reactive species. These reactive species can form complexes with amino acids, proteins, DNA and other macromolecules in the plasma and tissues of treated subjects [60]. Due to the fact that oxaliplatin converts into a larger number of platinum-containing products, platinum is the main feature assessed in the PK and PD of oxaliplatin. The binding of platinum to plasma proteins is considered moderate, between 79% and 87% of total platinum is found bound to proteins. It also exhibits no saturation over a large range of doses [61].

Oxaliplatin is detoxified by glutathione (GSH), which limits the therapeutic effect [62], if tumour cells over express GSH this could also lead to oxaliplatin resistance [63].

Oxaliplatin elimination in humans is predominantly through renal clearance with approximately 55% being cleared via urine and 2.1% through faecal clearance, 5 days post injection [44].

Oxaliplatin is associated with multiple mechanisms of action all relating to DNA damage. These fall into four main categories: DNA aducts, arrest of DNA synthesis, inhibition of RNA synthesis and triggering immunologic reactions [64]. There is also evidence that oxaliplatin kills cells by ribosomal biogenesis stress [65]. Ribosomal biogenesis is the process of creating ribosomes. Ribosomes are structures which create proteins required for many cell functions including proliferation [66]. Ribosomal biogenesis stress causes cell death by limiting the protein abundance [67], which is the energy source used to proliferate.

Oxaliplatin alone often shows low activity in many tumours, hence the use in combination therapy. The most common combination is when used alongside 5-fluorouracil. Experimental results suggest that oxaliplatin down regulates or inhibits the enzyme that degrades 5-fluorouracil [64] prolonging the effect of the drug.

These details of the PK and PD of oxaliplatin are required to build models which have a strong grounding in physiological reality.

Irinotecan

Irinotecan was developed in the early 1990's and gained FDA approval in 1996 for use on colorectal cancer. More recently irinotecan has been approved for use in pancreatic cancer as part of the FOLFIRINOX regime [55].

Irinotecan (CPT11) is a prodrug which means that it is considered to be relatively inactive compared to it's metabolite SN38.

The cellular absorption of CPT11 and SN38 is assumed to be either passive or by fluid phase endocytosis [68]. Irinotecan and its main metabolites SN38 and SN38G are transported out of the cells via ATP-Binding Cassette (ABC) transporters, as this has been shown to be the case in both humans and mice [69, 70].

Irinotecan is metabolised into SN38 by carboxylesterases [71]. The metabolite SN38 is approximately 100-1000 fold more toxic than the parent drug [72]. This activation occurs predominantly in the liver, small intestine and kidney for both humans and mice [72, 73]. SN38 is metabolised into a non-toxic SN38G via UDP glucuronosyltransferases (UGT) [74]. This detoxification step mainly takes place in the liver in humans [72].

The elimination of CPT11 and its metabolites is predominately faecal excretion in humans ($\approx 68\%$ of irinotecan), with renal and biliary elimination accounting for 10-22% and 3-22% of irinotecan respectively [72].

Irinotecan's mechanism of action involves topoisomerase I (TOP1) inhibition. TOP1 is a nuclear enzyme that relaxes supercoiled DNA and is important for replication and DNA decondensation [75]. TOP1 binds to supercoiled DNA and cuts one strand, allowing it to rotate and relax. TOP1 then dissociates and allows the strand to connect again. Irinotecan binds to these DNA/TOP1 complexes and

extends their lifetime by preventing the necessary unbinding of the complex. If the DNA/TOP1/irinotecan complex comes into contact with replication or transcription mechanisms, this can trigger cell apoptosis [76, 77].

This biological information is used to build realistic physiological models that can inform clinicians on processes that can be exploited to improve treatments.

5-Fluorouracil

5-Fluorouracil is part of a family of drugs known as Fluoropyrimidines which were developed in the 1950s. Fluoropyrimdines are a class of antimetabolites widely used for solid tumour treatments in cancers such as colorectal, breast and aerodigestive tract cancers [78].

5-Fluorouracill can be given intravenously in its main form or via either of the two pro-drugs capecitabine or tegafur. 5-Fluorouracil can be metabolised by different routes, with only some of them leading to activation of the drug. The main mechanism of 5-fluorouracil activation is the conversion to fluorodeoxyuridine monophosphate (FdUMP) [78]. The main transporters of 5-fluorouracil which have been reported are SLC22A7, ABCG2, ABCC3, ABCC4 and ABCC5 [79–82].

5-Fluorouracil is an analogue of uracil, which is one of the four nucleobases of RNA, and uses the same transport mechanisms to rapidly enter the cell [83]. Once converted into its active metabolites, i.e. FdUMP, it disrupts RNA synthesis and inhibition of thymidylate synthase which is required for DNA synthesis [83, 84].

Elimination of 5-Fluorouracil is through two main pathways, catabolism by the liver and urinary excretion [85]. Out of these two pathways liver metabolism is the primary route of elimination with urinary excretion only accounting for approximately 5% in normal individuals [86].

These key details can be used to help build more meaningful models to inform clinicians and improve patient care.

1.4 Circadian Rhythms

1.4.1 Definition and terminology

Circadian rhythms are the approximately 24-hour rhythms that are present within most organisms and are believed to be phylogenetically ancient [87]. The cellular mechanisms of the clock were first discovered in by Jeffrey C. Hall, Michael Rosbash and Michael W. Young in 1989 [88], who in 2017 were awarded the Nobel Prize for this discovery. Circadian rhythms are self-sustaining rhythms that are believed to have evolved to anticipate daily events and energy needs giving an advantage in regards to Darwinian fitness [89]. Although circadian organisation is present in most organisms,

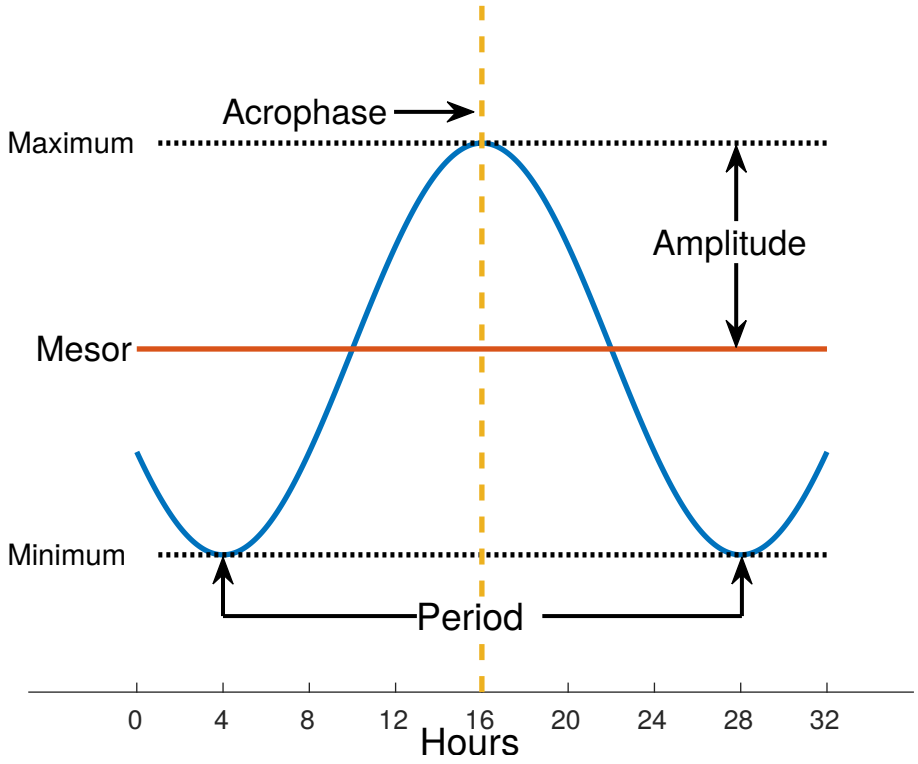

Fig. 1.1 Plot of circadian characteristics: level, amplitude, period and phase.

it is not necessarily set to the same time or phase. For instance diurnally active species and nocturnally active species will have a significantly different circadian clock as they have a roughly 12h shift in their rest-activity cycles [90]. As well as different species having different rhythms there are natural rhythm differences between sex and age [91]. Circadian rhythms are fully defined by their characteristics of: mesor, amplitude, period and acrophase (Fig. 1.1).

Mesor is the mean value or baseline around which the rhythmic variation occurs.

Amplitude is the magnitude of the rhythmic variation.

Period is the duration of a full cycle, usually taken to be approximately twenty-four hours although some rhythms have components with short periods.

Acrophase is the time for when the peak of a rhythm occurs.

In mammals many of the biological functions are organised by the circadian timing system, such as circadian rhythms, which are stimulated by external cues (Fig. 1.2). There is a central pacemaker for the circadian timing system which is located in the suprachiasmatic nuclei (SCN). The SCN then exert control over the peripheral organs through rhythmic regulations of different biological and physiological factors such as temperature, hormonal levels and the autonomous nervous system [92]. As

well as the master clock in the SCN, each nucleated cell is endowed with a molecular circadian clock that generates autonomous intracellular circadian variations. The peripheral clocks are then entrained by SCN-driven and tissue-level factors [1]. In fact, it has been shown that in mice and baboons at least the core clock genes exhibit similar phases throughout various tissues [93, 94].

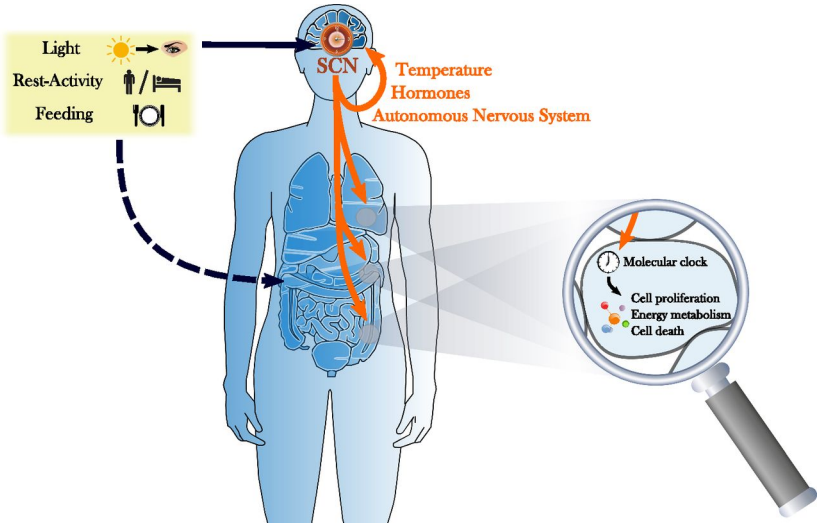

Fig. 1.2 The CTS. The CTS consists of a central pacemaker located in the SCN that displays circadian rhythms, but is also entrained by external cues. The SCN then generates rhythmic physiologic signals to control the molecular clocks present in nucleated cells. These signals induce oscillations in the expression of a large number of genes involved in key intracellular activities [1].

These rhythms are susceptible to disruption and one of the significant causes of this disruption is a modern industrialised lifestyle [95]. The development of artificial light has caused a fundamental change in the relationship between humans with their surroundings [95]. This modified relationship manifests itself in a multitude of ways but the most obvious are light-at-night and shift work. The impacts of these changes are not yet fully understood but have been shown to have a detrimental effect on health [96].

In particular, circadian rhythms are very important in cancer, since they influence many areas of the disease, and taking advantage of them in treatments can increase their efficacy and reduce toxicities.

1.4.2 The influence of circadian rhythms on cancer

Circadian rhythms influence many different areas of cancer, from development to treatment.

There is now a significant amount of studies that have linked circadian disruption with increased cancer risk [97–105], which has led to the International Agency for

Research on Cancer to classify night work and shift work with circadian disruption as "Probably Carcinogenic" [106]. The exact molecular events behind these increased risks are likely to be a multitude of interlinked factors from, melatonin suppression to faulty DNA repair [106].

Alongside the original development of cancers, it has also been shown that circadian disruption is linked to progression of tumours [107–111]. Indeed, circadian disruption achieved through either chronic jet lag or SCN ablation increased tumour growth rate in tumour engrafted mice. Next, the disruption of rest-activity rhythms in cancer patients was associated with a decreased quality of life and worse survival rates [1].

Circadian rhythms can have a large impact on the treatment of cancers. This is predominantly due to the chronopharmacology of different anti-cancer agents. There are approximately 50 different anti-cancer agents that display circadian variations in their pharmacology, related toxicities and/or anti-tumour efficacy [112, 113]. These circadian variations in pharmacology have numerous causes, absorption, distribution, metabolism or excretion, and it is most probably a combination of these [113, 32]. 24-hour rhythms in drug toxicity and efficacy, also called chronotoxicity and chronoefficacy, may arise from controls of the CTS at various levels of DNA damage sensing, DNA repair, cell cycle and cell death pathways [1, 114, 115].

The use of chronotherapy has already shown that the same drugs can produce better outcomes with proper timing. Building a deeper understanding of how this is possible has the potential to help clinicians develop better treatment regimes and schedules.

1.5 Chronotherapy

Chronotherapy is the term used for changing and adapting treatments relative to the biological rhythms of a patient over the 24-h span [1]. It can involve both pharmacological or non-pharmacological treatments, such as surgery [116], physical agents [117] and psychotherapy [118]. The goal is to optimise treatment efficacy, while minimising toxicity or adverse effects.

The potential benefit of chronotherapy has been demonstrated for various pathologies and for over 400 medications, including nearly 50 anticancer agents [112, 113]. Chronotherapy in terms of chemotherapy has been suggested as early as the late 1970's [119–121]. The use of circadian rhythms and chronotherapy, although being originally proposed nearly 50 years ago, and despite recent findings that circadian timing can modify the tolerability of anticancer agents by 2-10 fold [112], is still in its infancy. This is starting to change and in June 2016, there were 348 clinical trials worldwide involving chronotherapy or circadian biology according to the US National Institute of Health which is approximately 0.16% of existing trials and only

3.4% of these trials apply to cancer [32]. As of December 2018 the number of clinical trials related to chronotherapy or circadian biology has risen to approximately 600 [122]. This may be explained by the award of the 2017 Nobel prize of physiology or medicine awarded to Jeffrey C. Hall, Michael Rosbash and Michael W. Young for their discoveries of molecular mechanisms controlling the circadian rhythm. Furthermore, the benefits of chronotherapy for diseases such as hypertension, arthritis, asthma and peptic ulcers are significant, which has caused a sense of urgency in health professionals and regulatory services in implementing chronotherapy in clinical studies and evaluating trial results [32].

The evidence for chronotherapy for the particular drugs of focus in this thesis have been building for a number of years. The first experiments to show that there is a circadian variation in the pharmacology of 5-fluorouracil were done in the early 80's. These first experiments showed that the dose at which 50% of test animals die (Lethal Dose 50, or LD50) increased by approximately 70% for different injection times during the light dark cycle of mice, i.e. at certain times of the day the toxic effects are lower [123]. It was then shown that in addition to the toxicity, the efficacy is also affected by circadian timing. A study by Peters et al showed that the therapeutic efficacy of 5-fluorouracil against murine colon cancer was higher when administered at 0830 compared to 1830 [124]. Multiple studies then demonstrated the chronopharmacokinetics in human cancer patients receiving long term continuous infusions. This means that the level of 5-fluorouracil detected in the blood plasma fluctuated with a 24h rhythm even though the dose being delivered was at a continuous rate [125–127]. A phase I-II trial of chronomodulated delivery schedules of 5-fluorouracil alone and in combination with oxaliplatin have shown to have increased efficacy against metastatic colorectal cancer [128, 129].

Oxaliplatin, to my knowledge, is the only well-documented case in which a drug after failing a phase I clinical trial was later shown to be clinically effective with the integration of chronopharmacology [130]. Initial mouse experiments showed circadian differences in toxicity (Fig. 1.3) and tissue uptake in the late 1980's [2] which led to clinical trials showing the potential benefits of circadian timed delivery of oxaliplatin [131, 128, 132, 133]. With the discovery of more and more anti-cancer drugs being influenced by circadian timing, investigations into more recently developed drugs such as irinotecan were undertaken.

The first study to show irinotecan had circadian tolerability in mice was undertaken by Filipski et al in 2004 [134]. The molecular interaction of irinotecan was then investigated and modelled to understand the circadian influence at the cellular level [74]. The intersubject variability of circadian timing was investigated relative to irinotecan, showing that for three different strains of the C57BL/6 mouse (both sexes) there were three different chronotoxicity classes with distinct chrono-toxicity patterns [3] (Fig. 1.4). Then investigations have been done to identify a determinant

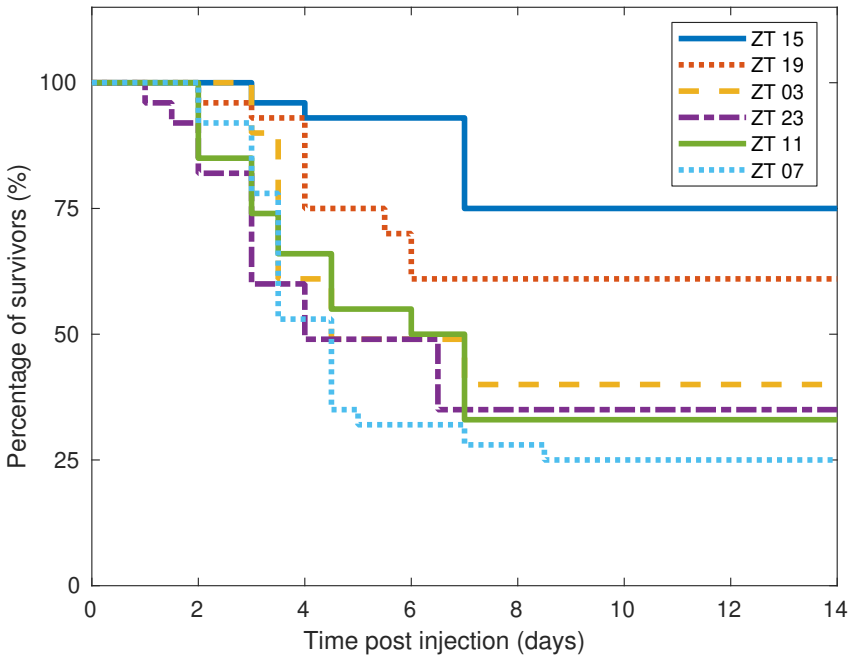

Fig. 1.3 Survival curves of male B6D2F$_1$ mice following i.v. administration of 17mg/kg of oxaliplatin at 6 different times of injection. Survival rate differed as a function of injection time with maximum difference in survival rate of 50%. Original data were collected over 40 days. Data shown here were truncated as survival percentage stays constant from day 9 until the end of the experiment. Original data can be seen in Boughattas et al 1989 [2].

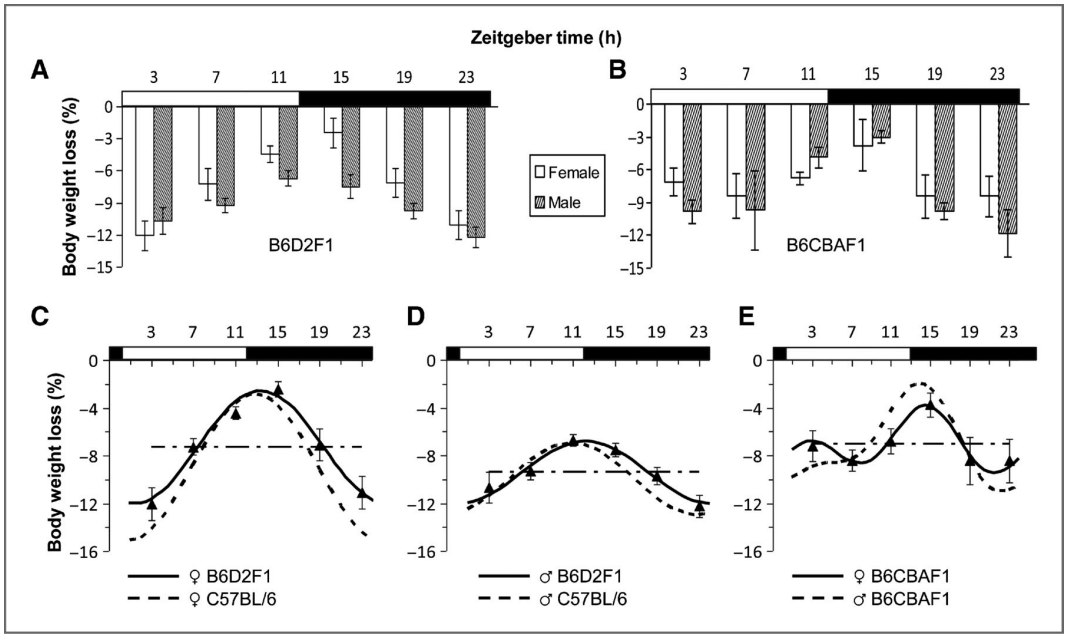

Fig. 1.4 Body weight loss (BWL) as a function of irinotecan dose timing in male or female mice from three mouse strains. Equally toxic doses of irinotecan were delivered daily for 4 days to C57BL/6 or B6D2F1 (50 mg/kg/d) or B6CBAF1 (80 mg/kg/d) at either 3, 7, 11, 15, 19 or 23 ZT. Top row, histograms of mean body weight change ±SEM against dosing time for B6D2F1 (A) and B6CBAF1 (B). Bottom row, cosinor analysis of 3 chronotoxicity classes based on reconstructed circadian patterns with 24-hour ± 12-hour rhythmic components: class 1, female B6D2F1 and C57BL/6 (C); class 2, male B6D2F1 and C57BL/6 (D); class 3, female and male B6CBAF1 (E). Data taken from Xiao Mei, li et al 2013 [3].

that could predict optimal circadian timing in cell cultures. This revealed that least irinotecan induced cell apoptosis occurred at a BMAL1 nadir (lowest levels in the 24h cycle) [135]. The discoveries made for circadian influence on all three of these drugs have led to the recent European study which shows the potential clinical benefit of chronomodulated infusion of a combined treatment [6].

Although chronotherapy has been shown to make large improvements in treatment efficacy, using a standardised approach for all patients is not optimal, specifically sex related differences in optimal timing can negate improvements made by circadian timing if every patient is treated the same.

For instance a meta-analysis by Giacchetti et al, has been shown that current chronotherapy schedules have different success rates for males and females. This work investigated three Phase III trials which compared the chronomodulated release or conventional release of FOLFOX which showed that the chronomodulated treatment improved overall survival for males from 17.5 months to 20.8 months, but for females actually decreased overall survival form 18.4 months to 16.6 months [136].

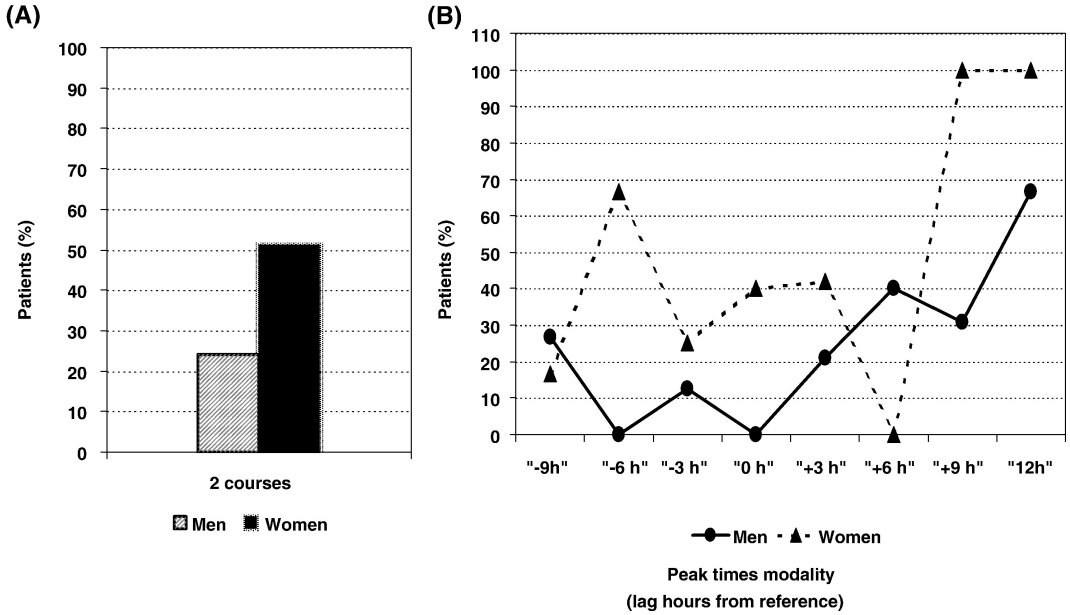

Fig. 1.5 Effect of patient's sex on chronotolerance for 5-FU and oxaliplatin in patients with metastatic colorectal cancer. (A) Overall incidence of severe toxicities of any kind over two courses of treatment; (B) Possible influence on circadian pattern of tolerability over two courses of treatment. The x-axis label is given in number of hours before (−) or after (+) the reference modality "0h". For the reference modality "0h", the peak times of delivery occurred at 4 pm for oxaliplatin and at 4 am for 5-FU. for other peak times the whole schedule was shifted by 3, 6, 9, or 12 h (hours) earlier or later. Taken from Levi et al 2008 [4].

The sex specific outcomes of chronomodulated treatments have also been observed in the combination of 5-fluorouracil, leucovorin and carboplatin (platinum based chemotherapy drug). Female patients experienced significantly higher toxicities than males under the same conditions [137]. This has been shown for 5-fuorouracil, leucovorin and oxaliplatin as well, where females were almost twice as likely to experience severe toxicities and had an optimal timing of delivery of potentially 6 hours later [4](Fig. 1.5).

Sex differences in tolerance of irinotecan have also been observed recently in a international time-finding study. This study demonstrated that optimal timing of irinotecan dosage, with respect to tolerability, occurs 4-7 hours earlier in males than in females [5, 138] (Fig 1.6). This phenomenon shows the need for a more detailed understanding of what influences optimal times and more personalisation when it comes to choosing delivery schedules.

Chronotherapy has been shown to improve efficacy and reduce toxicity. The example of oxaliplatin really emphasises the importance that circadian influences can have on drug efficacy and the significance circadian rhythms can have in preclinical and clinical trials [130]. Producing accurate physiological based models has the

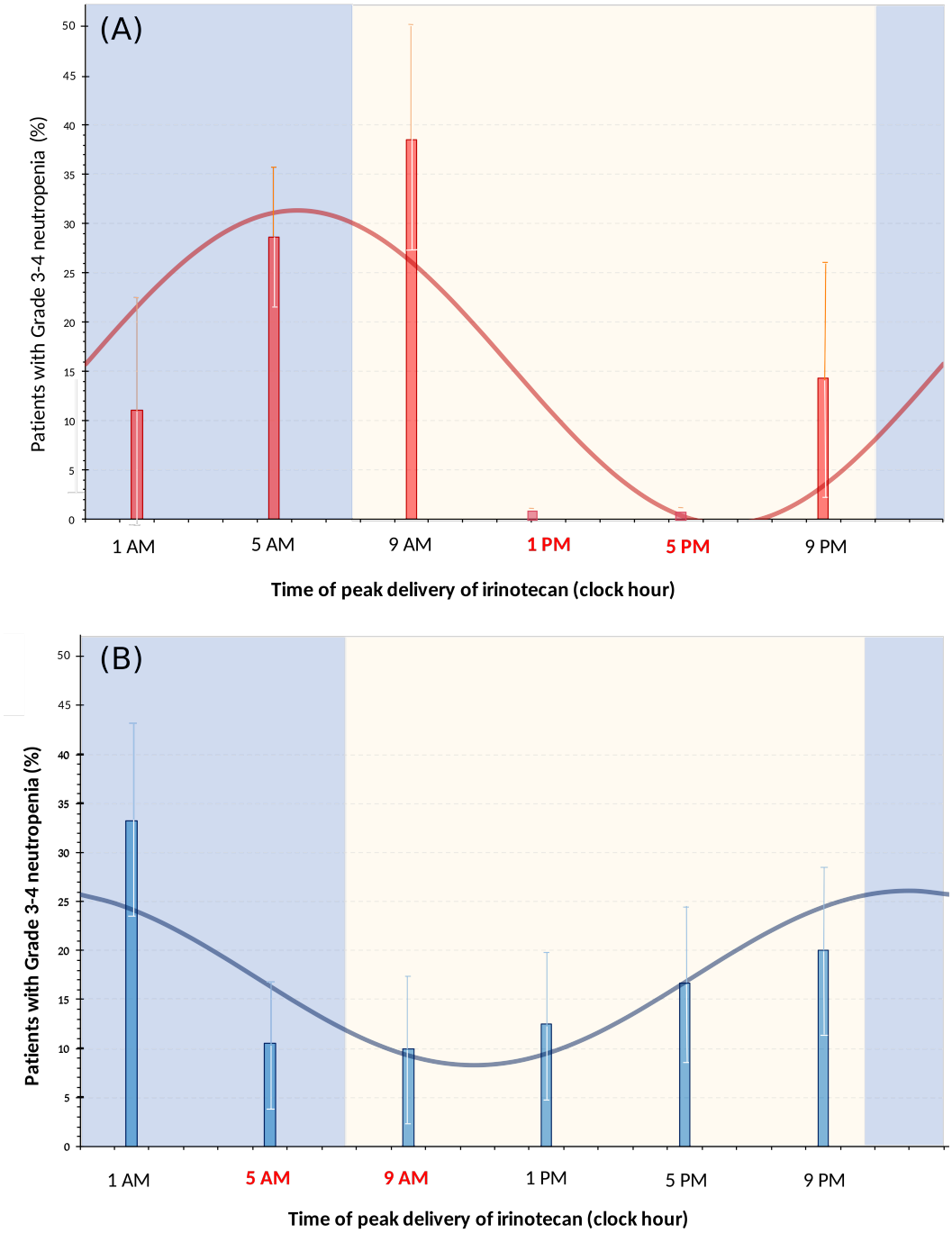

Fig. 1.6 Dosing time dependent incidence of severe neutropenia according to sex. Rates (±SE) of patients with Grade 3-4 neutropenia as a function of peak delivery timing of chronomodulated irinotecan in combination with chronomodulated 5-fluorouracil, Leucovorin and oxaliplatin, and corresponding best fit of 24-h cosine curve ($p<0.05$) (A) males (B) for females. Grey refers to night time and light refers to day time. [5]

potential to help to understand the processes behind the benefits of chronotherapies and can be used to further increase positive treatment outcomes.

1.6 Motivation

Gastrointestinal cancers are a significant burden on economy and health care systems and have a devastating effect on the lives of patients and their loved ones. Research shows that circadian rhythms have an impact on both the development and treatment of gastrointestinal cancers. Oxaliplatin and the full FOLFIRINOX regimen have been shown to have different toxicity levels for different times of administration, optimal timing being dependent on the patient's sex and geneteic background. Thus, modern medicine is now moving towards a more personalised treatment approach.

There are known sex specific differences in the toxicity of oxaliplatin, 5-fluorouracil and irinotecan. The development of mathematical models can help to direct and inform biological research and help create smarter ways to personalise treatments for patients.

1.6.1 Aims

This thesis aims firstly to improve currently used delivery profiles of chronomodulated drug infusion and provide a novel method of patient stratification based on semi-physiological pharmacokinetic parameters.

Secondly this thesis aims to use a quantitative systems pharmacology approach to build a fuller picture of the pharmacokinetics of oxaliplatin. Focusing on inter-species scaling of an in vitro model, and development of a whole body model that could be used to gain insight into the sex specific differences of oxaliplatin pharmacokinetics and pharmacodynamics.

1.6.2 Overview

With this in mind, chapter 3 of this thesis outlines an improvement to delivery profiles for chronomodulated drug infusion, and a method of patient stratification based on semi-physiological pharmacokinetics parameters. Chapter 4 then develops a novel mathematical model which is shown to be able to scale between animal and human pharmacokinetics of oxaliplatin. Model scaling is then used in a multi-scale modelling fashion to build a whole body pharmacokinetics mouse model. This model has been designed to explore the sex specific differences of oxaliplatin pharmacokinetics and pharmacodynamics and give more information on what processes cause the sexual dimorphisms which are observed.

Chapter 2

Mathematical methods

2.1 Pharmacokinetics-Pharmacodynamics modelling

Pharmacokinetics, sometimes known as what the body does to a drug, refers to the transport and transformation of the drug throughout the body. This includes absorption, bioavailability, distribution, metabolism, and excretion (ADME) [139].

Pharmacodynamics, sometimes known as what the drug does to the body, describes the effects of the drug on the organism, including DNA binding, DNA damage and drug-induced cell death [139].

2.1.1 Non-physiological VS physiologically-based modelling

Pharmacokinetic-Pharmacodynamic (PK-PD) modelling began with simple dose response curves, but over the last 60 years has developed into a range of sophisticated and complex models which give insight into underlying mechanisms of drug interactions [140].

The simplest PK models able to represent concentration-time profiles are based on compartments which do not normally hold a physiological interpretation. They are used for data description and interpolation, however they are very poor at extrapolation since the parameters have no strict biological meaning [141]. The size and complexity of the model usually increases with how physiologically-based the model is, and how much biological meaning can be attributed to the model structure and parameters [142]. The ultimate aim in achieving accuracy is to apply physiologically based PK (PBPK) models or whole body PK (WBPK) models. Originally, PBPK modelling was mainly focused on environmental toxicology, with any use within pharmaceuticals being based in academia, however it has in the

last 20 years been increasingly used in drug development and regulatory processes [143, 144]. These types of models use pragmatic compartmental structures to represent key anatomical features of the subject body, i.e. patient or animal. The parameters can then take on direct biological meaning and be used to inform users on previously unattainable information [142]. The downside to greater complexity is overparameterisation. This is often balanced by combining parameters together that have the same overall effect. For instance, if a drug can be metabolised in the liver as well as cleared from the liver via the bile duct, this can be "lumped" together as liver clearance. Another method to reduce overparameterisation is to consider semi-physiological models (such as [145]), this is often required for clinical models as human data may be more sparse than animal data.

Pharmacodynamics has moved from empirical to more qualitative descriptions due to advances in analytical methods, computer hardware and software, and to the increased interest from regulatory and academic organisations in precision medicine [146]. Early PK-PD models, based on empirical methodologies, describe the complex relationship between blood concentration and therapeutic effect by linking compartmental PK models with "effect models". These effect models define how the concentration in the compartment of interest translates to therapeutic effect. The aim of these models is to give a consistent mathematical structure to the effect of the drug. One of the most well used formulas is the Hill function, and can be used to describe specific binding patterns with each parameter having a physical meaning [147]:

$$E = \frac{C^n}{C^n + EC_{50}^n} \tag{2.1}$$

where the drug effect E is dependent on the drug concentration in the studied compartment C and the coefficient of half maximal effect EC_{50}, with n being the Hill coefficient which determines the steepness of the response, which can be seen in Fig. 2.1.

2.1.2 Main laws for the design of physiologically-based models

The structure of many PK-PD model parameters comes from three main principles: the law of mass action, Michaelis-Menten kinetics and Fick's first law.

Law of mass action

The law of mass action states that the rate of spontaneous chemical reactions is directly proportional to the product of the concentrations of the reactants. Consider the following reaction:

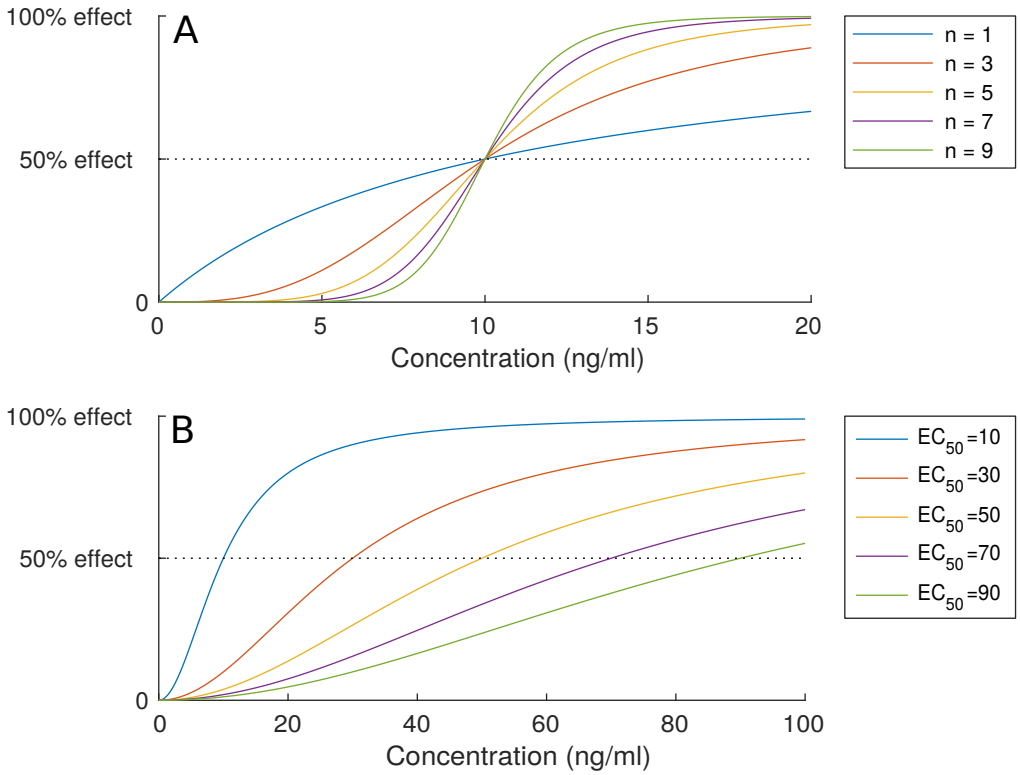

Fig. 2.1 A shows how the steepness of the Hill function changes with respect to the Hill coefficient n ($EC_{50} = 10$). B shows the influence of the half maximal effect coefficient EC_{50} on the Hill function curve ($n = 2$).

$$\alpha\mathrm{A} + \beta\mathrm{B} \overset{K}{\rightleftharpoons} \gamma\mathrm{AB}$$

from the law of mass action, the rate of the forward reaction is then:

$$K[A]^{\alpha}[B]^{\beta}. \tag{2.2}$$

This is often used in models with drug A binding to protein B. If the protein has much higher concentration than the drug, i.e. if the protein is in large excess, then the protein can be considered as constant and the reaction can be simplified to:

$$K^{*}[A]^{\alpha}, \tag{2.3}$$

where K^{*} incorporates the constant protein concentration. This manipulation is well used in the field of pharmacokinetic modelling to simplify models.

Michaelis-Menten kinetics

Michaelis-Menten kinetics typically represent the rate of enzyme reactions. This is often used in PK models to represent the metabolism of a drug catalysed by liver enzymes. Consider the following reactions:

$$E + S \quad \underset{K_{-1}}{\overset{K_1}{\rightleftharpoons}} \quad ES \xrightarrow{K_2} E + P$$

where the substrate S is converted into the product P though the activity of the enzyme E. This two-step process involves the reversible binding of the enzyme E to the substrate S to form ES complexes, followed by the transformation of the bound substrate into the product P and the concomitant release of unaltered enzyme E. The rate of production of product P is then:

$$V = K_2[ES] \tag{2.4}$$

The rate of formation of ES would then be:

$$\text{formation ES} = K_1[E][S] \tag{2.5}$$

and the breakdown of ES would be:

$$\text{breakdown ES} = (K_{-1} + K_2)[ES] \tag{2.6}$$

when the system is in steady state these would be equal and can be rearranged to:

$$[ES] = [E][S]/(\frac{(K_{-1} + K_2)}{K_1}) \tag{2.7}$$

Under the assumption that the total amount of enzyme (E_T) is unchanged ($E_T = E + ES$) (2.6) becomes

$$[ES] = ([E_T] - [ES])[S]/(\frac{(K_{-1} + K_2)}{K_1}). \tag{2.8}$$

Solving for $[ES]$ and simplifying gives:

$$[ES] = \frac{[E_T][S]}{\frac{(K_{-1}+K_2)}{K_1} + [S]} \tag{2.9}$$

if we multiply both sides of the equation by K_2 we get the rate of production of P (V) as:

$$V = K_2[ES] = \frac{K_2[E_T][S]}{\frac{(K_{-1}+K_2)}{K_1} + [S]}. \tag{2.10}$$

Since the concentration of the enzyme is assumed to be constant, notationally this is classically written as $V_{\max} = K_2[E_T]$ where $V_{\max}$ is the maximum possible rate of production of product, and $K_m = \frac{(K_{-1}+K_2)}{K_1}$ which is the concentration of substrate at which the rate is half its maximum, and the equation becomes:

$$v = \frac{V_{max}[S]}{K_m + [S]}. \tag{2.11}$$

Fick's first law for diffusion

In a spatial context, Fick's first law relates the drug diffusive flux through a point (1D) or a surface (2D) to the drug concentration as:

$$J = -D\frac{\partial C}{\partial x} \tag{2.12}$$

where J is the diffusive flux, D is the drug diffusion coefficient, C is the drug concentration and x is the spatial position. When this is restated for diffusion across a membrane barrier of thickness dx, concentration gradients ∂C is approximated by the concentration difference across the membrane i.e. concentration in compartment 1 minus concentration in compartment 2, $(C_1 - C_2)$. D/dx is then the first-order transfer constant k_d.

$$J = -D/dx(C_1 - C_2) = k_d(C_1 - C_2) \tag{2.13}$$

In a single compartmental model, C_2 is not considered and therefore the flux out of the comapartment can be writen as:

$$J = -D/dx(C_1) = k_d(C_1) \tag{2.14}$$

This law is used in the vast majority of PK models to represent drug transport between compartments and is equivalent to discarding the concentration gradients and only retaining the linear transfer property between compartments [148].. For example, the transfer of a drug between three compartments (A, B and C) represented as:

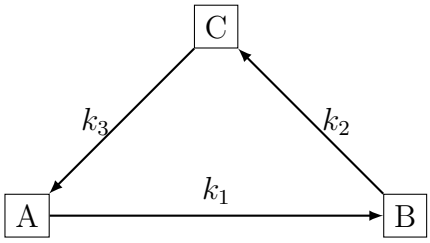

can be written as:

$$V_A \frac{dC_A}{dt} = k_3 V_C C_C - k_1 V_A C_A \tag{2.15}$$
$$V_B \frac{dC_B}{dt} = k_1 V_A C_A - k_2 V_B C_B \tag{2.16}$$
$$V_C \frac{dC_C}{dt} = k_2 V_B C_B - k_3 V_C C_C \tag{2.17}$$
$$\tag{2.18}$$

which simplifies to:

$$\frac{dC_A}{dt} = k_3 \frac{V_C}{V_A} C_C - k_1 C_A \tag{2.19}$$
$$\frac{dC_B}{dt} = k_1 \frac{V_A}{V_B} C_A - k_2 C_B \tag{2.20}$$
$$\frac{dC_C}{dt} = k_2 \frac{V_B}{V_C} C_B - k_3 C_C \tag{2.21}$$
$$\tag{2.22}$$

In this form the units of k_i would be rate $(1/t)$. It is also common for equations to be written in a different form.

$$V_A \frac{dC_A}{dt} = K_3 C_C - K_1 C_A \tag{2.23}$$
$$V_B \frac{dC_B}{dt} = K_1 C_A - K_2 C_B \tag{2.24}$$
$$V_C \frac{dC_C}{dt} = K_2 C_B - K_3 C_C \tag{2.25}$$
$$\tag{2.26}$$

This formulation incorporates the volumes directly into the parameters since $K_i = k_i V_j$ and has units volume per time (v/t). These three techniques make up the main toolbox of PK models and will be used in each of the models presented in this thesis.

2.2 Multi-scale modelling approach

Most real-world problems involve a range of different spatial or time scales, as well as different interacting processes. Taking these different scales and processes into account is known as multi-scale modelling [149, 150]. Multi-scale modelling can take many forms, in many different areas of research, from polymer composites [151] to crowd dynamics [152]. Biological experiments can be conducted at many different scales, looking at single proteins up to whole organisms which means data may exist for these different scales [153]. In the field of biology multi-scale modelling can be considered in two forms, the first look at intracellular, inter-cellular then whole body scales for the same species (Fig. 2.2A), the second is to use multiple species to develop models across in vitro, in vivo animal specimens and in vivo human (Fig. 2.2B). For both forms of multi-scale modelling the knowledge base is built upon at each step and translated to each different level of the multi-scale pipeline [154].

The main benefits of multi-scale modelling come from error reduction and increased understanding. Since the separation of these sets of processes means that the number of parameters fitted per data set is reduced, this leads to an overall increase in accuracy [155]. Also mathematical multi-scale models can give a complete overview of experiments, while still allowing the ability to focus in on particular key functionalities or structures [156]. These are necessary requirements in order to build informative models which can be used by clinicians to improve quality of treatment.

2.3 Parameter estimation and model identifiability

If we define a general dynamical system as:

$$\dot{x}(t) = f(x(t), p) + \sum_{i=1}^{m} g_i(x(t), p)u_i(t) \tag{2.27}$$

$$y(t, p) = h(u(t), x(t), p) \tag{2.28}$$

where x is the n-dimensional state variable i.e. concentration, u is the m-dimensional input vector of smooth functions e.g. drug delivery, y is the r-dimensional output vector i.e. concentration sample sites and f, g and h are assumed to be polynomial or rational functions of their arguments and p is a v- dimensional vector of unknown parameters, then this model is said to be identifiable if there exists a unique vector p of parameters [157]. In a mathematical description two parameter vectors are said to be indistinguishable, written as $p \sim \hat{p}$, if they give rise to identical outputs i.e:

$$y(t, p) = y(t, \hat{p}) \quad \text{for all } t \geq 0 \tag{2.29}$$

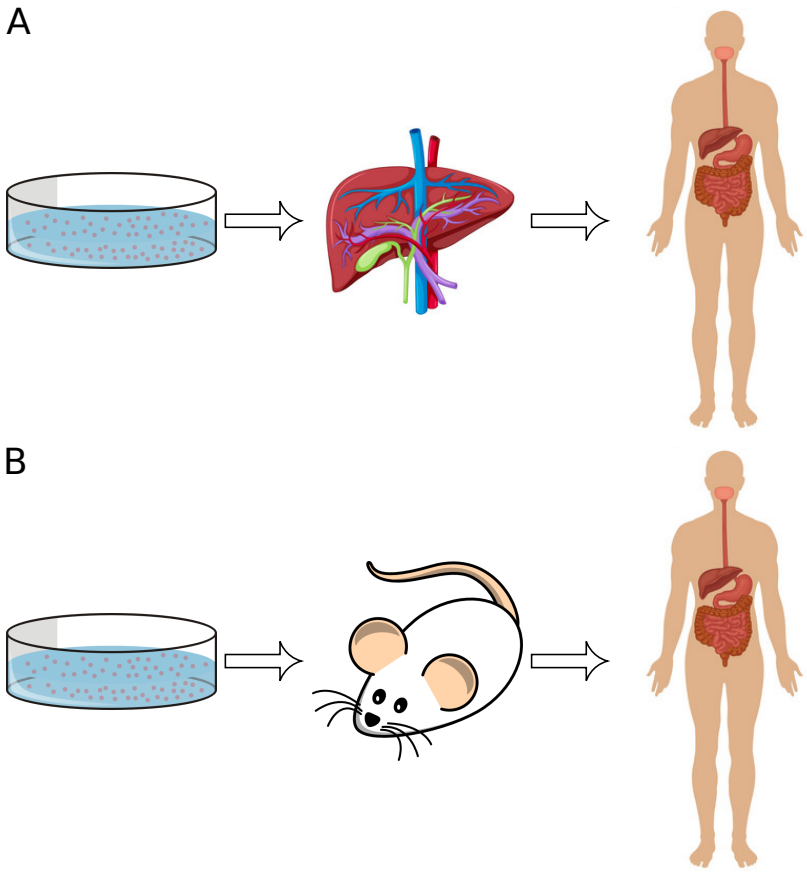

Fig. 2.2 Multi-scale modelling pipelines. A shows the advancement from in vitro intracellular to in vitro intercellular then in vivo, all within in the same species. B shows the advancement from in vitro to in vivo animal specimens and finally to in vivo humans.

If a parameter p_i is said to be locally identifiable then there exists a neighbourhood, N, of p such that:

$$\hat{p} \in N, \qquad p \sim \hat{p} \quad \text{implies that } p_i = \hat{p}_i \tag{2.30}$$

If the neighbourhood N encompasses the whole search space then the model is said to be globally identifiable, otherwise it is said to be nonuniquely or locally identifiable [158].

Identifiability is often split into two forms, structural and practical. Structural identifiability describes whether it is theoretically possible to determine the true value of a parameter from observations of the model output. In simple terms if a model is structurally identifiable then given the "ideal" data set the parameters would be uniquely identifiable. Practical identifiability relates to whether given the "real" data are the model parameters uniquely identifiable. Practical identifiability takes into account the limitations in quality and frequency of the data points to determine whether model parameters can be uniquely expressed [159].

2.3.1 Structural identifiability

Structural identifiability is an important part of model design and a necessary requirement for models to be informative [157]. There are a number of software packages that have been designed to analyse the structural identifiability of models. Three examples that have been designed to determine global identifiability are DAISY [160], GenSSI [161] and COMBOS [162]. DAISY and COMBOS use a combination of algerbraic transformations and computing Groëbner basis of model atirbutes. GenSSI is based on the generating series approach coupled with the use of identifiability tableaus [161] with the idea being to generate a non-linear system of equations on the parameters. If this system has a unique solution the the parameters are globally identifiable. All three methods will determine if a model is structurally globally identifiable, structurally locally identifiable and structurally non-identifiable. DAISY also gives the added benefit of saying whether initial conditions are required for identifiability. The main limitation of DAISY is that it can not deal with too many non-linearities and is restricted in the functional form of these non-linearities [160, 161]. Taking into account that the models used within this thesis do not have large amounts of non-linearities and the date the software was created the more well established software of DAISY was chosen to preform structural analysis.

2.3.2 DAISY

Differential Algebra for Identifiability of SYstems (DAISY) is a software tool created to perform global identifiability analysis on both linear and nonlinear dynamical

models represented by differential polynomials. It uses a bespoke algorithm to show whether model parameters are theoretically uniquely identifiable given certain input-output data. For the general dynamical system:

$$\dot{x}(t) = f(x(t), p) + \sum_{i=1}^{m} g_i(x(t), p)u_i(t) \tag{2.31}$$

$$y(t) = h(u(t), x(t), p) \tag{2.32}$$

where x is the n-dimensional state variable, i.e. concentration, u is the m-dimensional input vector of smooth functions e.g. drug delivery, y is the r-dimensional output vector, i.e. concentration sample sites and f, g and h are assumed to be polynomial or rational functions of their arguments and p is a v- dimensional vector of unknown parameters. Initial conditions are also included in the analysis and can be used to represent impulsive inputs. The algorithm's steps are as follows:

0. If any of the polynomials are rational they are reduced to the same denominator.

1. A binary matrix is created with each row representing an equation and each column representing a variable (inputs, outputs, states and their derivatives). The matrix entries for row one would be 1 if the corresponding column variable is present in equation one and zero otherwise.

2. The variables are ranked with respect to their derivatives i.e:

$$u_1 < u_2 < ... < y_1 < y_2 < ... < \dot{u}_1 < \ddot{u}_1 < ... < \dot{u}_2 < \ddot{u}_2 \tag{2.33}$$

$$< ... < \dot{y}_1 < \ddot{y}_1 < ... < \dot{y}_2 < \ddot{y}_2 < ... < x_1 < x_2 \tag{2.34}$$

$$< ... < \dot{x}_1 < \dot{x}_2 < ... \tag{2.35}$$

   Using this ranking the polynomials are then ordered by increasing size.

3. A comparison is made between the polynomial and the previous ones, if the rank is greater than or equal to the previous polynomials, then it is reduced with respect to the preceding ones via the pseudodivision algorithm (which can be seen in[160]).

4. Steps 1-3 are repeated until an auto-reduced set of minimum rank is reached i.e. no further reductions are possible. This is called the characteristic set.

5. If in the characteristic set a state component appears without its derivative then it is algebraically observable.

6. Extract the polynomials only containing the input and output functions i.e. without the x variable. These polynomials constitute the input-output relation of the dynamical system. Their coefficients are polynomial functions in p.

7. The coefficients of the polynomials and their derivatives are extracted and, along with any parameter equality constraints, provide an exhaustive summary of the original dynamic model.

8. A system of algebraic nonlinear equations in the unknown vector p is constructed, y evaluating each unknown p in the exhaustive summary at a randomly chosen numerical values.

9. The algebraic nonlinear equations are then solved symbolically using built in REDUCE, which is software designed for doing scalar, vector and matrix algebra, modules which then provides the identifiability results.

10. If initial conditions are known, then they are the corresponding polynomials of the characteristic set are evaluated at time $t = 0$. These known algebraic polynomial functions of p are then added to step 7 and continue through steps 8 and 9.

Full details of this algorithm can be seen in the Bellu et al paper [160]. The algorithm runs very fast for most models, however if there is more than one nonlinearity the algorithm may be unable to complete due to lack of memory.

The results obtained by running DAISY gives information on the structural identifiability of the model. The results can be from this list of possible answers:

- Globally identifiable, initial conditions not necessary. This means given the "ideal" data the model parameters can be uniquely define with out the extra information of initial conditions being required.

- Globally identifiable, initial conditions necessary. This means that with the inclusion of initial conditions the model parameters are identifiable.

- Locally identifiable, initial conditions not necessary. This means there a finite number of indistinguishable parameter values for this model without the inclusion of initial conditions.

- Locally identifiable, initial conditions necessary. This means only with the inclusion of initial conditions is there a finite number of indistinguishable parameter values for this model.

- Not identifiable. This means there is an infinite number of indistinguishable parameter values for this model.

2.3.3 Least squares estimation

Least squares estimation is a parameter fitting procedure which minimises the sum of squared residuals between a model and data. It has been used in data fitting since

1800's with the first clear description coming from Legendre in 1805 [163]. It was originally developed for fitting linear equations to data but since its inception has been used for many different model types including the models used in this thesis: ordinary differential equations (ODEs) [164]. The formulation of sum of squared residuals is:

$$SSR = \sum_{i=1}^{n} (y_i - f(x_i, \theta))^2 \tag{2.36}$$

where the y_i are the observed data, x_i is the location of the data points, and θ is the vector of unknown parameters in the model f. One of the advantages of the least squares method is that given the assumption that the noise in the data is normally distributed the maximum likelihood estimator is identical to that which minimises the sum of squared residuals. The assumption that noise is normally distributed is one that if often done in literature unless there is prior knowledge to the contrary. The noise in the data can be interrupted as the errors between predicted values and the data. This can be evaluated by plotting the residuals and observing whether they follow the normality line. The maximum likelihood estimator being identical to the least squares estimator is key for the likelihood profile methods discussed later.

2.3.4 CMAES

The covariance matrix adaption evolutionary strategy (CMAES) was derived from the concept of self-adaptation or evolutionary strategies (ES). It was created to deal with optimisation problems which were formulated to minimise an objective function (f), for which the only accessible information on f are cost function values. This has meant that it is particularly good for handling complex cost function landscapes, with small population sizes [165, 166] and has been shown to be highly competitive in a number of test cases, alongside its successes in real world problems [165]. The lack of information and complex cost function landscape also rules out the use of gradient based searches, as the chances of becoming "trapped" in local minima is too high [167]. A brief description of the algorithm is as follows:

1. Initialise parameters, evolutionary paths, sample mean and step-size.
2. Sample a new population of search points.
3. Select a certain number of "best" points to use to adapt mean and evolutionary paths.
4. Adapt the covariance matrix using evolutionary paths and sample points.
5. Repeat steps 2-4 until the termination criterion has been met.

A detailed description of the algorithm can be found in Hansen [165]. There are implementations in multiple languages to improve usability, with the implementations used within this thesis in MATLAB [168], or Python [169].

2.3.5 Likelihood profile

As stated above, parameter estimation is done by least squares estimation. Given the assumption that the error in the data is normally distributed i.e. $\epsilon \sim N(0, \sigma^2)$, the least squares estimator corresponds to the maximum likelihood estimate (MLE). Given the sum of squared residuals corresponds to the likelihood we can substitute it into the method of likelihood profiles described in [170]. This method can give asymptotic confidence intervals as well as practical identifiability. If a parameter is practically nonidentifiable, this means that the parameter has no significant effect on the likelihood. If a parameter has been shown to be structurally identifiable this does not imply it is practically identifiable, although the converse is true locally. Practical identifiability comes down to the amount and quality of the data available to fit a model. The method of likelihood profiles for identifiability defines practical nonidentifiability as having an infinite likelihood based confidence region. These confidence intervals are defined by:

$$\{\theta | \chi^2(\theta) - \chi^2(\hat{\theta}) < \Delta_\alpha\} \tag{2.37}$$

where the threshold is given by;

$$\Delta_\alpha = \chi^2(\alpha, df), \tag{2.38}$$

and χ^2 represents the likelihood, $\hat{\theta}$ is the optimal parameter set, α is the quantile used in the χ^2-distribution with degrees of freedom (df) either 1 for a pointwise confidence interval or the size of the parameter set for simultaneous confidence intervals. In order to actually test identifiability with this method the parameter space is explored to find the point where each parameter passes the threshold. Practically this involves the following steps:

1. Find the MLE of the parameter set $\hat{\theta}$
2. Now take a parameter θ_i from the parameter set to leave a new set ($\theta_{j \neq i}$) of size 1 less than the original parameter set $\#(\theta - 1)$.
3. Now move through the parameter range fixing θ_i at a new value.
4. Re-optimise all other parameters, i.e. find the MLE for $\theta_{j \neq i}$.
5. Repeat steps 2 and 3 until the likelihood profile passes above the threshold. This has been done by starting at $\hat{\theta}_i$ and moving in the positive direction until

the threshold has been met $\theta = \theta_+$ and then beginning at $\hat{\theta}_i$ and moving in the negative direction $\theta = \theta_-$.

The points at which the likelihood profile passes the threshold are the upper and lower confidence intervals, so for parameter i the optimal parameter is $\hat{\theta}_i$ between θ_- and θ_+, see Fig. 2.3A. If the parameter is nonidentifiable then the likelihood profile will only pass through the threshold once, see Fig. 2.3B. This method proves very useful in systems biology as it makes the defining of local identifiability and local confidence intervals possible for complex nonlinear systems [171].

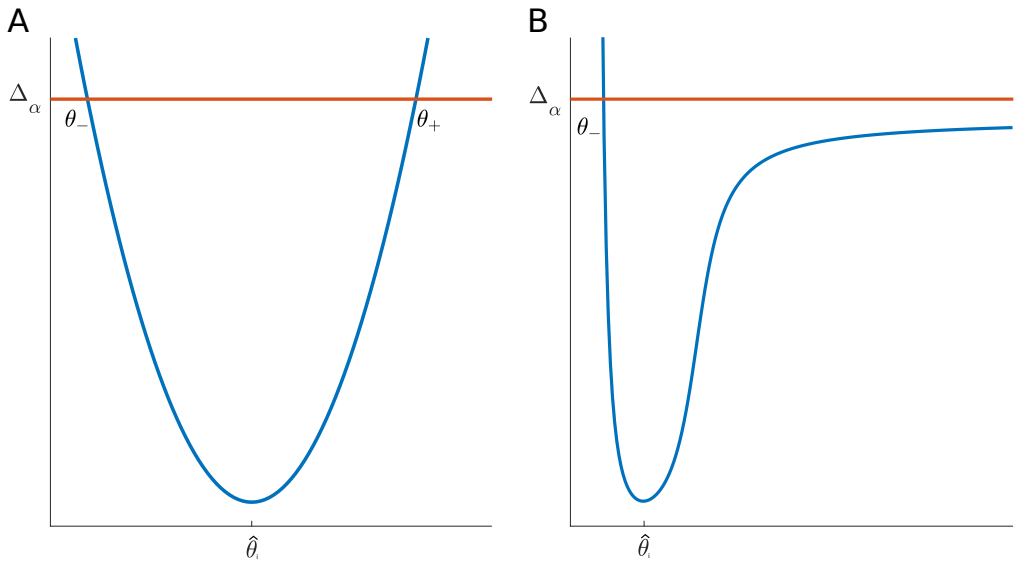

Fig. 2.3 Diagram of potential likelihood profiles. A shows an identifiable parameter $\hat{\theta}_i$ with confidence interval between θ_- and θ_+, B shows a nonidentifiable parameter since the profile only passes the threshold once.

2.3.6 Sobol sensitivity analysis

Sensitivity analysis allows for the identification and quantification of parameter influence on model output. The application of sensitivity analysis comes under four categories:

i Understanding the relationship between the input and the output

ii Determining the influence of parameter uncertainty on model variability

iii Identification of the most influential parameters

iv Guiding future experimental design

The main categories used within this thesis will be (iii) and (iv) since the number of parameters makes it impossible to understand the true relationships and parameter uncertainty has not been assessed in these models. There are two main types of sensitivity, local and global sensitivity. Local sensitivity refers to model output variations relative to single parameter changes, whereas, global sensitivity varies all the parameters simultaneously over their respective spaces and evaluates the relative contributions.

Sobol sensitivity analysis is a global sensitivity analysis method which is based on variance decomposition techniques. The Sobol method determines the contribution of each of the input parameters and their interactions to the overall model output variance. The results of the analysis are often split into first order interactions and total order interactions. First order is the fractional contribution of a single parameter on the output variance. Total order includes first order, second order and higher order effects on the output variance. The higher the interaction indices the more influential the parameter on the model output. There is no stringent value of these indices to determine what constitutes important or unimportant, although 0.05 is often used in the literature [172].

2.4 Model evaluation

2.4.1 Coefficient of determination

The coefficient of determination, often known as R^2 or R2, provides an indication of how well the observed outcomes are represented by a model [173]. There are several definitions of R^2, throughout this thesis the definition will be:

$$R^2 = 1 - \frac{\sum_i (y_i - f_i)^2}{\sum_i (y_i - \bar{y})^2} \tag{2.39}$$

where y_i refers to the data point i, $\bar{y}$ is the mean of the data points and f_i is the model output for the corresponding value of i. It can be thought of as a measure of how much better the fit of the model is relative to a straight line through the mean.

2.4.2 Sum of squared residuals

The sum of squared residuals (SSR) will also be used as a comparative measure of goodness of fit between the models within this thesis. The definition of SSR follows the same format as the least squares formula:

$$SSR = \sum_{i=1}^{n} (y_i - f_i)^2 \tag{2.40}$$

where y_i is the value of the data at point i and f_i is the value of the model corresponding to the data point i.

Chapter 3

Optimising circadian drug infusion schedules towards personalised cancer chronotherapy

3.1 Introduction

Cancer management is challenged by large inter- and intra-patient variabilities in both disease progression and response to treatments. Thus, the quest for accurate and personalised cancer therapies has fostered the development of new technologies enabling multi-type measurements in individual patients and complex drug scheduling. To translate datasets available for an individual patient into personalised therapies and further ensure their precise administration, new mathematical approaches are required. Indeed, systems medicine, that involves the implementation of theoretical approaches in medical research and practice, is critically needed as emphasised in the roadmaps of the Coordinated Action for Systems Medicine (CaSyM) from the European Union (https://www.casym.eu, [174]) and of the Avicenna action (http://avicenna-isct.org/), and in other international consortia [175, 156, 176, 177]. The final aim is a measurable improvement of patient health through systems-based practice which will enable predictive, personalised, participatory and preventive (P4) medicine [178].

Accuracy and safety of infusion pumps are mandatory to ensure that the correct drug dose is delivered to the patient over the intended period. Recurrent incidents related to devices delivering fluids such as nutrients or medications into the body have led the U.S Food and Drug Administration (FDA) to launch in 2010 an initiative to reduce infusion pump risks (https://www.fda.gov/medicaldevices/

productsandmedicalprocedures/generalhospitaldevicesandsupplies/infusionpumps/ucm202501.htm). Many of the reported events are related to deficiencies in the initial design of the device and of the embedded software. Adverse events may also arise from a defect appearing over the device's life cycle due to technical failure or lack of proper maintenance. However, due to the complexity of the equipment, user errors are also common [179].

Optimising the chemotherapeutics index, defined as the ratio between treatment antitumor efficacy and induced toxicities, is complex at multiple levels. First, large inter-patient variabilities are demonstrated in drug pharmacokinetics, tolerability and anti-tumour efficacy [175, 180, 26, 181]. Next, important intra-patient variabilities arise from the fact that a tumour and healthy tissues, rather than being static over time, display time-dependent variations, in particular over a 24h span, which are called circadian rhythms [1]. The circadian timing system controls most physiological functions of the organism resulting in drug Absorption, Distribution, Metabolism and Elimination (ADME) displaying 24h-rhythms with differences of up to several folds between minimum and maximum activities [137, 113].

Chronotherapy, that is administering drugs according to the patient's biological rhythms over 24 h, is a growing field in medicine and especially in oncology. Indeed, at least 22 clinical trials involving a total of 1773 patients with different types of metastatic cancers have demonstrated a significant influence of administration timing on the tolerability of 11 commonly-used anti-tumour drugs [182]. Two randomised phase III clinical trials in 278 metastatic colorectal cancer (mCRC) patients receiving irinotecan, oxaliplatin and 5-fluorouracil showed that cancer chronotherapy achieved an up-to-5-fold decrease in treatment side effects and nearly doubled anti-tumour efficacy compared to conventional administration of the same drug doses [112]. However, a meta-analysis of these two studies combined with another clinical trial involving 564 mCRC patients receiving the same drugs (497 men and 345 women in total) concluded that the chronomodulated drug modality significantly increased the efficacy and survival in men while reducing that in women as compared to conventional administration [136]. Such sex-specificity was further validated for irinotecan chronotoxicity in mouse experiments [3] and in a clinical trial involving 199 mCRC patients treated with oxaliplatin (infusion peak 4pm), 5-fluorouracil (infusion peak 4am) and irinotecan given at 6 different circadian times [5]. Both studies showed a higher circadian amplitude in females as compared to males and a difference of several hours between the optimal timing of each gender. Furthermore, circadian biomarker monitoring in individual patients recently revealed up to 12 h inter-patient differences regarding the timing of midsleep, the circadian maximum in skin surface temperature or that in physical activity [183]. These investigations have highlighted the need for the individualisation of drug combinations and chronoinfusion schemes to further improve treatment outcome, taking into account the patient's sex, chronotype

and genetic background. The accurate delivery of intended administration profiles is obviously critical in this context. Chronotherapy requires precise delivery with the error in drug infusion timing not to be greater than a few hours.

Clinical findings about cancer chronotherapy have motivated the development of innovative technologies for chronomodulated drug delivery including the Mélodie infusion pump (Axoncable, Montmirail, France, [6]). This portable electronic pump allows for the administration of up to 4 compounds according to pre-programmed schedules over the 24 h span. It was used in several clinical trials for the chronomodulated delivery of irinotecan (CPT11), oxaliplatin (L-OHP) and 5-fluorouracil (5-FU) into the central vein of metastatic colorectal cancer patients [113]. The Mélodie pump was recently used to infuse those three anticancer drugs directly into the hepatic artery of metastatic cancer patients in the translational European OPTILIV Study [6]. This uncommon delivery route into the hepatic artery and the use of an infusion pump to deliver the drugs according to chronomodulated profiles represent a novel chemotherapeutic approach which needs to be quantitatively investigated to maximise patient benefit. In this study, the plasma pharmacokinetics of oxaliplatin revealed inconsistencies between programmed delivery schedules and observed drug concentration within the patient blood including a delay in the time taken for the drug to be detectable in the blood and unexpected peaks in plasma concentrations during drug infusion. Such inconsistencies between targeted drug exposure patterns and plasma drug levels motivated the design of a mathematical model of fluid dynamics within the pump system presented hereafter. This pump-to-patient model was then connected to semi-physiological PK models to investigate the inter-patient variability in drug PK after hepatic artery administration. Thus, this systems pharmacology study aimed to develop predictive mathematical models allowing for the quantitative and general understanding of: i) the pump dynamics, irrespective of the drug delivery device, and ii) patient-specific whole-body PK of irinotecan, oxaliplatin and 5-fluorouracil after drug administration using an infusion pump. Such mathematical techniques would then allow for precise and personalised drug timing.

3.2 Methods

Ethics Statement

The pharmacokinetic data used in this investigation came from the Lévi et al pharmacokinetic investigation [6] and the comparison study companion study of the European OPTILIV trial (ClinicalTrials.gov study ID NCT00852228), which involved nine centres in four countries (France, Belgium, Italy and Portugal) [184]. The data have been analysed anonymously.

OPTILIV clinical datasets

The OPTILIV trial included 11 colorectal cancer patients with liver metastases (7 men and 4 women with median age of 60). The combination of irinotecan, oxaliplatin and 5-fluorouracil was delivered to patients by Hepatic Artery Infusion (HAI) using the Mélodie pump [6]. The patients received an intravenous administration of cetuximab 500 mg/m2 over 2 h 30 min on the morning of day 1 which was not modelled. From day 2, chronomodulated HAI of irinotecan (180 mg/m2), oxaliplatin (85 mg/m2) and 5-fluorouracil (2800 mg/m2) were given (Fig 3.1). Irinotecan was delivered as a 6h sinusoidal infusion starting at 02:00, with a peak at 05:00 on day 2. Oxaliplatin was administered as an 11h 30min sinusoidal infusion beginning at 10:15 with a peak at 16:00 on days 2, 3 and 4. 5-fluorouracil was also delivered as an 11h 30min sinusoidal infusion beginning at 22:15 with peak delivery at 04:00 at night, on days 3, 4 and 5. The superiority of this drug scheduling compared to non-circadian based administration was demonstrated for intravenous administration within several international clinical trials [74]. Between each drug infusion, there was a glucose serum flush which cleared the tubing. This was a 30-min sinusoidal infusion beginning at 09:45, and then again at 21:45, i.e. at the end of each infusion (Figure 3.1).

Plasma pharmacokinetic (PK) data were gathered after the first dose of irinotecan, oxaliplatin and 5-fluorouracil and measured longitudinally for each individual patient. Plasma concentrations of irinotecan and its active metabolite SN38 were determined in mg/ml at the start of infusion, then at 2, 3, 4, 6, 8 h 15 min and 31 h 45 min post HAI onset, for a total of seven time points, including baseline. Oxaliplatin concentrations were determined by measuring both platinum (Pt) plasma levels, unbound and total. Oxaliplatin binds to proteins in the blood and the free Pt fraction is the biologically active one. Thus, oxaliplatin concentrations were determined at the start time of the infusion, then at 3, 6, 9 h, 11 h 30 min and 17 h 15 min post HAI onset, for a total of six time points, including baseline. Plasma concentrations of 5-fluorouracil were determined at the start of infusion, then at approximately 3 h, 5 h 45 min, 9 h and 11 h 30 min post HAI, for a total of five time points, including baseline.

Plasma pharmacokinetic (PK) data were gathered after the first dose of irinotecan, oxaliplatin and 5-fluorouracil and measured longitudinally for each individual patient. Plasma concentrations of irinotecan and its active metabolite SN38 were determined, using high performance liquid chromotagraphy (HPLC), in mg/ml at the start of infusion, then at 2, 3, 4, 6, 8 h 15 min and 31 h 45 min post HAI onset, for a total of seven time points, including baseline. Oxaliplatin concentrations were determined by measuring platinum plasma levels using spectrophotometry, for both unbound and total platinum levels. Oxaliplatin binds to proteins in the blood and the free

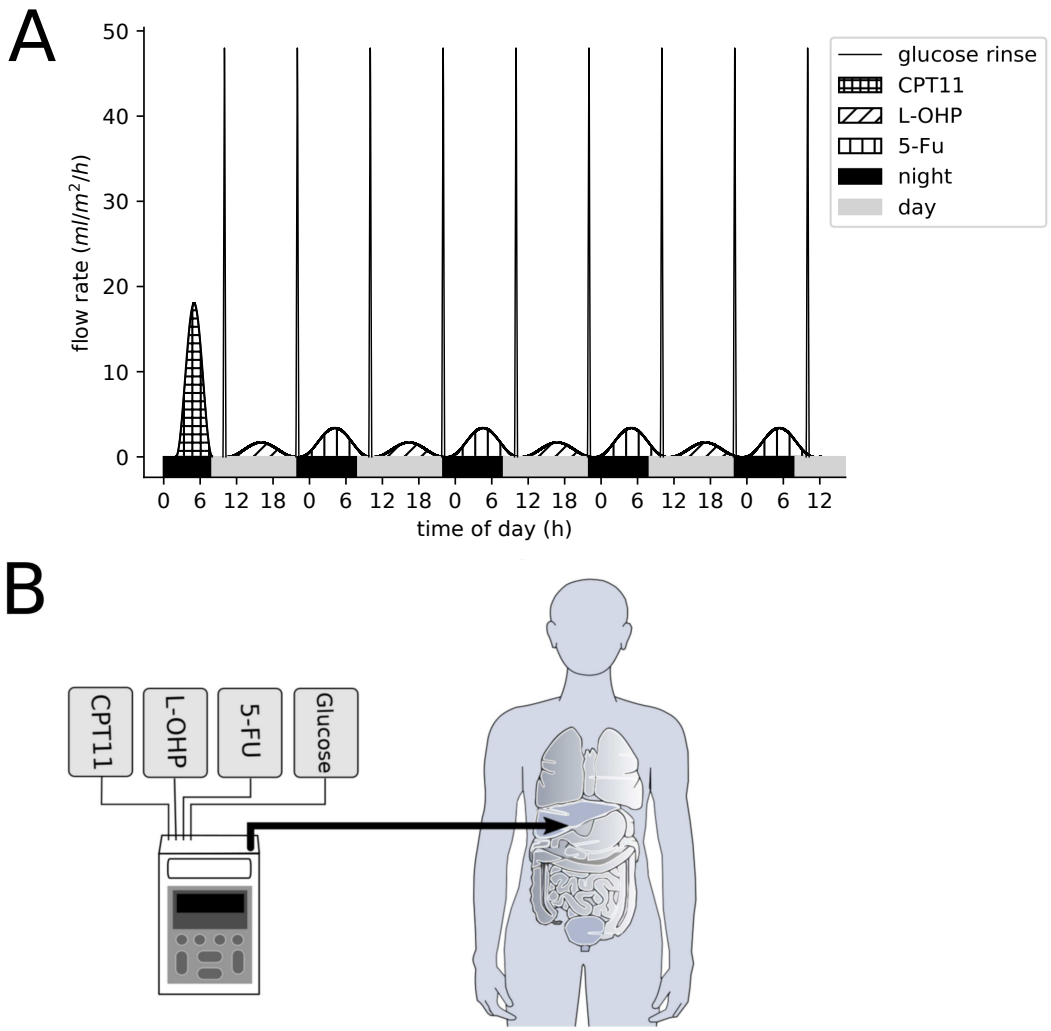

Fig. 3.1 (a) Delivery profiles of irinotecan, oxaliplatin, 5-fluorouracil and glucose flushes as administered in the OPTILIV clinical trial. (b) Schematic of the Mélodie infusion pump (Axoncable, Montmirail, France) used in the OPTILIV study for hepatic artery infusion [6].

Pt fraction is the biologically active one. Thus, oxaliplatin concentrations were determined at the start time of infusion, then at 3, 6, 9 h, 11 h 30 min and 17 h 15 min post HAI onset, for a total of six time points, including baseline. Plasma concentrations of 5-fluorouracil were determined using HPLC, at the start of infusion, then at approximately 3 h, 5 h 45 min, 9 h and 11 h 30 min post HAI, for a total of five time points, including baseline. The exact method used to assess plasma concentrations can be seen in the Levi et al paper of the OPTILIV study [6].

Pump description

The Mélodie pump system weighs 500 g when empty (excluding drug reservoirs and batteries) and measures 160 x 98 x 34 mm. The pump consists of four channels

which correspond to the four reservoirs that are connected to the pump. Each reservoir can have a maximum volume of 2 L. The four channels are controlled by four independent mechanisms which control the delivery to the infusion tube (Fig 3.1). For the OPTILIV study, the infusion tube comprised of two sections, the first was 135mm long with a diameter of 2.5mm, and the second section was 1500mm long with a diameter of 1mm. The two sections had a total volume of 1.84ml. The four pump reservoirs were loaded with irinotecan, oxaliplatin, 5-fluorouracil and 5% glucose solution respectively, with the latter used for washes in between drug infusions [185].

Mathematical modelling

A pump-to-patient mathematical model was designed as follows, irrespective of the drug delivery device. The drug solution's dynamics from the pump to the patient's blood were modelled using a Partial Differential Equation (PDE) considering time and 1 spatial dimension. This method was chosen as PDEs can take into account both time and space which was key for modelling systems such as pump delivery. The PDE was solved using a backward finite difference method written by the myself within Python 3.5.2 (https://www.python.org/). The drug PK models were based on Ordinary Differential Equations (ODEs) written in Python 3.5.2 and solved using the odeint function from the scipy library version '1.1.0' which is capable of solveing both stiff and non-stiff initial value first order ODEs such as are used in this thesis [186].

PK model parameter estimation involved a weighted least squares approach (Sec 2.3.3), with conditions also placed on the drug clearance routes. For the fit of the data of a given patient, the residuals were weighted by an estimated measurement error of 10% in line with precision values of the assay methods [187–189]. This method allowed correction of the residuals to be of the same order of magnitude for the parent drug CPT11 and the metabolite SN38, or for oxaliplatin free and bound concentrations. The minimisation of the least squares cost function was performed by the Covariance Matrix adaptation Evolution Strategy (CMAES) within Python which has been shown to be successful at handling complex cost function landscapes [166]. The fitting process was repeated 50 times for each patient with the best fit taken as final parameter values to reduce the chances of finding local minima. Parameter search ranges were chosen so the optimal value did not include the maximum of the ranges. Model goodness of fit was assessed using the sum of squared residuals (SSR) and R^2 values. PK model parameter numerical identifiability given the available data was investigated in a two-step process as follows. First, parameter sensitivity regarding the least-square cost function was computed via a global Sobol sensitivity analysis as a necessary condition for identifiability [172]. This method assesses

the relative contributions of each parameter to the variance in the cost function obtained when parameter values are varied, and thus allows for the identification of parameters which have no effect on the cost function and are therefore not identifiable from the available dataset. This step allowed a first reduction of the PK models. Next, likelihood profiles of parameters of the reduced models were derived following the procedure outlined in [170]. Additional biological constraints derived from the literature were added to ensure numerical local identifiability of all parameters. This two-step model design process was undertaken as computing likelihood profiles is associated with a high computational cost.

PK models were fitted to pooled data first to get an indication of general model fit then to single-patient plasma PK datasets independently to obtain patient-specific parameter values. Data were available for 10 to 11 patients which was too few to undertake mixed-effects population analysis and to reliably estimate the parameters' variances within a patient population [190, 191]. Sampling points at 6h post injection for irinotecan and 11h 30 mins post injection for oxaliplatin and 5-fluorouracil theoretically occurred at the same time as the start of the 30 min glucose flush, that is 9:45 for irinotecan and 5-fluorouracil, and 21:45 for oxaliplatin. As described in the results section, the flush was equivalent to the administration of the drug quantity remaining within the tube and logically influenced plasma drug concentrations. However, the exact time of patient blood collection was not reported and could vary by 10 to 15 minutes due to clinical constraints. Hence, the information of whether the blood sample was taken before or during the flush was not available. Thus, the collection time of the data points at theoretically 21:45 for oxaliplatin, 9:45 for irinotecan and 9:45 for 5-fluorouracil were unchanged if the drug concentration at the preceding data point was greater than the current one, indicating the flush might not have occurred yet. If not, the collection time was modified and set equal to the glucose peak time, which is 15min after its start time i.e. 22:00 for oxaliplatin and 10:00 for irinotecan and 5-fluorouracil, such a value leading to the best model fit. Overall, the collection time was changed compared to the theoretical one for patients 1, 2, 3 and 7 for oxaliplatin, for patient 5 for 5-fluorouracil, and for no patients for irinotecan.

Inter-patient variability and patient clustering based on PK parameters

Given the relatively small number of patients, the inter-patient variability in parameter values was assessed using a nearly unbiased estimator of coefficient of variation (CV),

$$\mathrm{CV} = \left(1 + \frac{1}{4n}\right) \times \frac{\sigma}{\mu} \times 100,$$

where μ is the parameter mean, σ the parameter sample standard deviation and n is the number of patients.

Next, fuzzy c-means clustering was used to define patient clusters based on individual PK parameters, for each drug separately. The fuzzy c-means clustering was done using a Python library sckit-fuzzy version '0.2' (http://pythonhosted.org/scikit-fuzzy/). The method is based on the determination of cluster centroids and classification of patient parameter vectors into the clusters such that the following quantity is minimised:

$$\sum_{i=1}^{n}\sum_{j=1}^{c} w_{ij}^2 \left(x_i - c_j\right)^2$$

where n is the number of patients, c is the number of clusters, x_i is the parameter vector of patient i, c_j is the centroid of cluster j, w_{ij} is the probability of patient i belonging to cluster j and can be expressed as:

$$w_{ij} = \frac{1}{\sum_{k=1}^{c} \left(\frac{x_i - c_j}{x_i - c_k}\right)^2}$$

Note that, for a given patient i, the following holds:

$$\sum_{j=1}^{c} w_{ij} = 1.$$

The validity function proposed by Fukuyama and Sugeno [192] was used to determine the number of clusters for each drug. The function is defined as:

$$V_{FS} = \sum_{i=1}^{n}\sum_{j=1}^{c} w_{ij}^2 (||x_j - c_j||^2 - ||c_j - \bar{c}||^2),$$

where $\bar{c}$ is the average of the centroids. The number of clusters was chosen between 2 and $n-1$ inclusively such that the $\mathrm{V_{FS}}$ was minimised. Plotting the clustering results was done using a multidimensional scaling (MDS) algorithm which projects multidimensional data onto a 2D plane while keeping a distance metric scaled relative to original data (Python library sklearn.manifold [193]). Correlation coefficients between the original Euclidean distance and the 2D-Euclidean distance were calculated

and were high for all models (> 0.98) which showed that the MDS projections were accurate [194].

3.3 Results

The overall objective of this study was to accurately investigate the inter-patient variability in the plasma PK of the three anticancer drugs administered during the OPTILIV trial. A first strategy consisted in using compartmental PK modelling taking the delivery profiles programmed into the infusion pump as inputs for the plasma compartments. However, such methodology revealed inconsistencies between the best-fit models and the data, including delays of several hours. I then concluded that the fluid dynamics from the pump to the patient had to be quantitatively modelled. Hence, I designed the complete model in two sequential mathematical studies. First, I studied the drug solution dynamics from the pump to the patient's blood for which the model was based on partial differential equations. This novel model of the pump delivery system took into account the specificity of the equipment used in order to accurately predict drug delivery in the patient's blood, although it could be easily adapted to any similar drug delivery device. Second, I connected this model to compartmental PK models based on ordinary differential equations. This complete framework allowed the investigation of inter-patient variability in drug PK after hepatic artery administration.

Pump-to-patient drug solution dynamics

Model design

The pump-to-patient model is a transport equation representing the dynamics of the drug solution along the administration tube, with respect to time (t) and one-dimensional space (x)(equation 3.1). This simplification neglects possible non-linear wave fronts across the diameter of the tube, however since the diameter is very small the effect of this would be negligible on the overall infusion profile. x is the distance along the tube from the pump ($x = 0$) to the patient ($x = L$). The drug solution was assumed to be incompressible so that the fluid velocity was considered as constant along the whole tube. Thus, the drug concentration in the tube $u(x, t)$ changes with respect to the following equation:

$$\frac{\partial u(x,t)}{\partial t} = -V(t)\frac{\partial u(x,t)}{\partial x} \qquad t \in [0, T], \quad x \in [0, L] \tag{3.1}$$

with a Dirichlet boundary condition of,

$$u(0,t) = \frac{S(t)}{sa \times V(t)}, \tag{3.2}$$

where $V(t)$ is the fluid velocity inside the tube, expressed in mm/h. The constant $sa = \pi r^2$ is the cross sectional surface area of the tube (in m^2), with r being the radius of the tube. The source term $S(t)$ represents the amount of drug delivered according to the infusion profile programmed into the pump and is expressed in mol/h. Initial conditions along the tube are $u(x,0) = 0$. The fluid velocity and source terms are controlled by the pump which imposes a fluid delivery rate expressed in ml/h. They are computed by converting the fluid delivery rate into mm/h and mol/h respectively using the tube geometry and the concentration of each drug solution. Hence, model simulations at the end of the tube ($x = L$) do not depend on the exact geometry of the tube but rather on its total volume. The input function for PK models depending only on quantities at the end of the tube, the original infusion tube which was constituted of two sections of different diameters was simplified in numerical simulations to a tube of radius 1mm and total length 2340mm that had the same total volume as the original set-up. The total tube volume was set to 1.84 mL for in the equipment used in the OPTILIV study. The transport equation with associated initial and boundary conditions can be solved using the classical method of characteristics [195] which gives:

$$u(t,x) = \begin{cases} 0 \quad \text{if} \quad \int_0^t V(r)dr < x \\ \frac{S(\tau(t,x))}{sa \times V(\tau(t,x))} \text{ otherwise} \end{cases},$$

where $\tau(x,t)$ is the time at which the drug reaching point x at time t initially entered the system, i.e.

$$\int_{\tau(t,x)}^{t} V(s)ds = x.$$

The input function for the PK models corresponds to the rate of drug infusion into the patient (i.e. at $x = L$) and can be obtained by:

$$d(t) = sa \times V(t)u(t,L) = \begin{cases} 0 \quad \text{for} \quad t \quad \text{such that} \quad \int_0^t V(r)dr < L \\ V(t)\frac{S(\tau_L(t,L))}{V(\tau_L(t,L))} \quad \text{otherwise, with } \int_{\tau(t,L)}^{t} V(s)ds = L \end{cases}$$

Note that, for all drug infusions apart from the glucose flushes, the source term $S(t)$ is proportional to the fluid velocity $V(t)$ as the drug is infused within the tube

at the same time as the fluid, so that $d(t)$ is proportional to $V(t)$ once the tube is filled, i.e. for times t such that $\int_0^t V(r)dr > L$. An example of the PDE model simulations in time and space for oxaliplatin delivery is shown in Fig 3.2 A.

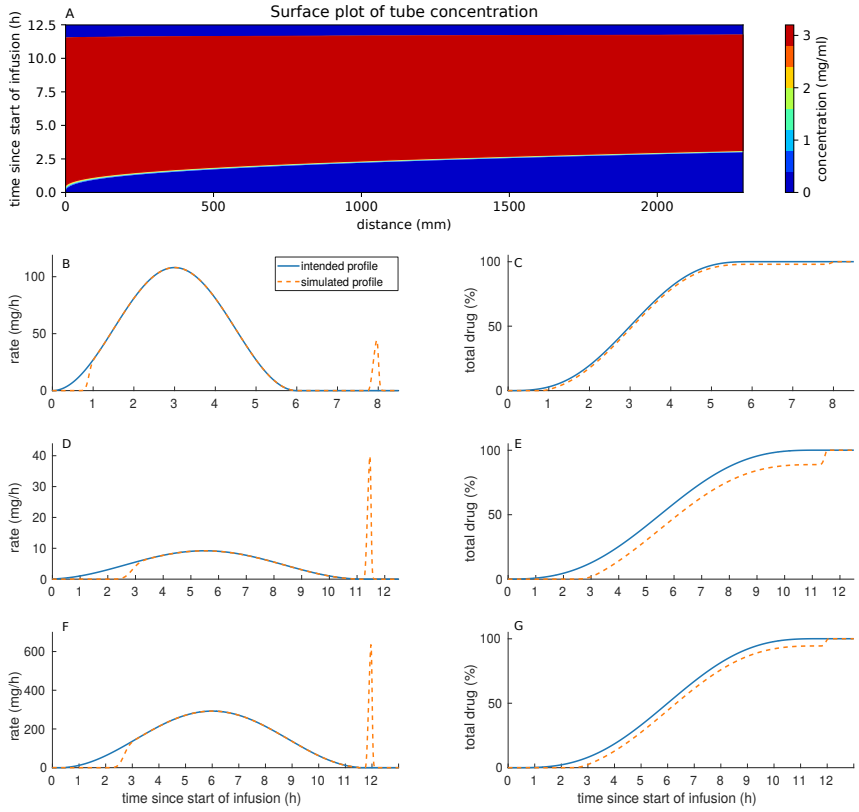

Fig. 3.2 (A) shows oxaliplatin concentration profile in the infusion tube. The x-axis represents the distance along the tube, the y-axis represents the time from the start of the pump delivery. For figures (B-G), the x-axis represents Clock time and starts at the beginning of the considered drug administration. The left column shows the both the intended delivery profiles and the simulated delivery profiles evaluated at the end of the tube (x=L), for irinotecan (B), oxaliplatin (D) and 5-fluorouracil (F). The right-hand column shows the cumulative percentage of drug delivered to the patient for the intended and actual profiles over time for irinotecan (C), oxaliplatin (E) and 5-fluorouracil (G). The initial delay between the intended and simulated profile is due to filling of the tubing. The spike at the end of the delivery is due to the glucose flush emptying the drug left in the tube in a short space of time. Dose was calculated using the surface area of a person as being 1.7m^2, representing an "average" person. For patient based simulations each patient's own surface area is used.

Differences between programmed infusion profiles and actual drug delivery in the patient's blood

The pump infusion schemes used in the OPTILIV trial were simulated for the three drugs: irinotecan, oxaliplatin and 5-fluorouracil. Whereas the drug profiles

programmed into the pump followed a smooth sinusoidal function, the actual drug delivery in the patient artery differed from the programmed profiles by two main features. First, the model predicted a significant time delay between the actual start of the drug delivery by the pump and the time the drug first reached the patient blood (Fig 3.2 B, D, F). This delay was evaluated by the model to be 3 h 5 min for oxaliplatin, 2 h 20 min for 5-fluorouracil and 51 min for irinotecan. The cause of this delay is due to the time taken to fill the infusion tube with the solution containing the drug at the beginning of the infusion. The delay was drug-specific as it depended on the drug solution concentration and the velocity of the solution in the tube driven by the programmed input profiles. Next, at the end of the infusion profiles, the pump stopped and did not administer the amount of drug left inside the tube. This remaining drug was flushed out by the glucose rinse subsequent to drug administration which induced a sudden delivery spike in the patient's artery (Fig 3.2 C, E, G). The amount of drug in this spike was expressed as a percentage of the total drug delivered and was estimated to be 10.7% for oxaliplatin, 5.36% for 5-fluorouracil and 1.85% for irinotecan.

Drug	Total dose (mg/m^2)	Drug solution concentration (mg/ml)	Main peak rate ($ml/m^2/h$)	Spike peak rate ($ml/m^2/h$)
CPT11	180	3.33	18.02	7.38
LOHP	28	3	1.63	7.28
5-FU	933	50	3.4	6.96

Table 3.1 Table describing the defining delivery values for CPT11, LOHP and 5-FU. Dose is given in mg per surface area of the patient (m^2). The main peak refers to the maximum flow rate from the intended delivery schedule. The spike peak rate refers to the maximum flow rate of the delivery caused by the glucose flush.

Our systems approach revealed important differences between the intended drug infusion profile and the actual administration into the patient artery. Hence, I developed optimised infusion profiles that strictly achieved the drug administration intended by clinicians. The same equipment was considered to avoid the cost of changing. Drug concentrations of the infusion solutions were kept unchanged in order to avoid possible problems of drug stability. In order to administer the drug in to the patient's blood following a smooth sinusoidal function, a profile in three parts is required as follows (Fig 3.3). The first part of the profile is an initial bolus to fill the tube between the pump and the patient with the drug solution. Once the tube is filled, the original sinusoidal profile starts. Then, to solve the problem of the amount of drug left in the tube when the pump stops, the original sinusoidal profile needs to be interrupted when the total drug amount has left the drug bag. Then, a

subsequent glucose rinse needs to be infused according to the final segment of the sinusoidal curve in order to deliver the drug remaining in the tube at the correct rate.

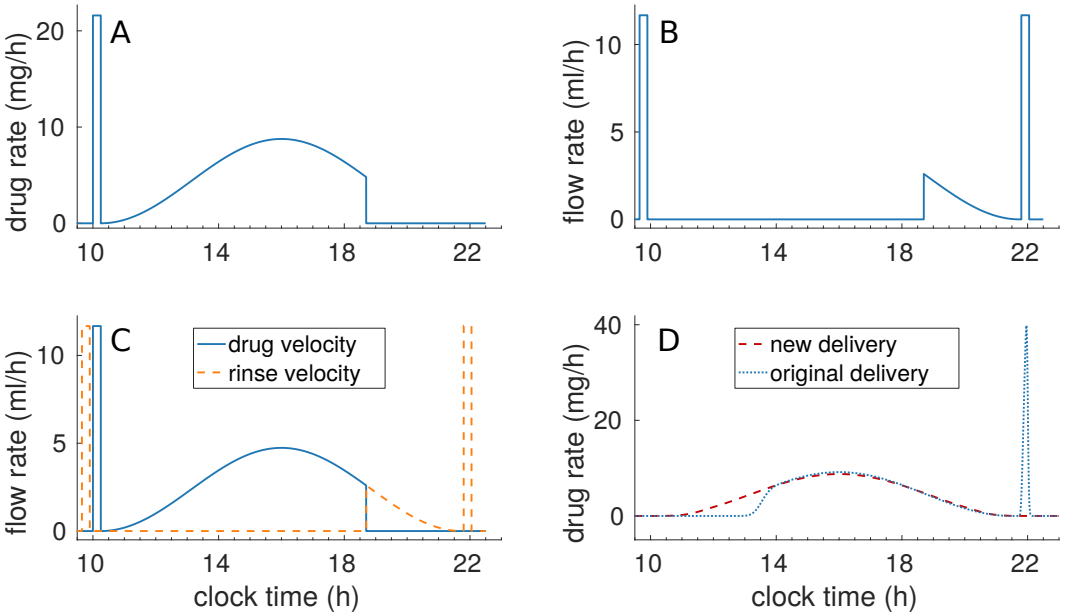

Fig. 3.3 Improved administration profiles. (a) shows the drug solution delivery profile which consists of an initial bolus to fill the tube entirely, followed by the original profile. (b) shows the rinse solution delivery rate which continues drug delivery at the correct rate while clearing the tube from any active substance, (c) shows how the flow rate along the tube is smoothly switched between the drug and the rinse and (d) shows the new drug delivery profile that will enter the patient compared to the original profile used in the OPTILIV study.

3.3.1 Inter-patient variabilities in irinotecan, 5-fluorouracil and oxaliplatin PK after chronomodulated administration

The pump-to-patient model provided educated predictions of the drug infusion into the patients' blood, which was a prerequisite to study the inter-patient variability in the PK of irinotecan, oxaliplatin and 5-fluorouracil. A compartmental physiological model was designed for each drug separately, since interactions between CPT11 and LOHP, and between LOHP and 5-FU have not been demonstrated [39, 40] and CPT11 and 5-FU also showed no interaction if CPT11 is delivered first as it is in this study [41]. All parameters were fitted for each patient independently.

Compartmental models of irinotecan, oxaliplatin and 5-fluorouracil pharmacokinetics

PK models represented the drug fate in: the Liver, to accurately represent hepatic delivery, the Blood, the measurement site, and the rest of the body known throughout this chapter as Organs. The volume of each compartment was individualised for each patient using the Vauthey method for Liver [9], Nadler's formula for Blood [10], and the Sendroy method for Organs [11]. For each formula below w is the weight of an individual patient and h is the height of the patient. Vauthey method for liver volume(V_l):

$$V_l = 191.80 + 18.51 * w$$

Nadler's formula for blood volume (V_b):

$$\text{Males} : V_b = 0.3669 * h^3 + 0.03219 * w + 0.6041 \tag{3.3}$$

$$\text{Females} : V_b = 0.3561 * h^3 + 0.03308 * w + 0.1833 \tag{3.4}$$

Sendroys formula for total body volume (V_t)

$$V_t = 50.6 * SA * (w/h)^{0.426} \tag{3.5}$$

where SA is surface area of the body, this was given for each patient in this study. This is then used to calculate organ volume by:

$$V_o = V_t - V_l - V_b \tag{3.6}$$

Each model assumed that the drug was delivered directly into the liver compartment to represent the Hepatic Artery Infusion (HAI, Fig 3.7, 3.8 & 3.9). All transports in between compartments were considered as passive and were represented by linear terms. Throughout this chapter, the terms Blood-Liver or Blood-Organ transport represent a bidirectional transport that encompasses the transfer across the blood vessel walls into/from tissues. This simplification has been adopted due to lack of data on the transport processes between compartments. In the models, the drug clearance terms accounted for all types of drug metabolism which were not explicitly modelled (e.g. hepatic CYP450 activity) and i) renal elimination for the Blood compartment, ii) intestinal elimination for the Organs compartment and iii) biliary excretion for the Liver compartment only for irinotecan and 5-fluorouracil since it could be neglected for oxaliplatin [60, 196, 86]. The Organs compartment did not include the intestinal lumen and only accounted for the intestinal cells composing the wall of the intestine which were exposed to the drug through blood circulation.

Patient	Volumes (ml)		
	Liver	Blood	Organs
1	1539	4737	65289
2	1236	3461	53139
3	1224	3658	50614
4	1798	4819	77765
5	1462	4636	61303
6	1690	5327	70900
7	1872	5832	78914
8	1537	4861	64437
9	1208	3517	51124
10	1618	4990	68479
11	1619	5238	67249

Table 3.2 Table of patient compartment volumes as determined by the Vauthey method for liver volume[9], Nadler's formula for blood volume [10]. Total volume was determined via the Sendroy method [11] then the blood and liver volumes were subtracted to give organ volumes.

The intestinal cells may expel the drug toward the lumen or transform the drug through metabolism, both phenomena being represented by the intestinal clearance in the models. The drug excreted through the bile directly reached the intestinal lumen - which was not considered as part of the Organs compartment- and the drug recirculation was neglected as no evidence has been found for any of the drugs when delivered intravenously [197, 198, 60] and the PK profiles did not show the multiple peaks associated with recirculation [199]. In the absence of quantitative data and to avoid model over-parametrisation, circadian rhythms were neglected in the PK models and all parameters were assumed to be constant over the 8h time window of PK measurements. Any chemical species bound either to plasma proteins or to DNA was assumed to be unable to move between compartments or to be cleared from the system.

Parameter identifiability assessed though sensitivity analysis to cost function variations revealed poor sensitivity of the clearance rate constant in the Organs compartment for the three drugs (see Methods). Hence, Organ clearance was neglected for 5-fluorouracil which is mainly cleared through hepatic metabolism, biliary excretion and renal elimination [86]. Organs clearance and liver clearance was neglected for oxaliplatin since majority of platinum is cleared via renal clearance and the total amount cleared after the end of treatment was set to 54% in line with the literature [60]. Irinotecan organ clearance was assumed to be scaled relative to that of the Liver compartment, this is since similar amounts of irinotecan are cleared via faecal clearance and biliary clearance [196]. In the model of 5-fluorouracil, poor sensitivity was also obtained for transport parameters between Blood and Organs.

Hence, transport rate constants were assumed to be proportional to compartment volumes for Blood-Liver and Blood-Organs transport, for each of the three drugs, thus neglecting organ-specific transporter expression.

Parameter likelihood profiles analysis revealed that additional constraints were needed to ensure the local identifiability of all parameters (see Methods and SI). Hence, information on renal, intestinal and hepatic clearance relative rates was inferred from literature as follows. For irinotecan, CPT11 drug amount though renal clearance and though combined intestinal elimination and biliary clearance were respectively set to 25% and 60% of the total administered dose [196]. As SN38, which is the active metabolite of CPT11, renal elimination was documented as negligible, the metabolite was considered to only be cleared through the Liver, via metabolism into SN38, or Organs and these cleared amounts were assumed to account for 15% of the total administered dose of irinotecan [196]. The amount of SN38 cleared via metabolism in the liver accounted for approximately 4% of the total administered does of irinotecan where as SN38 excretion into the intestinal lumen accounted for approximately 9% of the total dose of irinotecan therefore I have set the SN38 clearance via organs to be twice that of the liver clearance [196]. Oxaliplatin clearance was set such that 54% of the total administered drug amount was cleared via the kidneys [60]. The amount of platinum (Pt) bound within the Organs or within the Liver was set to 84% and 12% of the total dose, respectively [2]. The Boughattas et al paper [2] was used to give tissue concentrations, no data to our knowledge exists for humans so I have used these mouse data as a best approximation. The amount of platinum in the tissues was calculated from total amount found in the respective organs relative to total dose. 5-FU was shown to be mainly cleared through hepatic metabolism, so that the amount of drug cleared through the Liver was assumed to account for approximately 80% of the total dose [86]. With the addition of these constraints the models were all shown to be identifable.

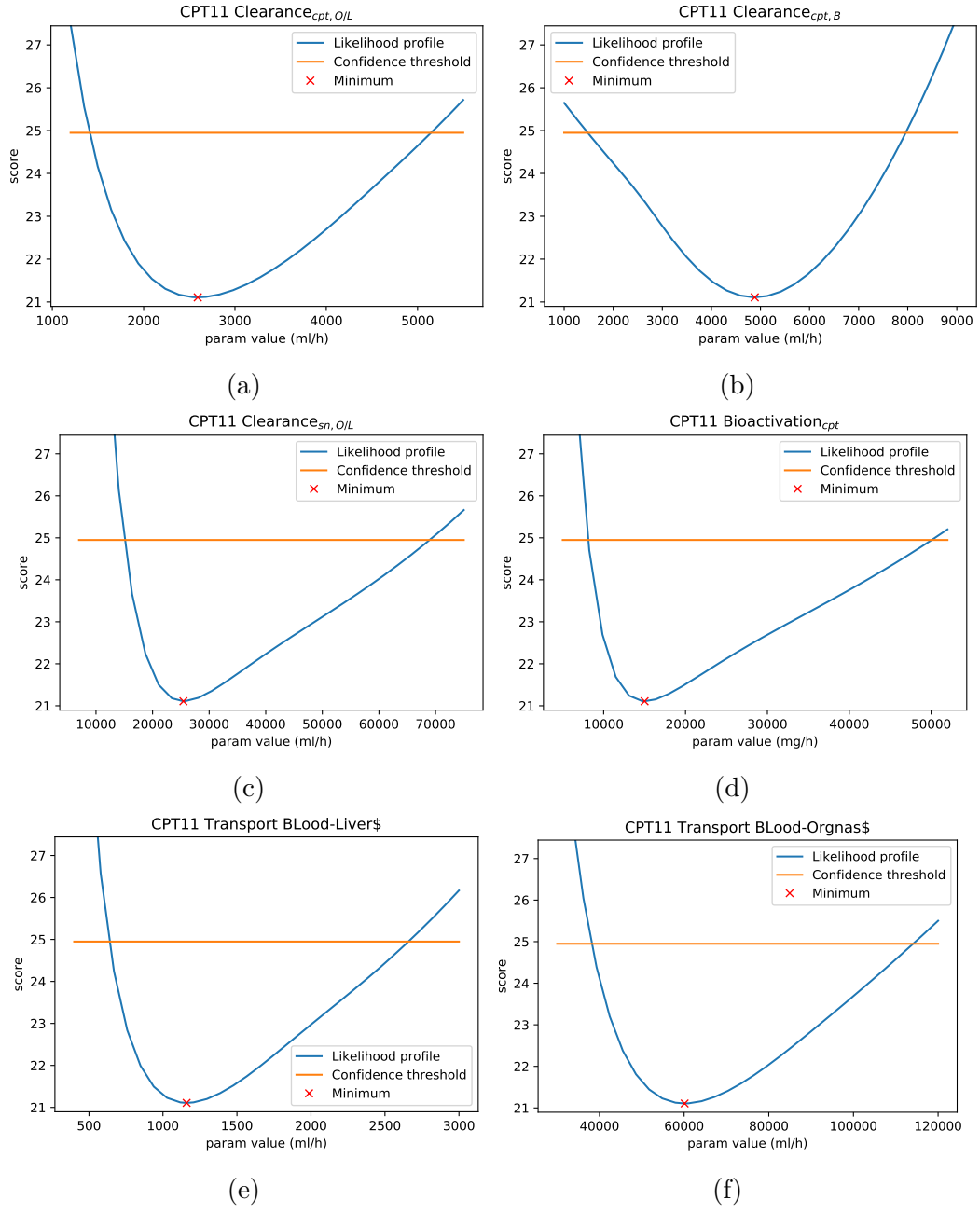

Fig. 3.4 Parameter Identifiability for irinotecan PK model.

The final irinotecan model had six compartments as each of the three Liver, Blood and Organs compartments, had two sub-compartments: the parent drug irinotecan, and its active metabolite SN38 (Fig. 3.7). Initial irinotecan administered in the liver was assumed to be only in the form of the parent drug. Irinotecan was converted into SN38 via Michaelis Menten kinetics within the liver and organs, since this is an enzymatic reaction [200], but not in the Blood since the activation enzymes carboxylesterases are not expressed in blood cells in humans [201]. The parameter estimate $K_m = 59.2\mu M$ which reflects the affinity of the substrate and the enzyme

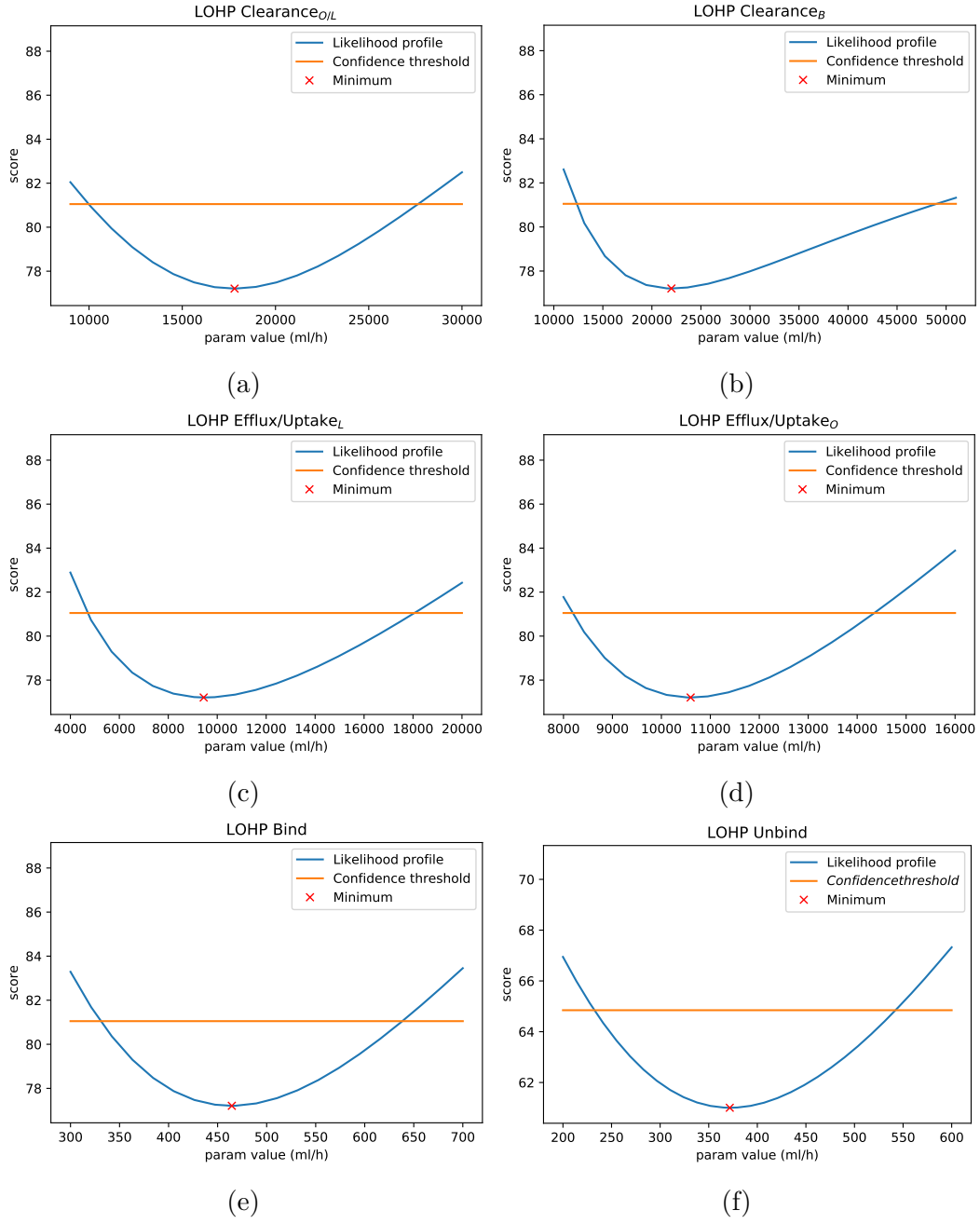

Fig. 3.5 Parameter Identifiability for oxaliplatin PK model.

was taken directly from an in vitro study in human liver cells [200], thus making the assumption that K_m values are unchanged from in vitro to in vivo as classically done in the literature [202, 203]. SN38 was considered to only be present in its bound form since the bound fraction is reported to be greater than 95% [204]. SN38 clearance terms accounted for SN38 elimination including its deactivation into SN38G though UDP-glycosyltransferases (UGTs) [74].

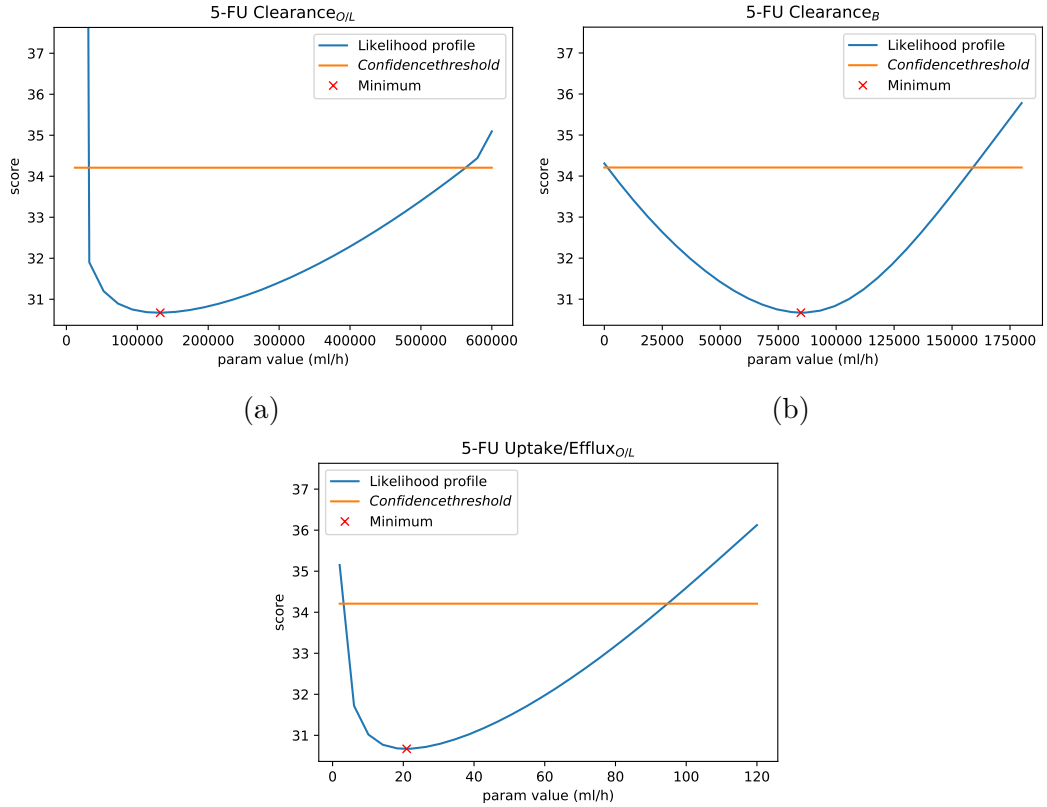

Fig. 3.6 Parameter Identifiability for 5-fluorouracil PK model.

The model equations for irinotecan are:

$$\frac{dL_{cpt}}{dt} = (d(t) - C_{cpt_{l/o}} * L_{cpt} - k_{b,l} * L_{cpt} + k_{b,l} * B_{cpt} - (V_{max}cp * L_{cpt})/(K_m + L_{cpt}))/V_l \tag{3.7}$$

$$\frac{dL_{sn}}{dt} = (-C_{sn_l} * L_{sn} - k_{b,l} * L_{sn} + k_{b,l} * B_{sn} + 0.67 * (V_{max}cp * L_{cpt})/(K_m + L_{cpt}))/V_l \tag{3.8}$$

$$\frac{dB_{cpt}}{dt} = (k_{b,l} * L_{cpt} - k_{b,l} * B_{cpt} + k_{b,o} * O_{cpt} - k_{b,o} * B_{cpt} - C_{cpt_b} * B_{cpt})/V_b \tag{3.9}$$

$$\frac{dB_{sn}}{dt} = (k_{b,l} * L_{sn} - k_{b,l} * B_{sn} + k_{b,o} * O_{sn} - k_{b,o} * B_{sn})/V_b \tag{3.10}$$

$$\frac{dO_{cpt}}{dt} = (k_{b,o} * B_{cpt} - k_{b,o} * O_{cpt} - C_{cpt_{l/o}} * O_{cpt} - (V_{max}cp * O_{cpt})/(K_m + O_{cpt}))/V_o \tag{3.11}$$

$$\frac{dO_{sn}}{dt} = (k_{b,o} * B_{sn} - k_{b,o} * O_{sn} - C_{sn_o} * O_{sn} + 0.67(V_{max}cp * O_{cpt})/(Kcp + O_{cpt}))/V_o \tag{3.12}$$

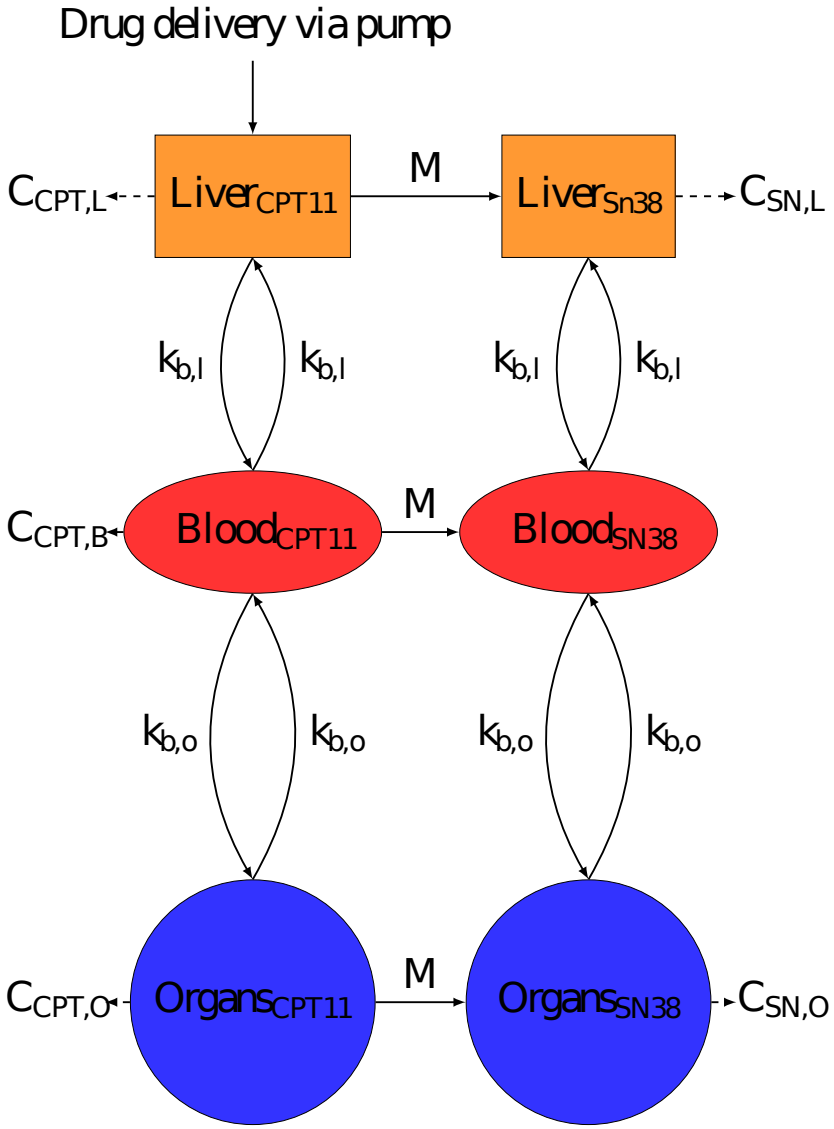

Fig. 3.7 Semi-physiological model of irinotecan PK. Compartments were minimised to the most important components, Liver to accurately represent drug delivery, Blood which is the measurement site and Organs to represent the rest of the body. C_i is the rate constant of clearance from compartment i. Irinotecan is bio-activated into its active metabolite SN38. Irinotecan was assumed to be delivered directly into the liver since hepatic arterial infusion was used.

where L_i, B_i and O_i represent the concentration in the Liver, Blood and Organs respectively, with *cpt* representing CPT11, and *sn* standing for SN38. $d(t)$ refers to the drug infusion function equal to the explicit solution of the PDE-based pump-to-patient model. The parameter values all included relevant compartment volumes, which means V_{max} is in terms of ml/h rather than the standard $mg/ml/h$. The weight conversion factor 0.67 in equation (3.4) and (3.8) is to account for the difference in molecular weight of SN38 compared to CPT11. Initial conditions were that all compartments had zero drug in them since this was the first dose in the course of

treatment.

$$x_0 = (L_{cpt_0}, L_{sn_0}, B_{cpt_0}, B_{sn_0}, O_{cpt_0}, O_{sn_0}) = \bar{0} \tag{3.13}$$

Model observations came from blood compartment for both CPT11 and SN38 separately.

$$B_{cpt}(T), B_{sn}(T) \tag{3.14}$$

where T is vector of times (h)

$$T = [0, 2, 3, 4, 6, 8.25, 31.75] \tag{3.15}$$

All parameters are in terms of ml/h.

The oxaliplatin PK model had six compartments corresponding to bound and free (Pt) molecules in the Liver, Blood and other Organs. Oxaliplatin is rapidly metabolised into platinum complex forms [60], which were not distinguished in the current data. In the absences of any data on the dynamics of these different metabolites they were all assumed to have the same PK properties in the model. Initial oxaliplatin administered in the liver was assumed to be free. Free Pt could bind to proteins and unbind from proteins, due to protein degradation [60], which was included in all compartments (Fig 3.8).

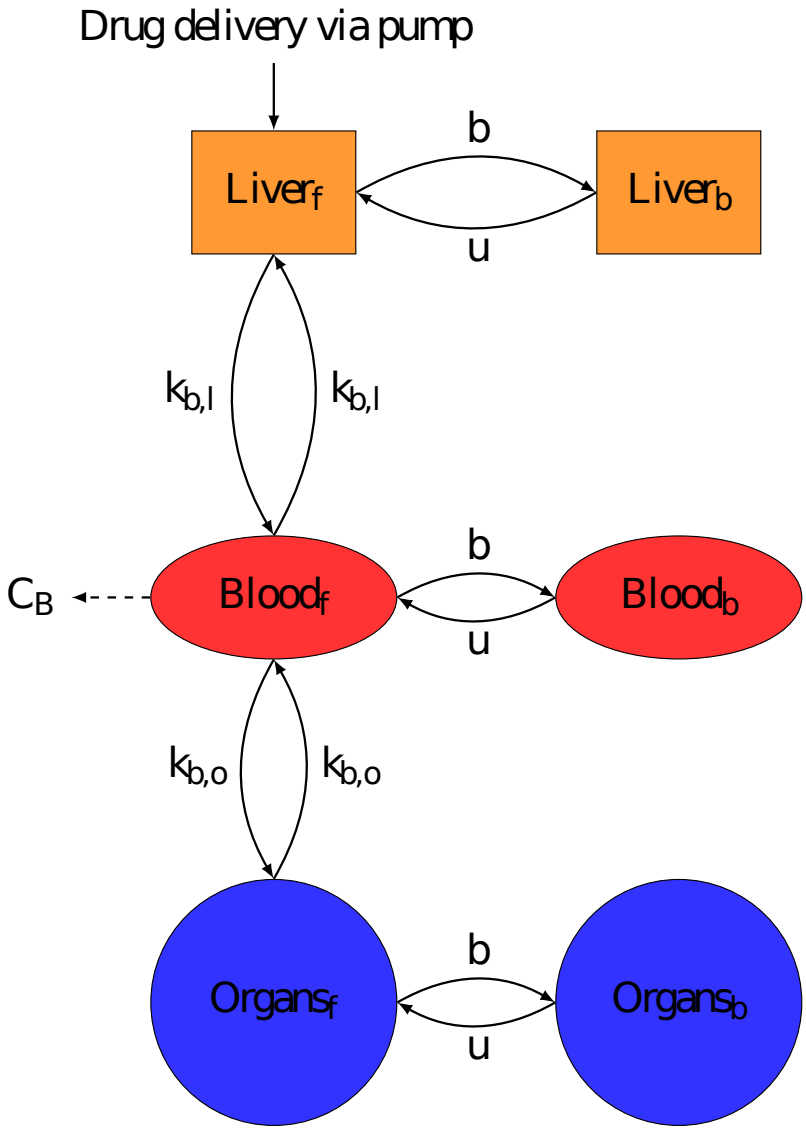

Fig. 3.8 Semi-physiological model of oxaliplatin PK. Compartments were minimised to the most important components, Liver to accurately represent drug delivery, Blood which is the measurement site and Organs to represent the rest of the body. C_i is the rate constant of clearance from compartment i. Each compartment contains a bound and unbound drug fraction and only unbound molecules can migrate between compartments. b and u are respectively the binding and unbinding rate constants of platinum to proteins. Oxaliplatin was assumed to be delivered directly into the liver in its unbound form.

The equations for oxaliplatin PK model are:

$$\frac{dL_f}{dt} = (d(t) - k_{b,l} * L_f + k_{b,l} * B_f - b * L_f + u * L_b)/V_l \tag{3.16}$$

$$\frac{dL_b}{dt} = (b * L_f - u * L_b)/V_l \tag{3.17}$$

$$\frac{dB_f}{dt} = (k_{b,l} * L_f + k_{b,l} * O_f - k_{b,o} * B_f - k_{b,o} * B_f - C_b * B_f - b * B_f + u * B_b)/V_b \tag{3.18}$$

$$\frac{dB_b}{dt} = (b * B_f - u * B_b)/V_b \tag{3.19}$$

$$\frac{dO_f}{dt} = (k_{b,o} * B_f - k_{b,o} * O_f - b * O_f + u * O_b)/V_o \tag{3.20}$$

$$\frac{dO_b}{dt} = (b * O_f - u * O_b)/V_o \tag{3.21}$$

where L_i, B_i and O_i represent the concentration in the Liver, Blood and Organs respectively, with i representing either the the bound drug b or the free drug f and $d(t)$ refers to the infusion function. The parameter values all included relevant compartment volumes. Initial conditions were that all compartments had zero drug in them since this was the first dose in the course of treatment.

$$x_0 = (L_{f_0}, L_{b_0}, B_{f_0}, B_{b_0}, O_{f_0}, O_{b_0}) = \bar{0} \tag{3.22}$$

Model observations came form the blood compartment for total platinum, i.e. sum of both free and bound, and free compartment.

$$B_{Tot}(T) = B_f(T) + B_b(T), B_f(T) \tag{3.23}$$

where T is vector of times (h)

$$T = [0, 3, 5.75, 9, 11.5] \tag{3.24}$$

All parameters are in terms of ml/h.

The final model for 5-fluorouracil had three compartments. The drug clearance accounted for both drug elimination and drug metabolism in each compartment (Fig 3.9). Protein binding of 5-fluorouracil was neglected in the model because of the low protein affinity of this drug [205]. Equations for the three models can be seen in SI.

The equations for 5-fluorouracil PK model are:

$$\frac{dL}{dt} = (d(t) - C_l * L - k_{b,l/o} * L + k_{b,l/o} * B)/V_l \tag{3.25}$$

$$\frac{dB}{dt} = (k_{b,l/o} * L + k_{b,l/o} * O - k_{b,l/o} * B - k_{b,l/o} * B - C_b * B)/V_b \tag{3.26}$$

$$\frac{dO}{dt} = (k_{b,l/o} * B - k_{b,l/o} * O)/V_o \tag{3.27}$$

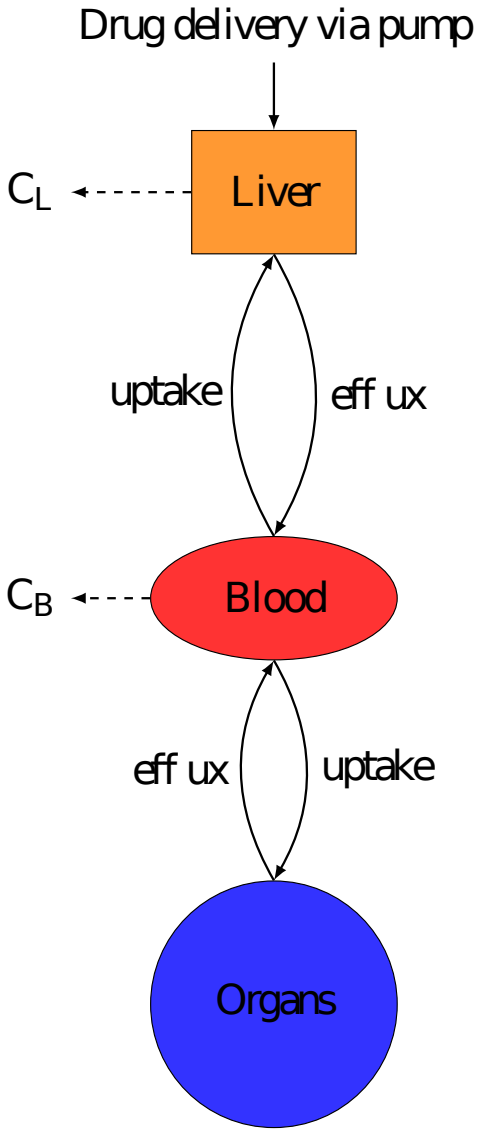

Fig. 3.9 Semi-physiological model of 5-fluorouracil PK. Compartments were minimised to the most important components, Liver to accurately represent drug delivery, Blood which is the measurement site and Organs to represent the rest of the body. C_i is the rate constant of clearance from compartment i. 5-fluorouracil was assumed to be delivered directly into the liver.

where L_i, B_i and O_i represent the concentrations of 5-fluorouracil in the Liver, Blood and Organs respectively and $d(t)$ refers to the infusion function. The parameter values all included relevant compartment volumes. Initial conditions were that all compartments had zero drug in them since this was the first dose in the course of treatment.

$$x_0 = (L_0, B_0, O_0) = \bar{0} \tag{3.28}$$

Model observations came from the blood compartment.

$$B(T) \tag{3.29}$$

where T is vector of times (h)

$$T = [0, 3, 6, 9, 11.5, 17.25] \tag{3.30}$$

All parameters are in terms of ml/h.

Inter-patient variability in irinotecan, oxaliplatin and 5-fluorouracil PK parameters.

Overall, each of the three drug models showed a very good fit to data as demonstrated by R^2 values averaged over all patients of 0.98 for irinotecan, 0.96 for oxaliplatin and 0.8 for 5-fluorouracil (Figs 1, 2 and 3 and table 4, 7 and 10 in SI). The results obtained using infusion rates computed through the pump-to-patient model were compared with simulations with infusion rates equal to the profiles programmed into the pump (see SI). Using the pump-to-patient model allowed an improvement of the model fit to pooled data for each drug (see SI) and the model fit to patient specific data for SSR values by an average of 4.9% for irinotecan, 43.4% for oxaliplatin and 12.5% for 5-fluorouracil, thus proving a measure of validity for our approach.

The irinotecan model had an almost perfect fit, it matched the linear increase of AUC compared to dose as described in the FDA drug label (SI Fig. 2) [206], and showed a rapid accumulation of both irinotecan and SN38 in the plasma of patients (Fig 3.10).

To test the validity of the PDE-based pump-to-patient model, I compared the goodness of this fit with that of the PK model with drug infusion rate equal to the infusion profile programmed in to the pump. Using the PDE to account for the properties of the system largely increased the model validity (Table 3.4, 3.5). The model was also fitted to the total data for one parameter set and then compared between using the intended delivery and the PDE derived delivery profile, this showed and increase quality of fit form a SSR of 7912.50 to 7828.28 and a R^2 of 0.89 to 0.92, which is an improvement of 1.1% for SSR and 3.4% for R^2. Pooled data agree with the improved fit our PDE model as the drug input but showed a worse fit to data.

No obvious impact on irinotecan and SN38 plasma concentrations was observed regarding the time needed to fill the infusion tube or the 30-min glucose delivery spike, as predicted by the pump-to-patient model.

The fit for the oxaliplatin PK model captured all general trends (Fig 3.11). The model fit for patient 7 did not fully capture the dynamics of total Pt plasma concentration but correctly simulated free Pt concentration. The model did predict i) a delay in plasma Pt concentrations at the start of the infusion due to the pump-to-

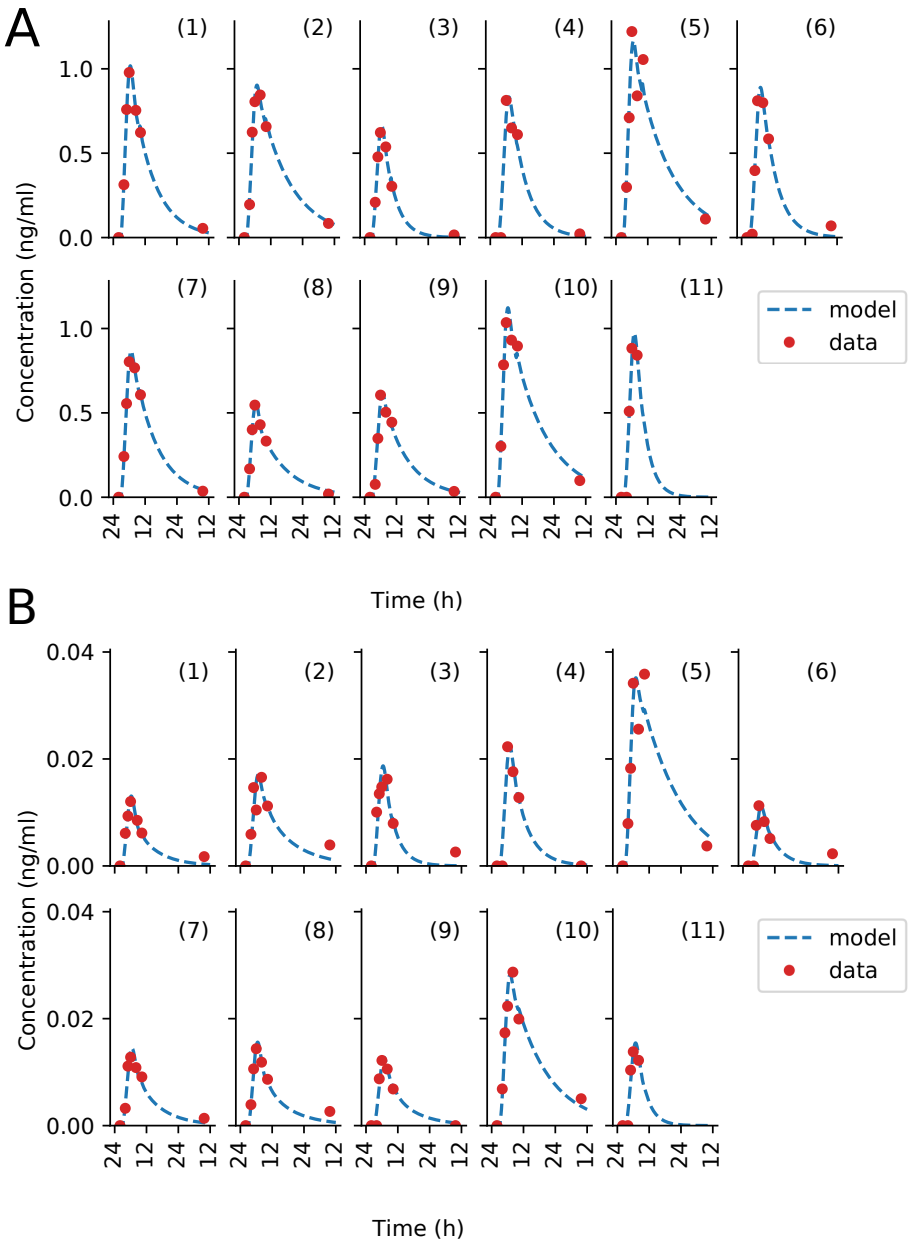

Fig. 3.10 Patient data best-fit of irinotecan PK model. Each subplot represents an individual patient dataset, fit to the model independently. (a) shows the fit of irinotecan plasma concentration, (b) shows that of SN38, the active metabolite of irinotecan.

patient drug transport and ii) a spike during the glucose flush for all patients. This drug spike had an effect on the time of maximum concentration tmax of the free Pt by shifting the time by up to 6 h. The model underestimated the free platinum peak concentrations after the glucose flush for the patients with the most significant rise in concentration, that are patients 2, 3 and 7.

To test the validity of the PDE-based pump-to-patient model, I compared the goodness of this fit with that of the PK model with drug infusion rate equal to the

Patient	Parameter Values					
	$C_{cpt_{l/o}}$ (ml/h)	C_{cpt_b} (ml/h)	C_{sn_l}& $C_{sn_o}/2$ (ml/h)	V_{max} (ml/h)	$k_{b,l}$ (ml/h)	$k_{b,o}$ (ml/h)
1	2.592e3	4.883e3	2.545e4	1.500e4	1.159e3	6.012e4
2	1.874e3	2.233e3	9.471e3	8.322e3	5.982e2	6.369e4
3	4.276e3	6.879e3	1.558e4	1.935e4	1.208e3	1.092e5
4	4.138e3	6.715e3	2.873e4	4.276e4	2.172e3	1.138e8
5	3.812e3	8.143e-1	3.900e3	6.665e3	1.430e3	6.813e4
6	2.483e3	9.758e3	3.657e4	2.654e4	1.370e3	8.997e7
7	2.876e3	5.202e3	2.592e4	2.100e4	1.170e3	1.092e5
8	1.777e3	4.386e3	1.105e4	1.206e4	3.157e2	3.524e4
9	8.231e2	4.928e3	1.137e4	9.328e3	2.054e2	3.722e4
10	2.326e3	2.547e3	5.431e3	6.452e3	9.495e2	6.315e4
11	1.799e3	1.675e4	2.818e4	2.234e4	1.414e3	1.166e8
Mean	2.6164e3	5.8446e3	1.8334e4	1.7258e4	1.0905e3	2.918e7
CV	42.4	77.9	61.3	64.5	52.6	176.3

Table 3.3 Individual Parameter Estimates of irinotecan PK model

Patient	Model SSR		
	Original profile	PDE profile	Improvement (%)
1	16.53	19.12	-15.6
2	140.17	145.69	-3.9
3	88.47	97.28	-9.9
4	171.51	150.32	12.3
5	480.52	417.51	13.1
6	93.84	83.01	11.5
7	15.35	13.36	12.9
8	10.30	10.18	1.1
9	45.73	38.79	15.1
10	74.23	73.48	1.0
11	96.76	81.2	15.9

Mean improvement	4.89

Table 3.4 Sum of Square Residuals (SSR) for the irinotecan PK model, with either the original delivery profile, or that simulated through the PDE pump-to-patient model. The table also shows improvement in percentages for most patients and an overall average improvement.

infusion profile programmed in to the pump. Using the PDE to account for the properties of the system largely increased the model validity (Table 3.7, 3.8). The model was also fitted to the total data for one parameter set and then compared between using the intended delivery and the PDE derived delivery profile, this showed and increase quality of fit form a SSR of 0.0033 to 0.0026 and a R^2 of 0.83 to 0.87,

Patient	Model R^2		
	Original profile	PDE profile	Improvement (%)
1	1	0.99	-1
2	0.98	0.99	1
3	1	0.99	-1
4	0.93	0.94	1
5	0.93	0.94	1
6	0.96	0.97	1
7	0.1	0.99	-1
8	0.99	1	1
9	0.97	0.98	1
10	0.99	0.99	0
11	0.96	0.96	0

Mean improvement	0.27

Table 3.5 R^2 values for irinotecan model, with either the original delivery profile, or that simulated through the PDE pump-to-patient model. The table also shows improvement in percentages for each patient and average improvement for all patients.

which is an improvement of 22% in SSR and 3.9% in R^2. Pooled data agree with the improved fit our PDE model as the drug input but showed a worse fit to data.

Patient	Parameter Values				
	C_b (ml/h)	$k_{b,l}$ (ml/h)	$k_{b,o}$ (ml/h)	b (ml/h)	u (ml/h)
1	1.780e4	2.198e4	9.447e3	1.059e4	4.644e2
2	1.198e4	6.784e4	6.635e3	4.202e3	1.806e2
3	9.812e3	1.049e6	5.011e3	4.312e3	2.629e2
4	8.418e3	1.544e4	4.008e3	5.485e3	7.080e2
5	6.104e3	9.188e3	4.323e3	5.918e3	5.481e2
6	1.380e4	4.303e3	9.096e3	7.701e3	7.327e2
7	1.185e4	7.017e7	7.655e3	3.689e3	1.899e2
8	7.322e3	2.601e3	5.951e3	8.886e3	1.070e3
9	4.292e3	3.931e3	2.316e3	4.094e3	6.873e2
10	9.102e3	6.526e3	6.382e3	7.053e3	5.926e2
Mean	1.0050e4	7.1356e6	6.0829e3	6.194e3	5.4370e2
CV	40.36	318.2	38.1	38.4	52.8

Table 3.6 Parameter Estimates of oxaliplatin PK model

The 5-fluorouracil model showed a very good fit to data, despite a slight systematic under-estimation of the third data point in time. Model fit was assessed through Sum of Squared Residuals (SSR) (Table 3.10) and R^2 values (Table 3.11). To test the validity of the pump-to-patient model, I compared the goodness of this fit with that

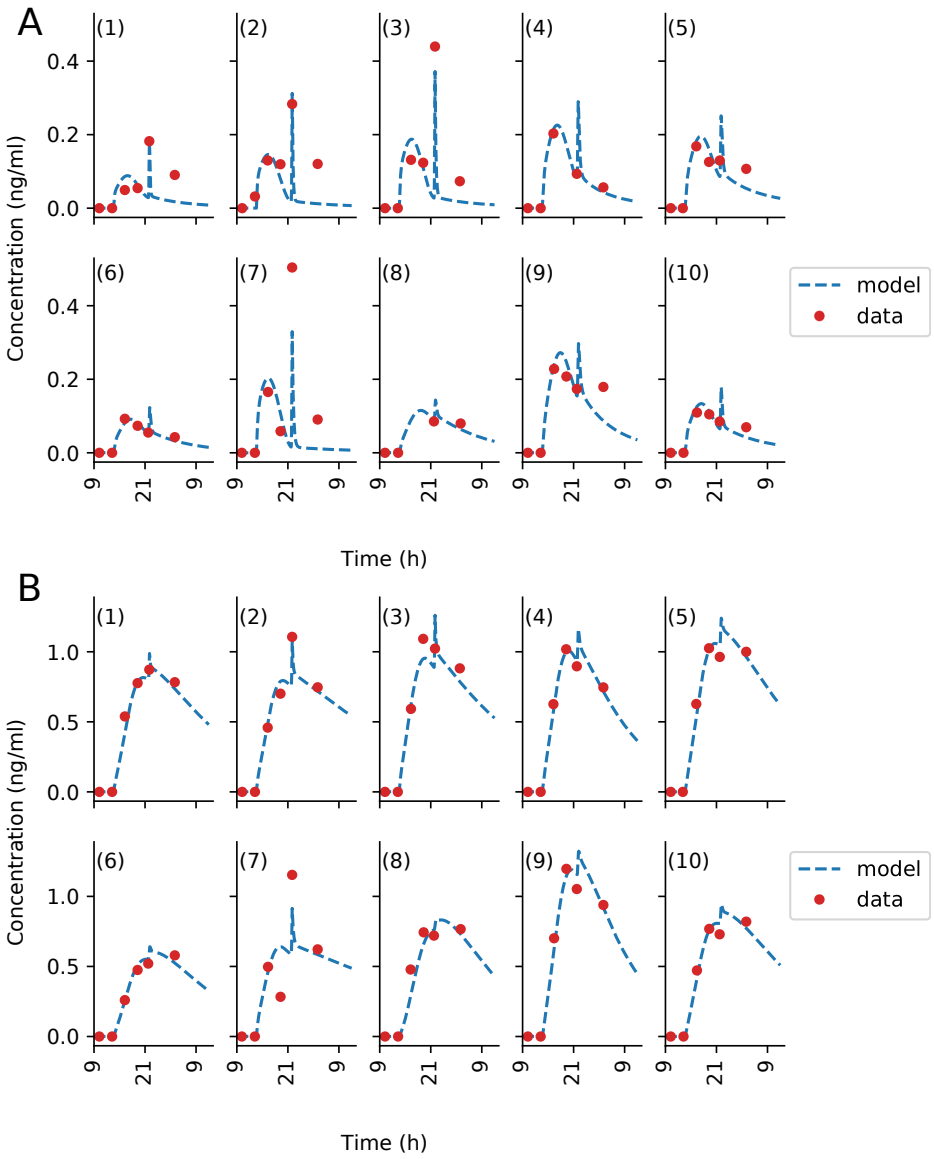

Fig. 3.11 Patient data best-fit of oxaliplatin PK model. Each subplot is an individual patient data fit to the model independently. (a) shows plasma ultrafiltrate platinum concentrations, and (b) shows plasma total platinum concentrations. PK data for Patient 11 were missing.

of the PK model with drug infusion rate equal to the infusion profile programmed in to the pump. Using the PDE to account for the properties of the system largely increased the model validity (Table 3.10, 3.11). The model was also fitted to the total data for one parameter set and then compared between using the intended delivery and the PDE derived delivery profile, this showed and increase quality of fit form a SSR of 2.6e-5 to 2.5e-6 and a R^2 of 0.44 to 0.47, which is an improvement of 3% for SSR and 6.7% for R^2. Pooled data agree with the improved fit our PDE model as the drug input but showed a worse fit to data.

Patient	Model SSR		
	Original profile	PDE profile	Improvement (%)
1	96.31	62.32	35.28
2	112.60	84.71	24.76
3	315.69	168.27	46.69
4	45.50	7.0	84.48
5	64.51	48.86	24.25
6	19.20	8.38	56.31
7	864.37	483.18	44.10
8	9.90	5.16	47.87
9	105.80	73.48	30.55
10	35.93	21.62	39.83

Mean improvement	43.4

Table 3.7 Sum of Square Residuals (SSR) for oxaliplatin model, with original delivery profile, and oxaliplatin model with the PDE simulated delivery profile. The table also shows improvement in percentages for each patient and average (mean) improvement for all patients.

Patient	Model R^2		
	Original profile	PDE profile	Improvement (%)
1	0.94	0.96	2.3
2	0.94	0.97	2.5
3	0.91	0.93	1.6
4	0.97	0.99	2.6
5	0.97	0.98	1.0
6	0.96	0.98	1.8
7	0.64	0.78	21.6
8	0.91	0.93	1.6
9	0.96	0.97	1.6
10	0.96	0.98	1.4

Mean improvement	3.9

Table 3.8 R^2 values for oxaliplatin model, with original delivery profile, and oxaliplatin model with the PDE simulated delivery profile. The table also shows improvement in percentages for each patient and average (mean) improvement for all patients. The much larger improvement in patient 7's R^2 value is because this patient shows the largest spike at the end of delivery and incorporating this into the delivery profile vastly improves the fit.

The model predicted that the glucose flush induced a late spike in plasma drug concentration which could not be seen in the data for all patients, probably because blood sampling frequency was not high enough (Fig 3.12). This model-predicted spike in 5-fluorouracil concentration changed the tmax value for Patients 5, 6 and 9.

The predicted spike AUC was equal to approximately 5% of the total AUC which was in agreement with the pump-to-patient model prediction. This was only calculable for 5-fluorouracil since its elimination was fast enough for its concentration to be close to zero by the time the glucose flush began.

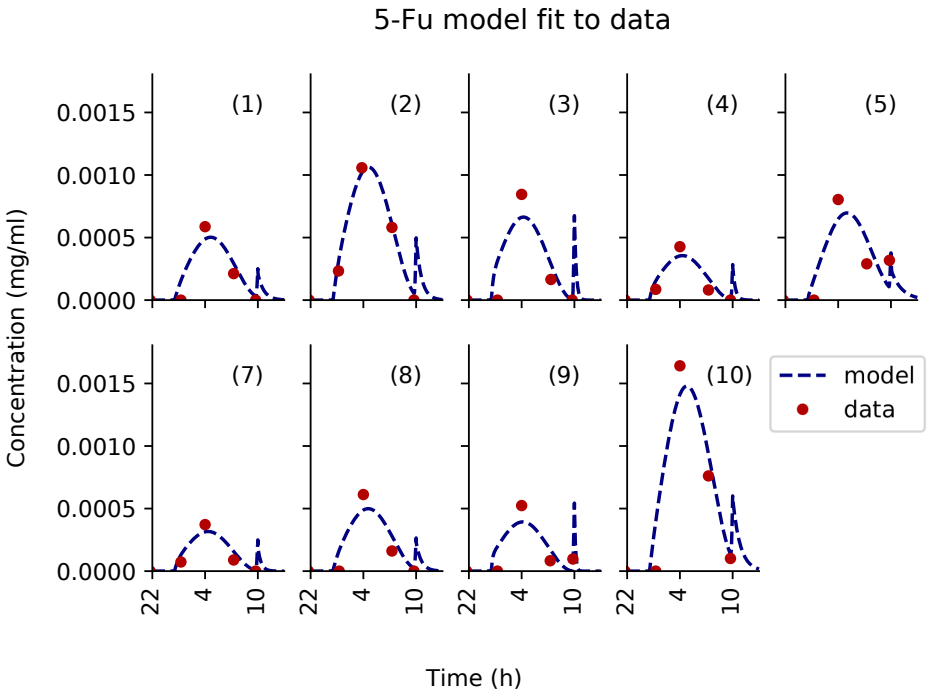

Fig. 3.12 Patient data best-fit of 5-fluorouracil PK model. Each subplot is an individual patient data fit to the model independently. PK data for Patient 6 and 11 were missing.

Patient	Parameter value		
	C_l, C_o (ml/h)	C_b (ml/h)	$Ef_{o/l}, Up_{o/l}$ (ml/h)
1	132384	84801	21.09
2	118360	46116	6540
3	125355	70614	38.89
4	334605	181219	86.54
5	349150	86562	2.682e+05
6	888311	221789	1.048e+06
7	131285	98929	23.68
8	523901	130879	1.618e+06
9	117557	36451	58.18
Mean	302323	106373	326127
CV	84.18	56.0	176.79

Table 3.9 Parameter Estimates of 5-fluorouracil PK model

Patient	Model R^2		
	Original profile	PDE profile	Improvement (%)
1	241.2	186.5	22.6
2	131.1	48.7	62.9
3	640.4	554.3	13.4
4	84.4	80.4	4.7
5	604.3	861.2	-42.5
6	57.6	57.5	0.01
7	306.8	256.6	16.3
8	308.2	294.2	4.5
9	1556.8	1076.4	30.8

Mean improvement	12.5

Table 3.10 Sum of Square Residuals (SSR) for 5-fluorouracil model, with original delivery profile, and 5-fluorouracil model with the PDE simulated delivery profile. The table also shows improvement in percentages for each patient and average (mean) improvement for all patients.

Patient	Model R^2		
	Original profile	PDE profile	Improvement (%)
1	0.79	0.84	6.3
2	0.96	0.99	3.1
3	0.73	0.77	5.5
4	0.85	0.86	1.2
5	0.69	0.55	-20.0
6	0.86	0.86	0.0
7	0.75	0.79	5.3
8	0.64	0.65	1.5
9	0.83	0.88	6.0

Mean improvement	49.5

Table 3.11 R^2 values for 5-fluorouracil model, with original delivery profile, and 5-fluorouracil model with the PDE simulated delivery profile. The table also shows improvement in percentages for each patient and average (mean) improvement for all patients.

The model fit to each individual patient PK data allowed an investigation of the inter-patient variability in the resulting PK parameters (Fig 3.16 A, B, C). The CV of each PK parameter was calculated among the patient population (see SI). Then, the mean CVs for the entire parameter set of each drug model were calculated as a single measure of inter-patient variability. Irinotecan had the smallest mean CV with a value of 79.18%, and a range from 42.48 to 176.25%. Oxaliplatin had the second smallest value of mean CV, 97.56%, with the largest range from 38.1 - 318.2%.

5-fluorouracil had the largest mean CV at 112.10%, with the smallest range from 59.4 to 187.51%. In all three models the parameters which showed the largest inter-patient variability were transport parameters specifically, for irinotecan Blood-Organ transport, for oxaliplatin Blood-Liver Transport and Blood-Liver/Organ transport for 5-fluorouracil.

For each drug model, individual patient parameter sets were then utilised to identify patient clusters. The numbers of clusters were determined by minimising the validity index of Fukuyama and Sugeno V_{FS} as described in [207]. Clustering for different numbers of clusters and their respective V_{FS} can be seen in the (Figs. 3.13, 3.14, 3.15). For irinotecan, the minimum value of V_{FS} was achieved for four clusters. One cluster was composed of Patients 1, 2, 3, 5, 7, 8, 9 and 10, the other three patients were in a cluster on their own. The analysis for oxaliplatin concluded to two clusters, a cluster of only one patient, patient 7, and the rest of the patients being clustered together. The analysis for 5-fluorouracil revealed four clusters: 5 patients were grouped in the largest cluster (Patients 1, 2, 3, 7, and 10), two patients in the second cluster (Patients 4, 5) and the final two patients were in clusters on their own. Only patients 1, 3 and 10 were consistently clustered together for all three drugs.

Once the patient PK parameters had been clustered, the mean of the parameter CVs was reassessed for each cluster with 2 or more patients within. Irinotecan mean CV in the largest cluster was 51.52%, which represented a large decrease compared to the mean CV for the entire patient population equal to 79.18%. The oxaliplatin main cluster which was constituted of all patient but patient 7 had a mean CV of 87.37% as compared to 97.56% for the entire population. 5-fluorouracil's largest cluster had a CV of 32.37% and the smaller cluster had a CV of 72.87%, which corresponded to a drastic decrease of inter-patient variability as the population mean CV was equal to 112.10%. All other clusters for each drug had only a single patient and therefore the CV could not be assessed. Clustering was compared to covariates of patients, such as gender, age and gene polymorphism, to see if there was any correlation however none was found.

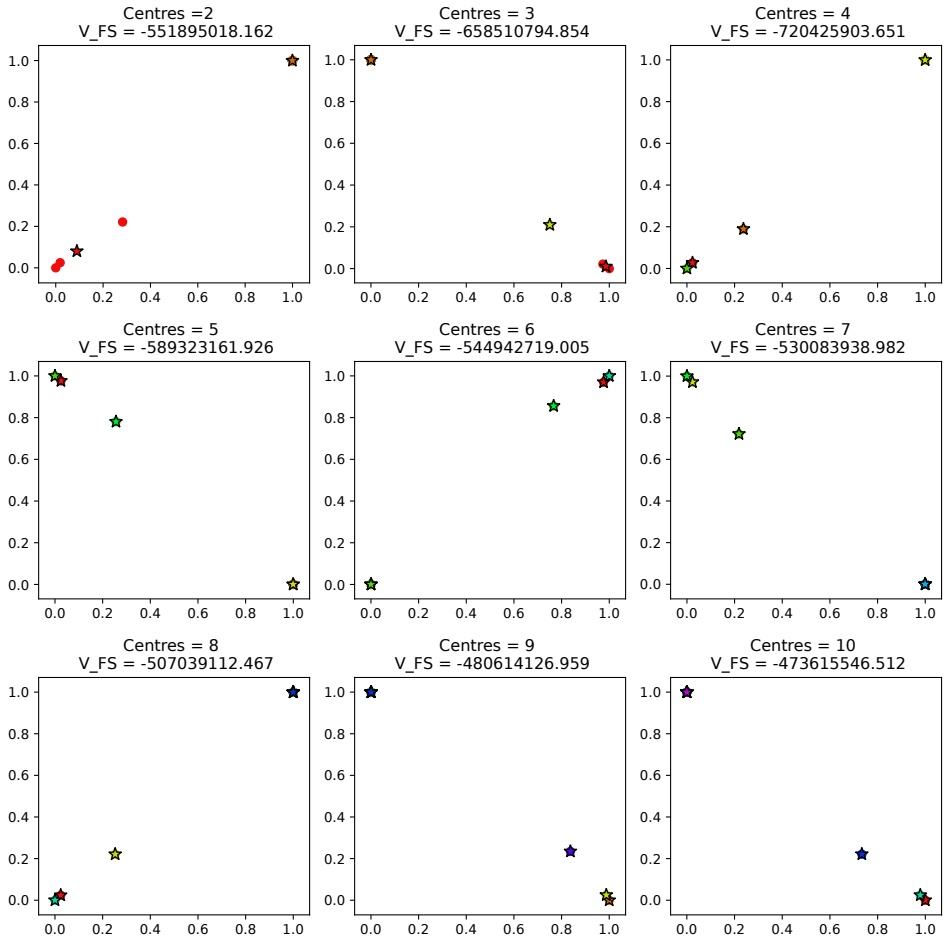

(a)

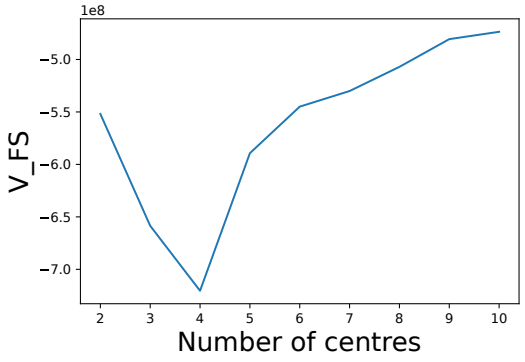

(b)

Fig. 3.13 Patient parameter clustering analysis for Irinotecan. (a) 2D visualisation of patient clusters for different number of clusters. Centroids (stars) and patients (dots) are shown, (b) V_{FS} values for different numbers of clusters.

3.4 Discussion

Precision and personalised medicine requires accurate technologies for drug administration and proper systems pharmacology approaches for individual patient

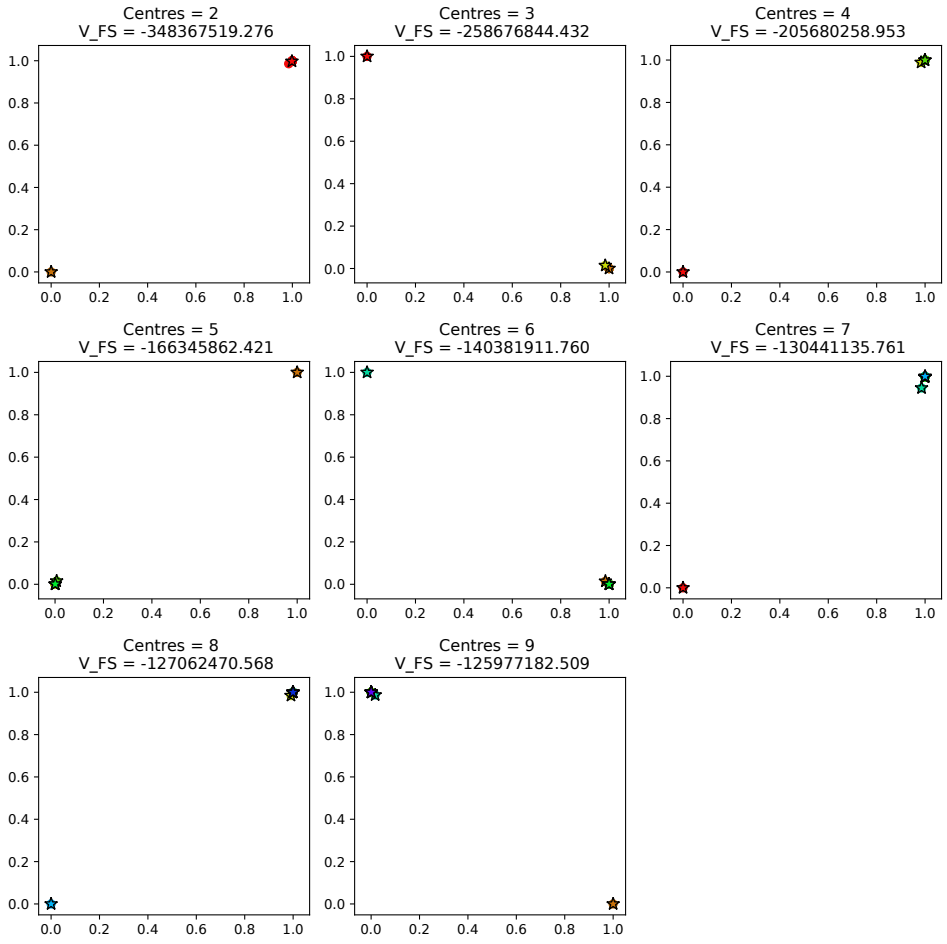

(a)

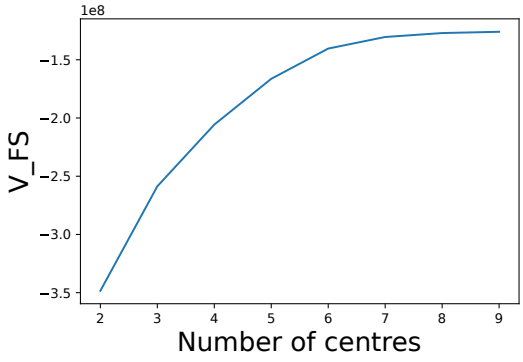

(b)

Fig. 3.14 Patient parameter clustering analysis for oxaliplatin. (a) 2D visualisation of patient clusters for different number of clusters. Centroids (stars) and patients (dots) are shown, (b) V_{FS} values for different numbers of clusters.

multidimensional data analysis. Here, plasma PK data of the OPTILIV trial in which patients received irinotecan, oxaliplatin and 5-fluorouracil through a chronomodulated schedule delivered by an infusion pump into the hepatic artery were mathematically analysed. To allow for an accurate analysis of PK patient data, a model of the

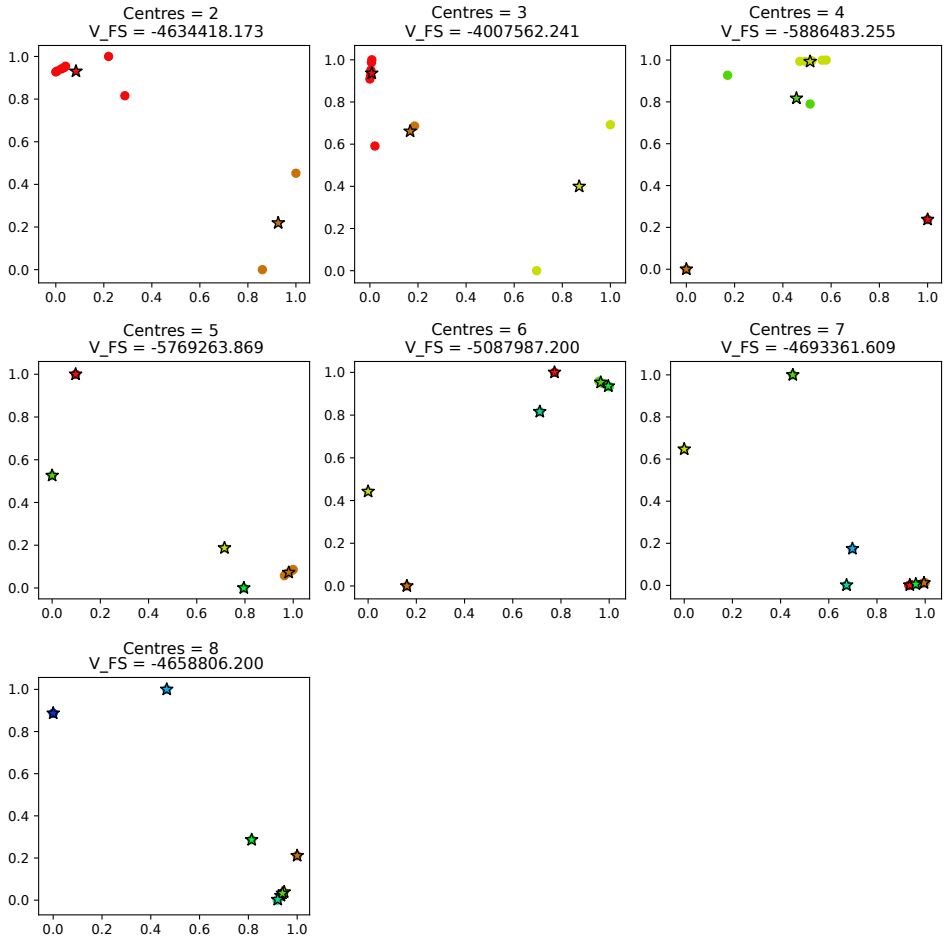

(a)

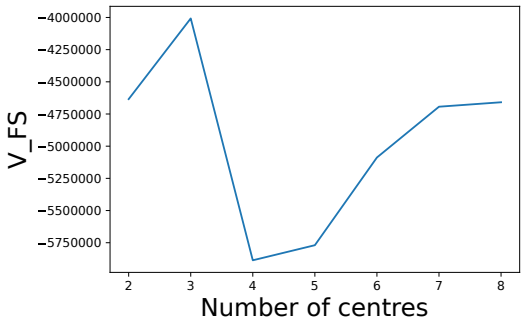

(b)

Fig. 3.15 Patient parameter clustering analysis for 5-fluorouracil. (a) 2D visualisation of patient clusters for different number of clusters. Centroids (stars) and patients (dots) are shown, (b) V_{FS} values for different numbers of clusters.

pump drug delivery was successfully designed and connected to semi-mechanistic PK models. Although no data were available to directly validate the model-predicted drug infusion rates, the overall framework achieved a very good fit to individual time-concentration profiles which showed model accuracy. The validity of the ap-

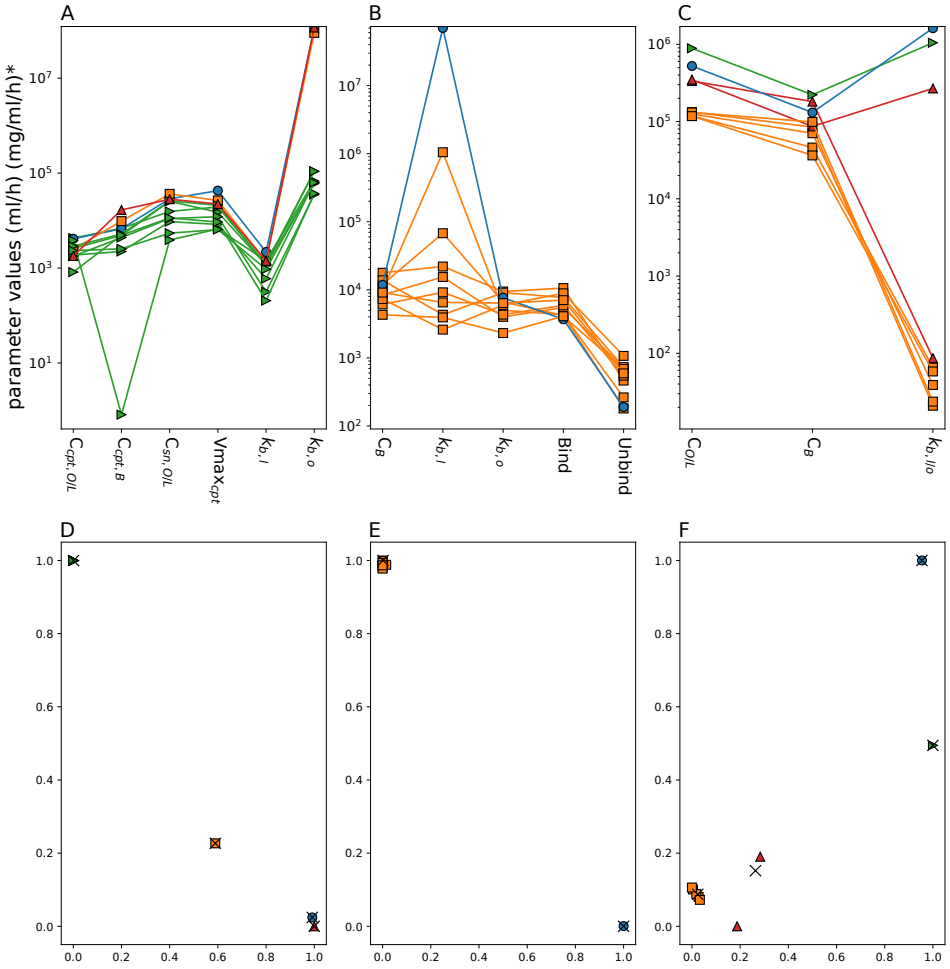

Fig. 3.16 Inter-patient variability in drug PK parameters. The first line shows parameter variability across the considered patient population for irinotecan (A), oxaliplatin (B) and 5-fluorouracil (C), the colour and symbols represent the clusters each parameter set belongs to. The parameters are named with reference to the schematics of the models, the subscripts refer to the blood (b), organs (o) and liver (l). In the irinotecan parameters, additional subscripts cpt and sn refer to irinotecan and SN38 respectively. The second line shows multidimensional scaling representation of patient clustering based on their PK parameters for irinotecan (D), oxaliplatin (E) and 5-fluorouracil (F), the x refer to the cluster centroids and the points refer to patient PK parameters projected onto 2D plot.

proach was further demonstrated by the modestly improved data fit using the PDE model's explicit solution connected to PK models compared to PK models directly integrating infusion profiles that were programmed into the pump (see SI). This study gave insights into inter-patient variability and paved the path to treatment optimisation.

The simulations for the pump-to-patient model showed and quantified a delay between the actual start of the pump and the time when the drug appeared in

the patient blood which was due to the delay needed for the drug solution to fill up the infusion tube and eventually reach the patient. A validation of this model prediction could be seen directly in the data as 5-fluorouracil and oxaliplatin plasma concentrations were close to zero for the first two measurement times. The length of this delay depends on both the drug solution concentration and the volume of the infusion tube, so that its importance was high for oxaliplatin, intermediate for 5-fluorouracil and minor for irinotecan. Temporal accuracy is key for precision medicine especially in the context of chronotherapy and chronomodulated drug delivery. Thus, the programming of any drug administration devices need to account for these delays. The pump-to-patient model that I present here allows to adaption to any infusion scheme for any drug administration devices in order to properly administer the treatment schedules initially intended by the oncologists.

In addition to such "pump-to-body" delay, the increase in free Pt concentration near 22:00 shown in the PK data was explained by a spike in oxaliplatin delivery resulting from the glucose rinse flushing out the residual oxaliplatin left within the infusion tube. This phenomenon was well captured and quantified by the oxaliplatin PK model which predicted that the quantity of drug delivered in the final spike was equal to 10.7% of the total dose. The model also showed that the t_{max} of oxaliplatin plasma concentration was shifted by several hours due to this delivery profile spike. In silico simulations also predicted that the glucose flush would alter the PK of 5-fluorouracil. The spike only accounted for a small amount of 5-fluorouracil dose of 5.36% and may not have caused any significant detrimental effect. More data points covering the time of unexpected drug administration due to the glucose flush would have further validated the model which already achieved a very good fit to the available data points. However, free oxaliplatin plasma concentration displayed complex patterns with high values at the start of the glucose flush for patients 1, 2, 3 and 7 which left no doubt on the large impact of the glucose flush on oxaliplatin administration. Similarly, unexpectedly high plasma concentrations of 5-fluorouracil were observed at the start of the glucose flush for patient 5 and 9 which partially validated the model. The delivery spike due to the glucose rinse did not seem to have influenced the plasma concentration profile of irinotecan because the drug concentration in the solution was much lower and the flow rate programmed into the pump was much higher as compared to oxaliplatin and 5-fluorouracil administration. Indeed, the spike only accounted for less than 2% of the total dose of irinotecan.

The pump-to-patient model further showed that these inconsistencies between the simulated and intended drug administration could be overcome with a simple and easily constructed adaptation of the infusion profiles, given the specific dimensions of the infusion tube. The new profile showed a much better match with the original intended administration profile.

Several published clinical studies propose mathematical models of the PK of 5-fluorouracil, oxaliplatin or irinotecan with various levels of complexity. First, a physiologically-based PK model of capecitabine, a pro-drug of 5-fluorouracil, was designed for humans [203]. However, the data available in the OPTILIV study would not allow for estimating parameters of such a detailed model. Next, numerous clinical studies have performed compartmental analysis of plasma PK data from cancer patients receiving either 5-fluorouracil, oxaliplatin or irinotecan [208]. These models were designed for intravenous injection and could not be readily used for intra-arterial hepatic administration, this also meant that comparison of parameter values was limited between our model and the literature. Thus, the development of new semi-physiological PK models was necessary to include the drug delivery site as a separate compartment, that was different from the Blood compartment for which data were provided. This meant that it was difficult to compare parameter values from the literature to the parameter values obtained in our analysis. The parameter values we obtain were very large with some having large confidence intervals but apart from via quality of fit to data there was no way to assess biological relevance of these vales which is a limitation of this model and the data set. The intention was also to develop more physiologically-relevant models in view of future account of circadian rhythms and chronotherapy optimisation investigations. Indeed, the developed models are called semi-physiological as the compartment volumes together with relative fractions of clearance routes were inferred from the literature. The quantity of data available for this study limited the models to being semi-physiological in nature. However, these models could be further extended to physiologically-based models, with increased data sets, by detailing the "Organs" compartment and be connected to mechanistic PD models to represent organ-specific drug PK-PD. Furthermore, the current models do not account for any circadian rhythms although they may largely impact on drug PK-PD. Thus, new circadian clinical studies are needed to improve the models towards drug chrono-administration optimisation.

Inter-patient differences in maximum plasma drug concentrations and in the time at which it occurred led us to further investigate variability in between subjects. Although there is only a small sample size in this study the methods used could be easily applied to larger data sets and can still give useful information on this data set. Irinotecan showed the lowest mean variability. Clustering analysis indicated that patients could be classified into five clusters with respect to irinotecan PK parameters. The second largest inter-patient variability was found for 5-fluorouracil. Clustering for 5-fluorouracil showed there were four clusters. Regarding oxaliplatin, there was the largest variability between patient's PK model parameters with all parameters showing high variance. The fitting process was repeated for each patient many times to reduce the chance that the large variance was due to finding different local minimums. Clustering according to oxaliplatin PK parameters split patients

into two clusters leading to isolation of patient 7. This clustering of the patients led to a reduced inter-patient variability for all drugs, especially for irinotecan and 5-fluorouracil. This decrease in CVs is not unexpected, but the significant level of reduction means this method could be used as a way to stratify patients into treatment groups with less inter-patient variability in PK profiles. The measure of inter-patient variability could be interpreted as an indicator of the need for personalisation as high differences between subjects implies high potential benefit of drug administration personalisation. Here, I demonstrated that the PK of all three considered drugs displayed important inter-subject variability. The remaining clinical challenge lays in determining clinical biomarkers for stratifying patients before drug administration, in order to reach the intended plasma PK levels. In order to do so, patient clusters were compared to known covariates such as age, gender and gene polymorphisms. However, none showed significant correlation. I then performed modelling analyses and identified the PK parameters which were critical for inter-patient variability for irinotecan, 5-fluorouracil and oxaliplatin which were the transport parameters between the Blood and either the Liver or the Organs compartments.

Conclusion

In conclusion, a mathematical framework was designed to allow for accurate analysis of patient PK data. A model of the dynamics of the drug solution from the pump to the patient's blood was designed, irrespective of the drug delivery device. It was used to represent the chronomodulated drug administration though the Mélodie infusion pump into the patient hepatic artery of irinotecan, oxaliplatin and 5-fluorouracil. The model revealed significant inconsistencies between the drug profiles programmed into the pump which corresponded to the drug exposure intended by clinicians and the actual plasma PK levels. Importantly, it allowed for the design of innovative drug infusion profiles to be programmed into the pump to precisely achieve the desired drug delivery into the patient's blood. Next, the pump-to-patient model was connected to semi-physiological models of the PK of irinotecan, oxaliplatin and 5-fluorouracil. The overall framework achieved a very good fit to data and gave insights into inter-patient variability in the PK of each drug. Potential clinical biomarkers for treatment personalisation were suggested although further investigations in larger cohorts of patients are required. Overall, this complete framework informs on drug delivery dynamics and patient-specific PK of irinotecan, oxaliplatin and 5-fluorouracil towards precise and personalised administration of these drugs.

Acknowledgements

I would like to thank Sami Al-Izzi of the University of Warwick Mathematics Institute and Dr Thomas Lepoutre (Inria, team Dracula, Lyon, France) for their discussions.

Chapter 4

Physiologically-based modelling of oxaliplatin pharmacokinetics based on preclinical studies

4.1 Motivation

The motivation behind this chapter came from available experimental and clinical evidence of sex-related differences in tolerability and optimal timing of oxaliplatin. Indeed, clinical investigations of the sexual dimorphism in circadian-dependent tolerance of FOLFOX revealed that the sex was a significant determinant of the drug schedule tolerability. Optimal times of delivery for men and women could differ by up to 6 hours [4]. To further investigate this phenomenon at the molecular scale, oxaliplatin sex-dependent chronotoxicity is studied in mice.

A dose finding experiment was done which demonstrates the sex specific differences of oxaliplatin treatment. The mice were given a single injection at ZT 7, the most toxic time for males, and then tracked for 2 weeks to see the survival rate for different doses. Female mice were more sensitive to oxaliplatin with lethal toxic doses first evident at 13 mg/kg compared to 19 mg/kg for male mice (Fig 4.1). Body weight losses were consistent with these survival results (data not shown).

This experiment shows sex dimorphism in response to oxaliplatin treatment. Two mathematical models have been developed in a multi-scale modelling frame work to accurately predict oxaliplatin PK/PD and better understand sex dimorphism in a preclinical setting. The first model is an in vitro model which quantifies how drug-protein binding occurs in the blood of different species. This model can then be used as, firstly, a proof of the structure of oxaliplatin dynamics and secondly as the first step in a multiscale modelling approach for the whole body model. The whole body model has been designed to give information on the differences in chronotoxicities

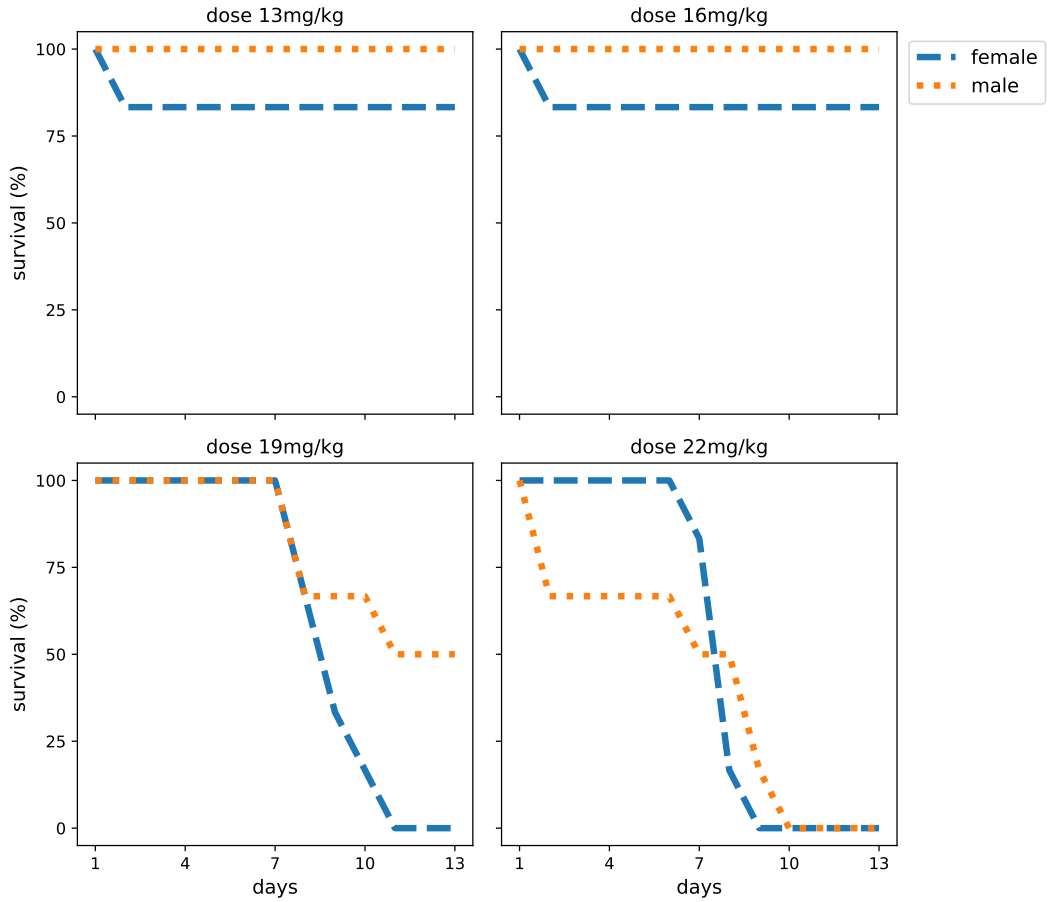

Fig. 4.1 Dose finding experiment showing the percentage survival of male and female mice after different doses of oxaliplatin given at ZT 7, which was chosen as it was the worst timing for male mice. No deaths were observed for either sex at lower doses.

between male and female mice. The aim of this model is to be able to inform future work on sex dimorphisms in human patients by connecting differences in model parameters with specific measurable processes.

4.2 Oxaliplatin blood PK: an in vitro study in mice, rats and humans

4.2.1 Introduction

One of the early steps in drug development is animal testing during which 11% of drugs fail due to unacceptable toxicity levels in animals [209]. However, it is unknown whether the tolerability problems in animals would translate into humans, since animal models do not relate very well at all to human results [210]. Even if drugs make it through the preclinical stages to phase I clinical trials the percentage of

drugs that make it to approval is only 13.8% [211]. This lack of success has in part been attributed to the inability to make accurate predictions in humans based on preclinical animal models [212]. Thus, there exists a need for quality scaling and extrapolation methods between species.

One method to tackle this problem has been physiologically-based (PB) modelling and quantitative systems pharmacology (QSP) which has been developing since the 90s. CaSyM [174] and Avicenna [213] European consortia recently recommended developing systems pharmacology approaches based on physiology, as these methods do not subdivide living organisms into independent components. Physiologically based approaches instead recognise that genes, proteins, cells and organs interact with each other and with the environment in complex ways that can vary over time. Indeed, anticancer drug toxicity and efficacy are ultimately determined at the molecular scale by the response of gene and protein networks involved in the drug pharmacokinetics (PK) and pharmacodynamics (PD) in different cell populations, healthy or tumour, located in different organs. Hence, theoretical models of whole-body drug PK-PD and cell type-specific regulatory pathways constitute a reliable physiological basis from which the drug can be selected for further investigations. Such detailed molecular and dynamical mathematical modelling further allows for the direct integration of the patient's and tumour's molecular profiles into treatment decision.

Because the complex molecular physiology of healthy and diseased tissues together with their temporal organisation are unlikely to be completely assessed directly in individual cancer patients, multi-scale methodologies integrating in vitro, pre-clinical and clinical investigations are required [214]. Mathematical models which are not based on the physiology only allow for allometric animal-to-human scaling typically using body weight or body surface area. These methods have been proven inaccurate in part because they do not consider the species-specific metabolic rates and expression of transporters and intracellular proteins [215]. In contrast, mathematical variables and parameters of physiologically-based models do have a biological meaning which is conserved across species [216]. Hence, extrapolation from rodent studies to clinical investigations is made possible by keeping the model structure and re-sizing parameters. Current challenges in the field of QSP lie in developing reliable scaling methods to extrapolate human parameter values from preclinical datasets [217]. Empirical allometric procedures have been used for decades. One of the first papers to combine the idea of physiological modelling with allometric scaling was Johnson et al in 1992 [218]. The premise behind allometric scaling is that since many physiological parameters are a function of the size of an animal, pharmacokinetic parameters may also be a function of the size [219]. The use of these empirical scaling techniques and physiological modelling has now become common-place within the pharmaceutical industry [220, 221]. There have been recent examples of successful translational

scaling of PBPK models between multiple species [222–224]. However, in 2015 the FDA still deemed the predictive power of PBPK modelling to be inadequately demonstrated which may be due to deficient inter-species scaling methodologies [225]. Indeed, a recent study of temozolomide brain disposition demonstrated that scaling transport parameters from mice to humans using organ volumes was far from accurate [226]. Thus, as will be shown here, there are still scenarios in which allometric scaling methods cannot bridge species gaps.

It is known that the binding of cancer metal-drugs with plasma proteins largely impacts on their pharmacokinetics and antitumour efficacy [227]. Protein binding has been shown to be of importance for oxaliplatin as only 13-21% of the drug is in an unbound state 6h after administration in humans [60]. The plasma binding rate for a given drug is known to vary across species probably as a result of different plasma proteins present at different relative concentrations in the blood [228]. However, to our knowledge, scaling methods do not exist to predict drug binding in humans based on rodent studies. Hence, this study aimed to investigate oxaliplatin binding and transport in the whole blood of mice, rats and humans, with the aim of being able to use the information gained from these models to better inform whole-body PBPK models of oxaliplatin. To this end, an in vitro PK model has been designed to assess the plasma protein binding of oxaliplatin together with its transport between the different components of the blood for different species.

4.2.2 Methods and Materials

Data sets

The data sets used in this work are from two species, Wistar male rats and humans.

The rat data were originally presented by Luo et al in "Biotransformations of oxaliplatin in rat blood in vitro" [7]. The rats were male, 6-8 weeks of age and approximately 225g of body mass. They had been kept in 12 hour light/dark cycle at a temperature of 22°C for at least one week prior to the experiment. Animals were sacrificed and 4.75ml of heparinized blood (250 units heparin/ml) from the rats was mixed with 0.25ml of oxaliplatin stock solution (400 μg/ml or 1 mM) to obtain an initial oxaliplatin concentration of 50μM. The mixture was then incubated in 5% CO_2 at 37°C for up to 24 hours. Aliquots of 0.5ml were taken at 0, 0.5, 1, 2, 4, 7, 9, 12 and 24 hours after initial mixing. The samples were then analysed for platinum content in the red blood cells (RBC) and plasma. The platinum in the plasma and RBC was evaluated as bound platinum and ultra-filtrate platinum (i.e. unbound fraction). Full details of the exact experimental procedure can be found in the original article [7].

The human data were taken from the Pendyala et al paper "In Vitro Cytotoxicity, Protein Binding, Red Blood Cell Partitioning, and Biotransformation of Oxaliplatin"

[229]. Oxaliplatin was mixed with human whole blood and incubated at 37°C. 1 ml aliquots were taken from the whole blood sample at 0, 1, 2, 3, 4, 5 and 6 hours post mixing, and analysed for platinum content in the RBC and the plasma, the platinum in the plasma was evaluated as bound platinum and ultra-filtrate platinum. Three separate experiments were undertaken for oxaliplatin concentrations of 5, 10 and 20 μg/ml. The results were collated since there was no significant effect of the initial drug concentration on the percentage of total platinum recovered in each compartment. Full details of the experiment can be found in the original article [229].

Mathematical modelling

The in vitro PK models were based on physiologically-based compartmental models using Ordinary Differential Equations (ODEs) programmed using MATLAB [230] and solved using ode45 in the standard MATLAB library.

PK model parameter estimation was achieved using a weighted least squares approach, with the weighting set as the standard deviation of the data from original papers. The minimisation of the least squares cost function was performed by the Covariance Matrix adaptation Evolution Strategy (CMAES) within MATLAB [231] which has been shown to be successful at handling complex cost function landscapes [166]. Model goodness of fit was assessed using R^2 values. PK model parameter identifiability was assessed using the software DAISY [160], written in REDUCE, for structural identifiability and likelihood profiles for practical identifiability, following the procedure outlined in [170].

4.2.3 Results

Model structure

The model for oxaliplatin in vitro blood PK includes two compartments, plasma and RBC, with each compartment having a bound platinum and free platinum fraction (Fig. 4.2). The bound platinum was assumed not to be able to move between compartments. Binding in plasma and RBC was linearly dependent on platinum concentration within the given compartment, as was unbinding or dissociation. Unbinding was included since this is the only way equilibria with non-zero values of unbound platinum could be reached, especially considering that binding saturation is not seen within the concentration profiles [229]. Binding and unbinding rates were assumed to be different for plasma and RBC compartments. The transport between compartments was also assumed to be linear with respect to compartment concentrations.

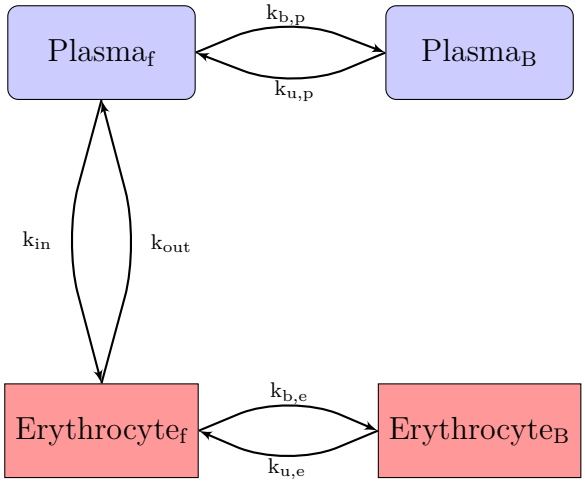

Fig. 4.2 Schematic of in vitro blood binding model.

The model equations are given by:

$$\frac{dP_f}{dt} = (-k_{\mathrm{b,p}} * P_f - k_{\mathrm{in}} * P_f + k_{u,p} * P_b + k_{\mathrm{out}} * E_f)/V_p \tag{4.1}$$

$$\frac{dP_b}{dt} = (k_{\mathrm{b,p}} * P_f - k_{u,p} * P_b)/V_p \tag{4.2}$$

$$\frac{dE_f}{dt} = (k_{\mathrm{in}} * P_f - k_{\mathrm{out}} * E_f - k_{\mathrm{b,e}} * E_f + k_{u,e} * E_b)/V_e \tag{4.3}$$

$$\frac{dE_b}{dt} = (k_{\mathrm{b,e}} * E_f - k_{u,e} * E_b)/V_e \tag{4.4}$$

where P and E refer to plasma and RBC (erythrocytes which is another term for red blood cells), with subscripts f and b referring to free (ultrafiltrate) and bound respectively. The model has 9 parameters which are: volumes of plasma and RBC (V_p, V_e), oxaliplatin binding rates in plasma and RBC $(k_{b,p}, k_{b,r})$, unbinding rates $(k_{u,p}, k_{u,r})$ and transport rates between plasma and RBC cytoplasm (k_{out}, k_{in}). For the rat data, observations were taken from free platium and total platinum in both the plasma and the RBC's, the human data was observed from free and total platinum in the plasma and total platinum in the RBC's: for rats

$$P_f(T), \quad P_{tot}(T) = P_f(T) + P_b(T), \quad E_f(T), \tag{4.5}$$

$$E_{tot}(T) = E_f(T) + E_b(T) \tag{4.6}$$

where T in vector of time points (h)

$$T = [0, 0.5, 1, 2, 4, 7, 9, 12, 24] \tag{4.7}$$

and for humans

$$P_f(T), \quad P_{tot}(T) = P_f(T) + P_b(T), \quad E_{tot}(T) = E_f(T) + E_b(T) \tag{4.8}$$

where T in vector of time points (h)

$$T = [0, 1, 2, 3, 4, 5, 6] \tag{4.9}$$

Initial conditions were set as the total drug unbound in the plasma compartment and all other compartments were empty.

The volumes were all fixed using parameters from the literature and all other parameters were shown to be structurally globally identifiable without the need for initial conditions to be present, using DAISY as described in 2.3.2.

Table 4.1 Volumes of blood compartments fixed for the in vitro model [12].

Organ	Volume (ml)	Symbol
Plasma	1.0	V_p
RBC	0.7[1]	V_r

[1] Total blood minus plasma.

Parameter estimation for Rats and Humans

The model was then fitted to both the rat and human data simultaneously. Parameters were scaled using allometric measures taken from the literature as follows. The volumes of plasma (V_p) and RBC (V_e) were calculated from species haematocrit, which is the ratio of the volume of RBCs to the total volume of blood measured as a percentage (Table 4.2). Next, the transport rates between compartments were scaled by the total surface area of RBCs in the blood which was calculated by RBC count in each species (#RBC) multiplied by the surface area of a single RBC of that species (SA):

$$k_{in}^S = K_{\text{in}} \times \#\text{RBC}^S \times \text{SA}^S$$
$$k_{\text{out}}{}^S = K_{\text{out}} \times \#\text{RBC}^S \times \text{SA}^S.$$

The superscript S denotes the species and is equal to either rats or humans. Oxaliplatin binding parameters in the plasma was scaled by the species-specific total plasma protein concentration and the binding parameter in the RBC was scaled using Haemoglobin levels since they are the most abundant protein in the RBC and

have well documented measurements in all analysed species [232]:

$$k_{\mathrm{b,p}}{}^{S} = K^{S}_{\mathrm{Bind_{Plas}}} \times \text{Total plasma protein}^{S}$$
$$k_{\mathrm{b,e}}{}^{S} = K_{\mathrm{Bind_{E}}} \times \text{RBC Haemoglobin}^{S}.$$

Unbinding was considered a passive action and no scaling was applied to these parameters.

Allometric scaling	Species	
	Rat	Human
Total plasma protein (g/dl)	6	7
RBC Haemoglobin (g/dl)	13	15
RBC count (10^6 cells/mm^3)	6.46	5.4
RBC surface area (mm^2)	1.04	1.36
Haematocrit (%)	36%	42%

Table 4.2 Physiological parameters used for scaling parameters of the in vitro oxaliplatin PK model. Rat parameters came from [13] except surface area which was from [14]. Human parameters came from [15–17, 14, 18].

Using the above equations, parameters were fitted simultaneously to rat and human datasets by estimating the quantities $K_{bind_{plas}}$, K_{bind_E}, $k_{u,p}$, $k_{u,r}$, K_{in}, and K_{out}. However this first model calibration strategy failed to provide a good fit to data, thus given the assumption that our model is correct purely allometric scaling fails for this study (Fig. 4.3 and Table. 4.3)). I have not been able to find an equivalent model within the literature for oxaliplatin so model comparison or validation was not possible in this way.

Next, to provide a better data fit and understand the species difference between human and rat PK, only one of the estimated parameters was allowed to be different with respect to species. The model fitting was run while changing which of the parameters was estimated directly for each species (Table. 4.3).

The final model kept all parameters scaled to each species except for the plasma binding parameter since this had higher a R^2 value than all other options (Fig.4.4). The model fit was good with an R^2 of 0.96. Model long term behaviour is shown to not have settled down completely after 24hours is may be a limitation of the model however no details exist over this time frame so can not be verified. The values and confidence intervals of all parameters can be seen in Table 4.4 and Fig 4.5. The final values for binding rates in the plasma for humans was twice as large as that for rats whereas the maximum difference in protein levels was approximately 1.2 times as large. No other protein level could be found within the literature that could

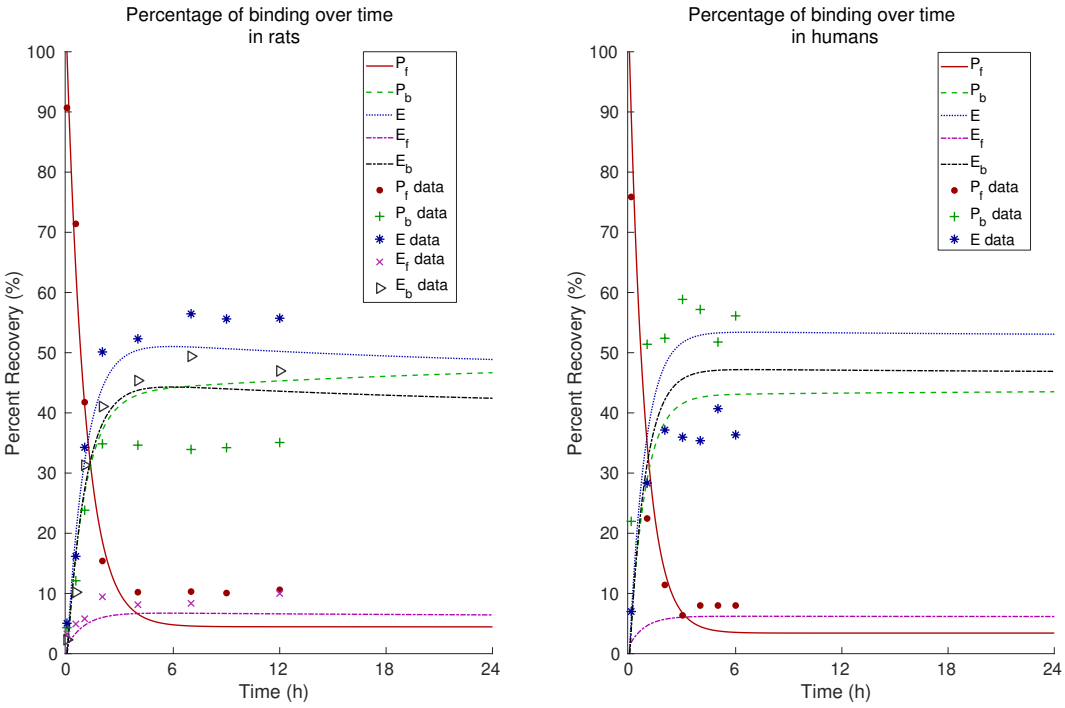

Fig. 4.3 Version 1 of the in vitro model where all parameters are kept equal for both species while being scaled with allometric values.

Parameter fitted by species	R^2		
	Rat	Human	Combined
None	0.9220	0.3994	0.7677
Plasma binding	0.9711	0.9477	0.9641
RBC binding	0.9350	0.8434	0.9080
Unbinding Plasma	0.9385	0.8773	0.9204
Unbinding RBC	0.9307	0.8369	0.9031
Uptake	0.9377	0.8440	0.9101
Efflux	0.9363	0.8526	0.9116

Table 4.3 R^2 values for the different versions of the model. The first column describes which parameter was fitted directly to each species. R^2 values are shown for the rat data the human data and the combined data (R^2 of model fit to both data sets simultaneously). Note the fitting process was always done on the combined data.

replicated this large difference. All parameters were shown to be practically locally identifiable from these datasets using likelihood profiles (see Fig. 4.5).

Next, the developed scaling method was used to investigate oxaliplatin in vitro PK in mice, as they are one of the main species utilised in preclinical studies. All parameters except the plasma binding rate were scaled using allometric equations as described above. Mouse values were 5.6 g/dl of total plasma protein, 14.2 g/dl of haemoglobin, cell count of 9.48 million cells/mm^3, a haematocrit of 46% [233] and

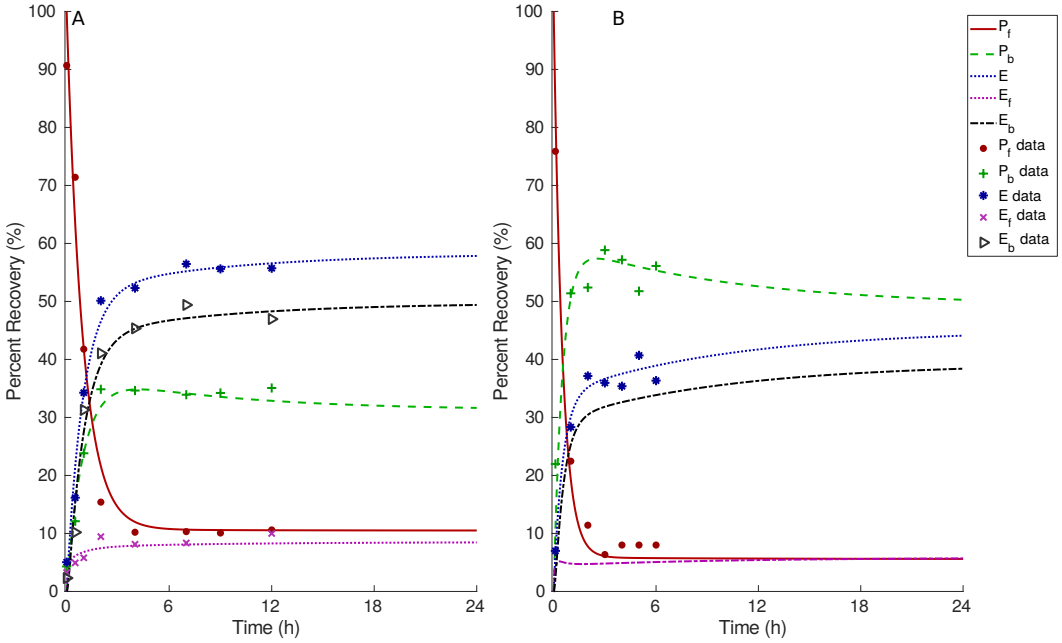

Fig. 4.4 Fit of oxaliplatin in vitro PK model to in vitro blood binding data for rats (A), and humans (B) taken from [7, 8], with plasma protein binding parameters differing between species. f and b subscripts refer to the free and bound sections within each compartment.

Symbol	Parameter Description	Value (ml/h)	Confidence interval (ml/h)
$k^r_{bind_{plas}}$	Plasma binding rat	0.2066	0.198-0.216
$k^h_{bind_{plas}}$	Plasma binding human	0.4900	0.473-0.508
k_{bind_E}	RBC binding	0.6747	0.895-1.860
$k_{u,p}$	Unbinding plasma	0.4093	0.370-0.449
$k_{u,r}$	Unbinding RBC	2.6399	1.891-4.302
K_{in}	RBC uptake	0.2775	0.264-0.290
K_{out}	RBC efflux	0.1919	0.165-0.224

Table 4.4 Best-fit parameters for oxaliplatin in vitro PK model. Confidence intervals were obtained using likelihood profiles.

a surface area of 0.91 mm^2 [14]. The plasma binding rate was assumed to vary in the interval [0.2, 0.5] which corresponds to the union of the parameter confidence intervals obtained for rat or human data, this was chosen as no information could be found on possible variations between mice and humans or rats. Time-concentration profiles for 10 different values of plasma binding rates are shown in Fig 4.6. The change in proportion of platinum found in each of the compartments is significant and can also be seen in the data for rats and humans, with humans having the majority of platinum in the plasma and the larger plasma binding rate while rats having the converse.

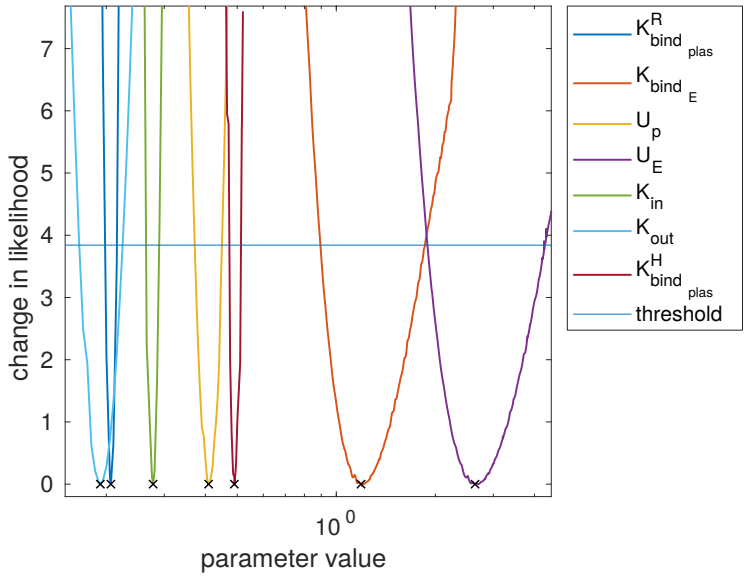

Fig. 4.5 Local identifability plot for parameter of the in vitro PK model. For a parameter to be identifiable the likelihood needs to cross the threshold twice. The threshold is set at 0.95 quantile of the χ^2-distribution with degrees of freedom of 1. The width between the two crossing points is the pointwise confidence interval of the parameters.

4.2.4 Discussion

A physiologically based model of oxaliplatin in vitro PK together with a scaling method were developed in order to reliably predict the drug transport and binding for different species. The model obtained a good level of fit (R^2=0.96, Table 4.3) to the rat and human data while only having a single parameter (plasma protein binding) differ between the two species, all other parameters being scaled using physiological measurements. The model was also shown to be structurally globally identifiable and locally practically identifiable. The scaling of the parameters could account for the variance between the drug PK in the two different species. In order to keep parameter overlap at a maximum and increase translational potential, only single parameter changes were investigated. Model fits may be improved if more parameters were fitted for each species but this would also be counter productive for the purpose of the model and has therefore not been investigated in this work. The parameter which was changed in order to provide the best fit was binding of platinum in plasma proteins. No allometric scaling related to the concentration of the most abundant proteins in the plasma could be found to explain the large difference in binding rates between the two species (albumin, globulin, total protein etc) and binding in the plasma is predominantly to albumin [60]. The molecular weight of albumin was also investigated as a potential scaling method, however this could not account for such a large difference in binding rates of the two species either. The affinity of oxaliplatin

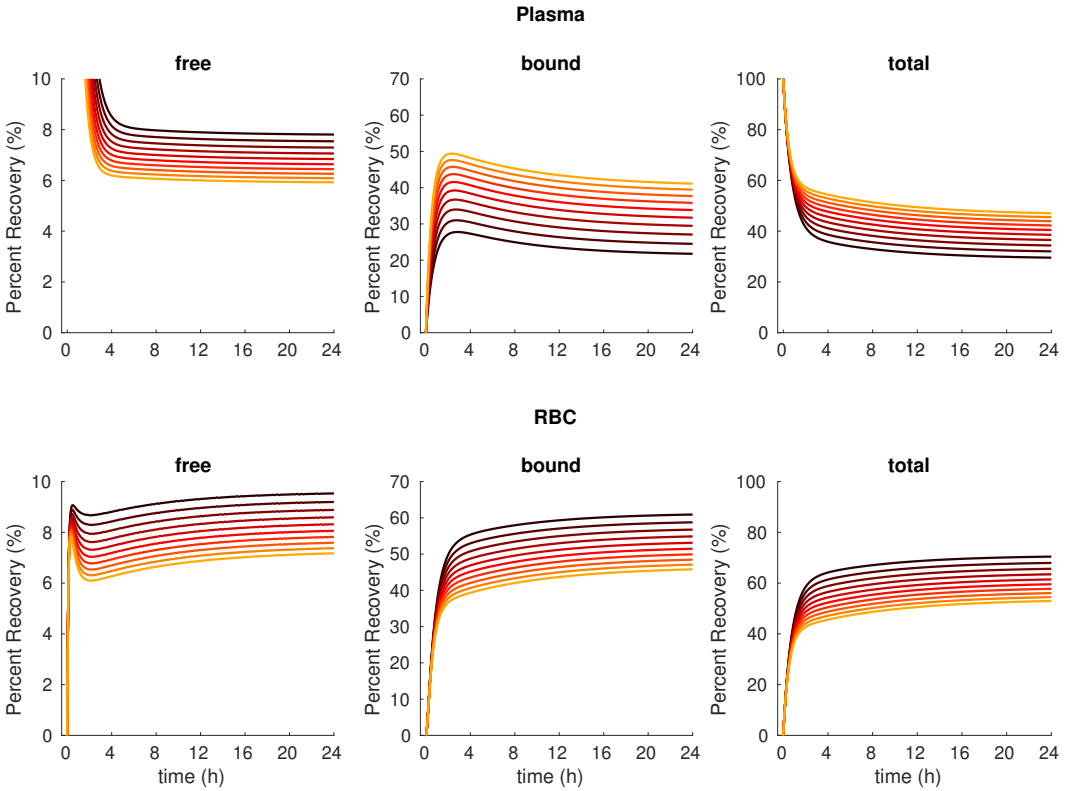

Fig. 4.6 Output of oxaliplatin in vitro PK model calibrated for mice, with plasma binding parameter varied between 0.2 (orange) and 0.5 (black), with a set size of 0.03.

binding to most abundant proteins in the blood should therefore be investigated in order to create a better scaling method, which could then be used to create a translational model of oxaliplatin.

With a model that can now accurately predict oxaliplatin in vitro PK for humans and rats, an example of potential dynamics was shown for mice. Varying the plasma binding rate has an impact on the percentage of the dose that is recovered from each compartment (Fig 4.6). In particular the change in binding has a large impact on whether the RBC or the plasma has the majority of the total dose. This shows that for this model to be used for another species, quantitative information on the binding affinity of oxaliplatin with the different plasma proteins in each species would be required. This study clearly demonstrates that in order to create translational PBPK models, details on the exact reactions and interactions of drugs at the cellular level need to be incorporated in the inter-species scaling. This model can now be used to give smaller search ranges based on confidence intervals for parameters in a larger more complex whole body PBPK models.

The model of oxaliplatin in vitro PK in the whole blood and the developed scaling method can be used in the design of a whole body model of oxaliplatin PK. The in vitro model will be used as the blood compartments of the whole body model. The

parameters of binding/unbinding and RBC transport can now be used directly to reduce the number of unknown parameters in the whole body model. This multi-scale method of fitting models is very important for creating identifiable models that can describe the complex drug PK at the level of a whole organism [155].

4.2.5 Future Work

To verify the quality of this model and its ability to scale between species, in vitro data of Pt PK in mouse whole blood will be incorporated into the model. The data will be from an experiment which is currently running at INSERM U935 (Villejuif, France). The data will be as close to the available experimental datasets in rat and human blood as possible and will consist of PK longitudinal measurements of bound and free platinum amounts in the plasma and RBC.

In order to verify the model, all parameters will be kept the same except the plasma binding. Each of the allometric scaling values will be updated with the mouse equivalent. The plasma binding parameter will then be fit to the new data using the CMAES algorithm and a least squares cost function. Achieving a good fit to the new data will show that this method can be used as a basis for predicting species-specific oxaliplatin PK and corresponding parameter values.

4.3 Physiologically based whole body model of oxaliplatin pharmacokinetics: A framework to explore sex dimorphism in circadian toxicity

4.3.1 Introduction

Standardised guidelines for medical treatment have been the status quo for many years, however recently the idea of personalised medicine has begun to gain traction with the UK and USA bringing in strategies and initiatives to develop methods to replace the “one size fits all” approach [22]. Personalised medicine can be broken down into different levels of personalisation, from stratification, which is reducing population to smaller biologically relevant groupings, to precision, which is designing treatment to the exact biology of an individual patient. Each level can lead to improved outcomes, however, each level of personalisation also comes at a cost, and this cost needs to be balanced with the benefits of the personalisation [234]. Therefore methods need to be designed with a simple stratification or test that will still bring benefits to patients.

One of the possible types of personalisation is chronotherapy, which is giving treatment relative to a patient's circadian clock. The benefit of giving treatments relative to optimal circadian timings has been shown in both preclinical and clinical settings [1, 2, 235] although it is still not broadly applied in medical practice [32]. One of the problems that is limiting the use of chronotherapy is the lack of reliable, inexpensive and noninvasive measurement methods of key circadian rhythms [32]. Initial and promising work has been done, by multiple groups to try and build such methods [135, 236, 237]. If the connection between important pathways relating to the PK of a drug can be linked to specific circadian biomarkers this could vastly improve the personalisation of chronotherapy.

An intuitive method of stratification within the human population is by sex. It has been evident, for a number of years, that there is a sexual dimorphism in human disease, drug pharmacokinetics (PK) and pharmacodynamics (PD), and in the circadian timing system (CTS) [238–240]. The sex specific difference in efficacy of chronotherapy treatment has been demonstrated in mice for irinotecan [3] and more recently in humans [5]. In fact the recent clinical trial from Levi et al suggests that the optimal timing of irinotecan for females is between 4-7 hours later than males, and when taken at its optimal timing can reduce the chance of high grade toxicities significantly [5]. These findings motivated the exploration of whether similar phenomena exists for oxaliplatin. It has already been shown that oxaliplatin has circadian influences on PK and initial unpublished results have shown that there is also a sex specific difference in both timing and maximum tolerated dose. It is now important to understand what drives circadian differences in PK/PD effects and sex specific timings.

In order to build the required understanding a mathematical framework has been developed. This framework draws upon mathematical tools to develop models in order to simulate the pharmacokinetic profiles. Since the data will be from mice, the data can come from a large range of organs and therefore allow the use of whole body models. Whole body pharmacokinetic models (WBPK) or physiologically based pharmacokinetic models (PBPK) aim to be a physiologically realistic representation of the body with parameters taking on biological meaning [241]. Although there is no concrete definition of either WBPK or PBPK they are usually related to whether the overall structure has been developed based on physiological structure and before the fitting stage has taken place, rather than being determined by the best fit to data [242]. The use of this type of model can help inform biologists and clinicians which parameters have the largest influence on different features of treatment and can give the opportunity to find specific biomarkers to link between pathways and treatment outcomes.

4.3.2 Model Design

A whole body pharmacokinetic (WBPK) model has been developed in order to understand the cause of circadian differences in PK levels of oxaliplatin observed within data. This WBPK model of oxaliplatin takes into account the most significant physiological compartments, with regard to desired clinical effect, toxicity and clinical measurement sites.

The blood is an important compartment to model as it will be the main connecting compartment for the whole model, the site for delivery of the initial dose of oxaliplatin and is also the main site of clinical measurements of PK data in humans. Blood is split into two sub-compartments, plasma and red blood cells (RBC). This is to capture the dynamics, demonstrated in section 4.2, of oxaliplatin moving into the RBCs and no longer being able to move to other compartments. Within the blood sub-compartments, plasma and the RBC, binding to proteins can also occur. This is key to the dynamics since if oxaliplatin is bound to proteins it is assumed to be unable to move between compartments. Oxaliplatin can however unbind from these proteins and become free to move between compartments again. This behaviour of binding and unbinding to proteins is considered in all compartments within the model. Alongside this blood is considered to be the main route of clearance representing the renal clearance pathway, which accounts for 60% of total drug clearance after 24 hours within humans [60], this is used in the absence of available data for mice.

The organ compartments are: jejunum, liver and non-eliminating tissue (NET). The jejunum has been included into the model since one of the toxicities often observed with oxaliplatin is gastrointestinal i.e. nausea, vomiting and diarrhoea. The jejunum is also a clearance pathway from the body accounting for clearance of approximately 5% of the total delivered dose in humans [60], this is used in the absence of available data for mice. The liver is one of the main targets of oxaliplatin when used in colorectal cancer, since colorectal cancer metastasises to the liver [243] and is therefore of particular clinical significance. The final compartment included in the model is the NET. The NET is an aggregate of all tissues which oxaliplatin is likely to move between but no significant evidence of its effect can be found and no clearance can be achieved. The model schematic summarises the WBPK model (Fig. 4.7).

The model equations have been developed using the mathematical tools described in Section 2.1 and can be seen in equations 4.11[a-k]. Circadian oscillations were added to clearance from both the blood and the jejunum, as well as the transport parameters to liver and to the jejunum from the plasma and the binding in the red blood cells. This oscillation took the form of:

$$\left(1 + A \times \cos[\frac{2\pi}{24}(t - \phi)]\right) \tag{4.10}$$

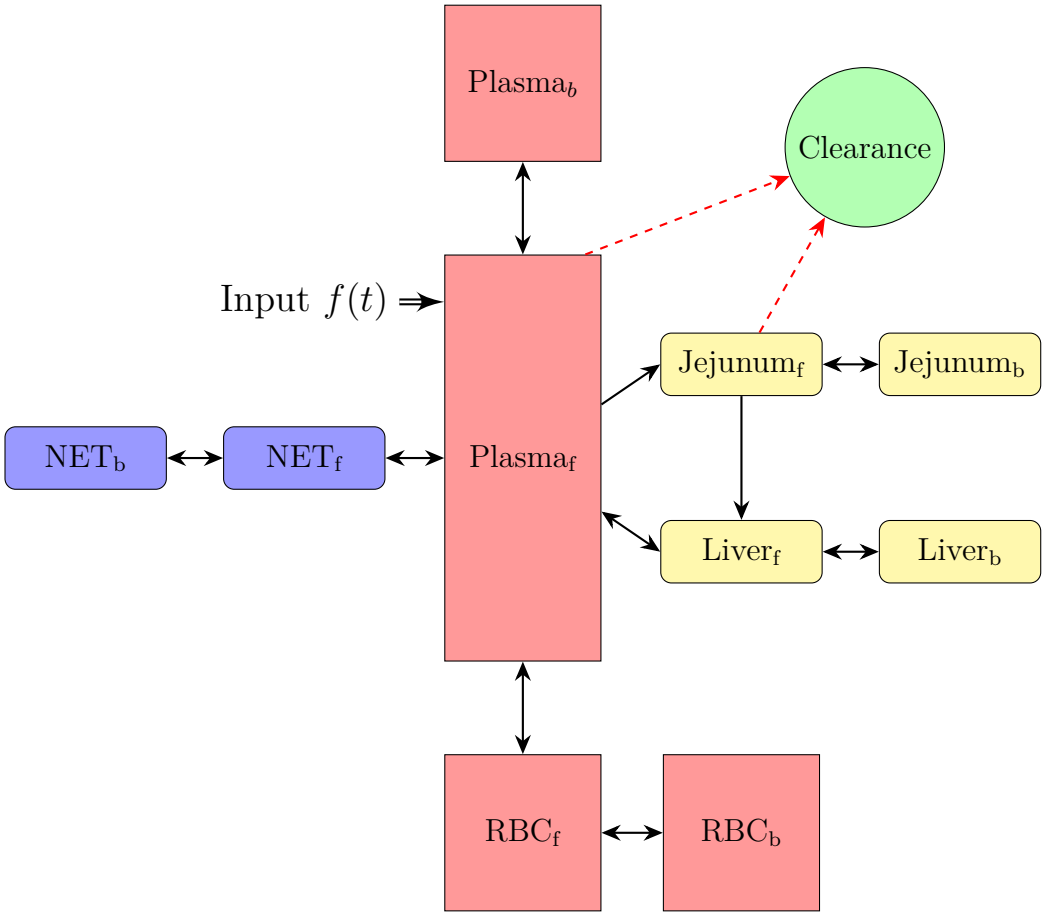

Fig. 4.7 Schematic of whole body pharmacokinetics model of oxaliplatin in mice. Red compartments are blood compartments, yellow represent the different tissues of interest and blue is the NET compartment for which we have no data since it consists of a large range of different tissues. The red arrows represent clearance from the system.

where A is the amplitude of the oscillations relative to the mean and ϕ is the time of the peak [244]. It is known that the clearance for both the blood and jejunum are likely to have their phase during the dark phase (since mice are nocturnal) [245, 246] so the phase will be restricted to the dark ZT i.e. 12-24 hours. The parameter names and description can be seen in table 4.5.

$$\frac{dP_f}{dt} = (f(t) + k_{(l,p)}L_f + k_{(n,p)}N_f + k_{(r,p)}R_f + k_{\text{unbind}}P_b - (k_{(p,l)} + k_{(p,n)} + k_{(p,r)} + +k_{(p,j)} + k_{(\text{bind},p)} + C_{blood})P_f)/V_p \quad (4.11a)$$

$$\frac{dP_b}{dt} = (k_{(\text{bind},p)}P_f - k_{\text{unbind}}P_b)/V_p \quad (4.11b)$$

$$\frac{dR_f}{dt} = (k_{(p,r)}P_f + k_{\text{unbind,e}}R_b - (k_{(r,p)} + k_{(\text{bind},r)})R_f)/V_r \quad (4.11c)$$

$$\frac{dR_b}{dt} = (k_{(\text{bind},r)}R_f - k_{\text{unbind,e}}R_b)/V_r \quad (4.11d)$$

$$\frac{dN_f}{dt} = (k_{(p,n)}P_f + k_{\text{unbind}}N_b - (k_{(n,p)} + k_{(\text{bind},n)})N_f)/V_n \quad (4.11e)$$

$$\frac{dN_b}{dt} = (k_{(\text{bind},n)}N_f - k_{\text{unbind}}N_b)/V_n \quad (4.11f)$$

$$\frac{dL_f}{dt} = (k_{(p,l)}P_f + k_{\text{unbind}}L_b + k_{(j,l)}J_f - (k_{(l,p)} + k_{(\text{bind},l)})L_f)/V_l \quad (4.11g)$$

$$\frac{dL_b}{dt} = (k_{(\text{bind},l)}L_f - k_{\text{unbind}}L_b)/V_l \quad (4.11h)$$

$$\frac{dJ_f}{dt} = (k_{(p,j)}P_f + k_{(c,j)}C_f + k_{\text{unbind}}J_b - (k_{(j,l)} + k_{(\text{bind},j)} + C_{Jej})J_f)/V_j \quad (4.11i)$$

$$\frac{dJ_b}{dt} = (k_{(\text{bind},j)}J_f - k_{\text{unbind}}J_b)/V_j \quad (4.11j)$$

(4.11k)

Observations for the data will be taken from the plasma, RBC, liver and jejunum as both free and total platinum.

$$P_f(T), \quad P_{tot}(T) = P_f(T) + P_b(T), \quad (4.12)$$

$$R_f(T), \quad R_{tot}(T) = R_f(T) + R_b(T), \quad (4.13)$$

$$L_f(T), \quad L_{tot}(T) = L_f(T) + L_b(T), \quad (4.14)$$

$$J_f(T), \quad J_{tot}(T) = J_f(T) + J_b(T) \quad (4.15)$$

where T in vector of time points (h)

$$T = [0.1667, 0.6667, 6, 24, 48, 72] \quad (4.16)$$

The input was considered as an initial condition, taken to be the total total dose and only present in the plasma_f compartment, all other compartments were considered empty. All compartmental volumes have been taken directly from literature.

Alongside the PK model there is also a PD model for the key area of toxicology, jejunum. The model is based on the Hill function discussed in section 2.1 and describes cell death due to drug concentration in the compartment. This process could be modelled in multiple ways depending on what the data require. The drug

effect could be considered as an inhibition of the production of cells (equation 4.17), or a stimulation of cell death (equation 4.18).

$$\frac{dR}{dt} = k_{in}\left(1 - \frac{E_{max}C^n}{C^n + EC_{50,j}^n}\right) - k_{out} \tag{4.17}$$

$$\frac{dR}{dt} = k_{in} - k_{out}\left(1 + \frac{E_{max}C^n}{C^n + EC_{50,j}^n}\right) \tag{4.18}$$

where E_{max} is the maximum effect of the drug, EC_{50} is the concentration in which the drug is at 50% maximum effect, k_{in} is production of new cells and a constant, k_{out} is natural cell death which is also constant, C is the concentrations of drug in the specific compartment and R is the response which in our case is the cell count in the effected tissue. The E_{max} parameter may also be considered circadian and becomes:

$$E_{max} = e_{max}\left(1 + A\cos[\frac{2\pi}{24}(\phi - t)]\right).$$

Parameter description	Parameter symbol
Transport from plasma to NET	$k_{(p,n)}$
Transport from plasma to red blood cells (RBC)	$k_{(p,r)}$
Transport from plasma to liver	$k_{(p,l)}$
Transport from plasma to jejunum	$k_{(p,j)}$
Transport from NET to plasma	$k_{(n,p)}$
Transport from RBC to plasma	$k_{(r,p)}$
Transport from liver to plasma	$k_{(l,p)}$
Transport from jejunum to liver	$k_{(j,l)}$
Unbinding of oxaliplatin from proteins in tissues and plasma	$k_{(\text{unbind})}$
Unbinding of oxaliplatin from proteins in RBC	$k_{(\text{unbind},e)}$
Binding in the plasma compartment	$k_{(\text{bind},p)}$
Binding in the NET compartment	$k_{(\text{bind},n)}$
Binding in the RBC compartment	$k_{(\text{bind},r)}$
Binding in the liver compartment	$k_{(\text{bind},l)}$
Binding in the Jejunum compartment	$k_{(\text{bind},j)}$
Clearance from Blood compartment	C_{blood}
Clearance from Jejunum compartment	C_{jej}

Table 4.5 Descriptions of parameters and the symbols used within the whole body pharmacokinetic model. The parameters units are ml/h.

The parameters in Table 4.5 will be fitted using CMAES and least squares methods discussed in section 2.2, except the parameters taken from the in vitro model. These are transport to and from RBC and the binding and unbinding in the RBC, as well as unbinding in plasma. The additional coefficients representing physiological values are taken from Brown et al [12], which gives a comprehensive list of physiological parameters and conversion methods for scaling between mass and volume, see Tables 4.6 and 4.7.

Table 4.6 Composition of NET and conversion from weight to volume. Relative weights of each organ and conversion to volume [12].

Organ	% of body weight	Conversion (g:ml)	Volume (ml)
Muscle	38.4	1:1	9.5
Skin	16.53	1:1.4519	6
Adipose tissue	6.84	1:2.1427	3.664

Table 4.7 Relative weights of each organ and conversion to volume [12].

Organ	% of body weight	Conversion (g:ml)	Volume (ml)
Bone Marrow	5.8	1:1	1.48
Liver	5.49	1:1	1.37
Jejunum	2.5[1]	1:1	0.625
NET	Shown above	n/a	19.164

[1] Total small intestine

4.3.3 Model fitting to published data

In order to give a proof of concept for the model, existing data were taken from two papers by Boughattas et al from 1989 and 1994 [2, 8]. The first data set was a single time point 24h post injection of oxaliplatin 17mg/kg. The data were mean values of four repeats for tissue concentration of platinum from three different times of injection (Halo, after light, 0, 8 and 16). The tissues data used in the fitting came from liver, RBC and jejunum but only at a single time point as data at any great level of detail are impractical in humans. The second data set consisted of 6 time points for mean concentration of platinum in RBC and both free and total platinum in the plasma for 162 male B6D2F1 mice given 17mg/kg of oxaliplatin at three different times of injection (Halo 0, 8 and 16) although data were combined as limited differences were observed in the experiments. The data were then combined into the three delivery times for blood, liver, RBC and jejunum. The data were fitted using least squares residuals and the CMAES algorithm in Python.

The fit to the published data set is good and, with the addition of circadian rhythms in relevant transport parameters, shows the model can successfully fit to

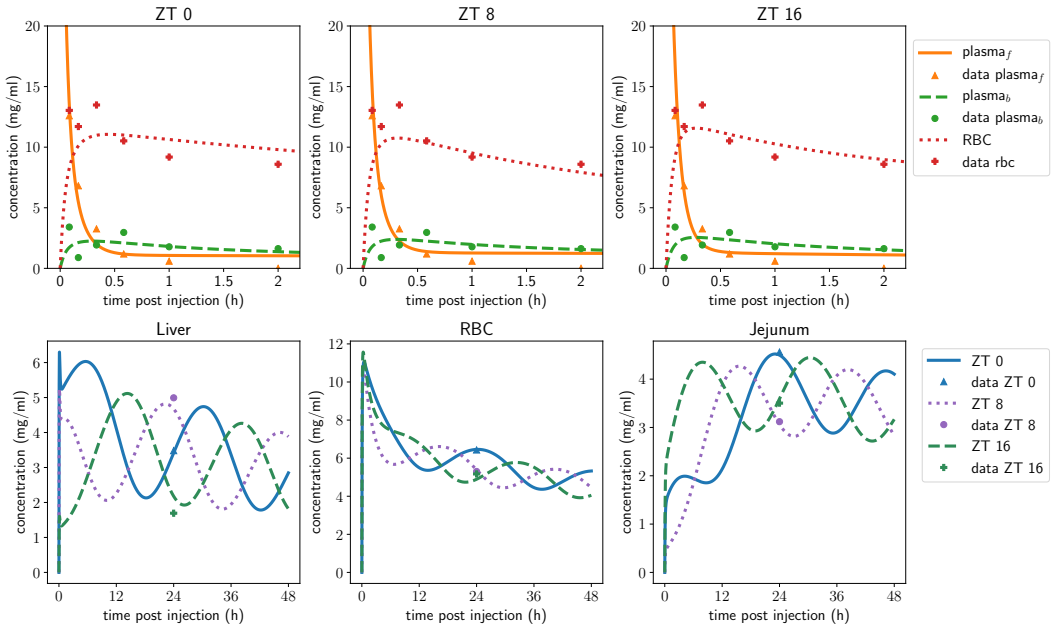

Fig. 4.8 Fit of whole body model to historical data taken from Boughattas et al 1989 and 1994. The top row shows the fit to blood samples at each different time of administration. The bottom row shows fit for each different time of administration in the liver red blood cells (RBC) and the jejunum.

real data. The data are obviously very sparse which would be a problem for practical identifiability. The inclusion of the circadian parameters was necessary to capture the significant differences in organs values for different delivery schedules.

4.4 Model identifiability

4.4.1 Structural identifiability

With the level of complexity and biological relevance in our model comes a large amount of parameters, which opens the model up to the problem of identifiability. The first step in assessing identifiability was to use the Differential Algebra for Identifiability of SYstems (DAISY) which is a package written in REDUCE that determines structural identifiability of models, further details can be found in section 2.3.2. Both the published data and the experimental data that will be available in the future take samples from each compartment of the model except the NET. The location of observations was input into DAISY alongside the model equations and initial conditions, input was considered as an initial condition, and analysed. The analysis revealed that the model was structurally globally identifiable with out the need for initial conditions to be included. It is important to note that structurally identifiable is not the same as practically identifiable. Structurally identifiable only says that theoretically given the “ideal” data in the indicated compartments the

model parameters will be identifiable. Practical identifiability is, given the actual data the parameters are identifiable. This is important since actual data will be noisy, sparse or both and this can effect the ability to find parameters accurately. Another limitation of DAISY is that it cannot give any indication on whether our circadian parameters are identifiable since there is no input of sample times of data.

4.4.2 Practical identifiability

Practical identifability will be evaluated by looking at the sensitivity of the cost function to the parameter set. Global sensitivity will be produced using Sobol sensitivity as outlined in Section. 2.3.6. Local sensitivity will be done by finding the best fit parameters then varying a single parameter at a time and observing the change in the cost function. Each parameter will be varied between lower and upper bounds with a thousand points and plotted. Sensitivity is determined by a change in cost as the parameter is varied. Parameter sensitivity does not guarantee practical identifiability however it is a necessary condition [172].

Published data

Sobol global sensitivity analysis, as described in section 2.3.6, shows that the model is most sensitive to transport from liver to plasma, platinum unbinding and clearance from the blood. It also shows that circadian parameters have negligible effect relative to the other parameters. This is not unexpected since any effect of the circadian parameters will be dependant on the transport or binding parameter they influence i.e. for the equations:

$$k_{i,j}\left(1 + k_{i,j_A} * \cos[\frac{2\pi}{24}(k_{i,j_\phi} - t)]\right) \tag{4.19}$$

$k_{i,j}$ would have more of an effect than the amplitude k_{i,j_A} or the phase k_{i,j_ϕ} (Fig 4.9).

Local analysis shows that the cost function is sensitive to all parameters apart from blood clearance phase and amplitude (Fig. 4.10). It can be seen from the scales of the plots the magnitude of the change for the circadian parameters is significantly lower which agrees with the global sensitivity.

Future experimental data

The synthetic data are created by first using the parameters fitted to the published data. The output from the model is then reduced to be the same number of time points and repeats as the experimental data. Multiplicative noise is then introduced to the data to make the data “realistic”, this is in the form of Gaussian white noise

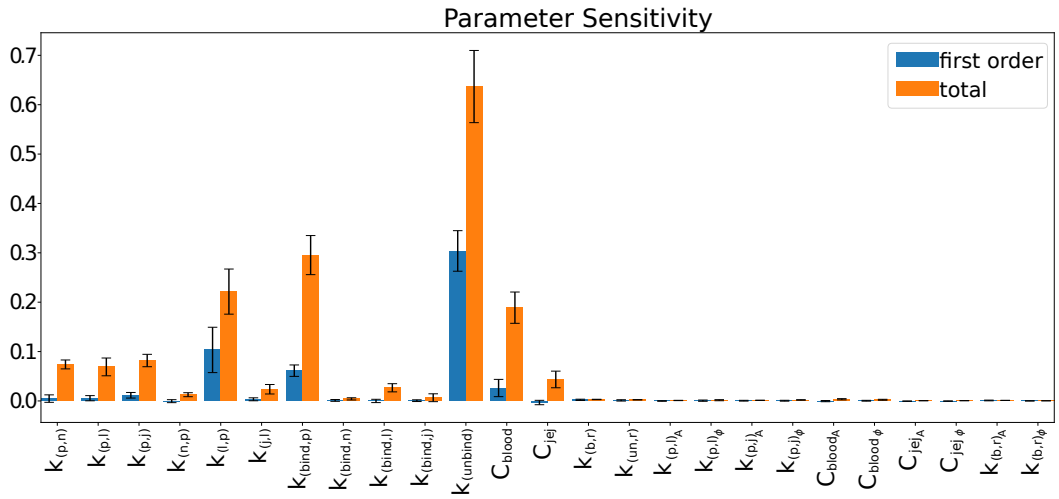

Fig. 4.9 Parameter sensitivity to cost function of published data from Boughattas et al 1989 and 1994 for whole body mouse model.

with mean 1 and standard deviation of 0.1. The cost function is then the least squares distance of the model from this data.

Global sensitivity was then assessed for these data. The sensitivity showed that the cost function was most sensitive to transport and binding/unbinding parameters and presented negligible relative sensitivity for the circadian parameters (Fig. 4.11).

Local sensitivity demonstrates the cost function is sensitive to all parameters apart circadian parameters for blood clearance and circadian parameters for plasma to liver transport (Fig. 4.12). The scales show again that the magnitude of effect on the cost function is significantly lower for circadian parameters.

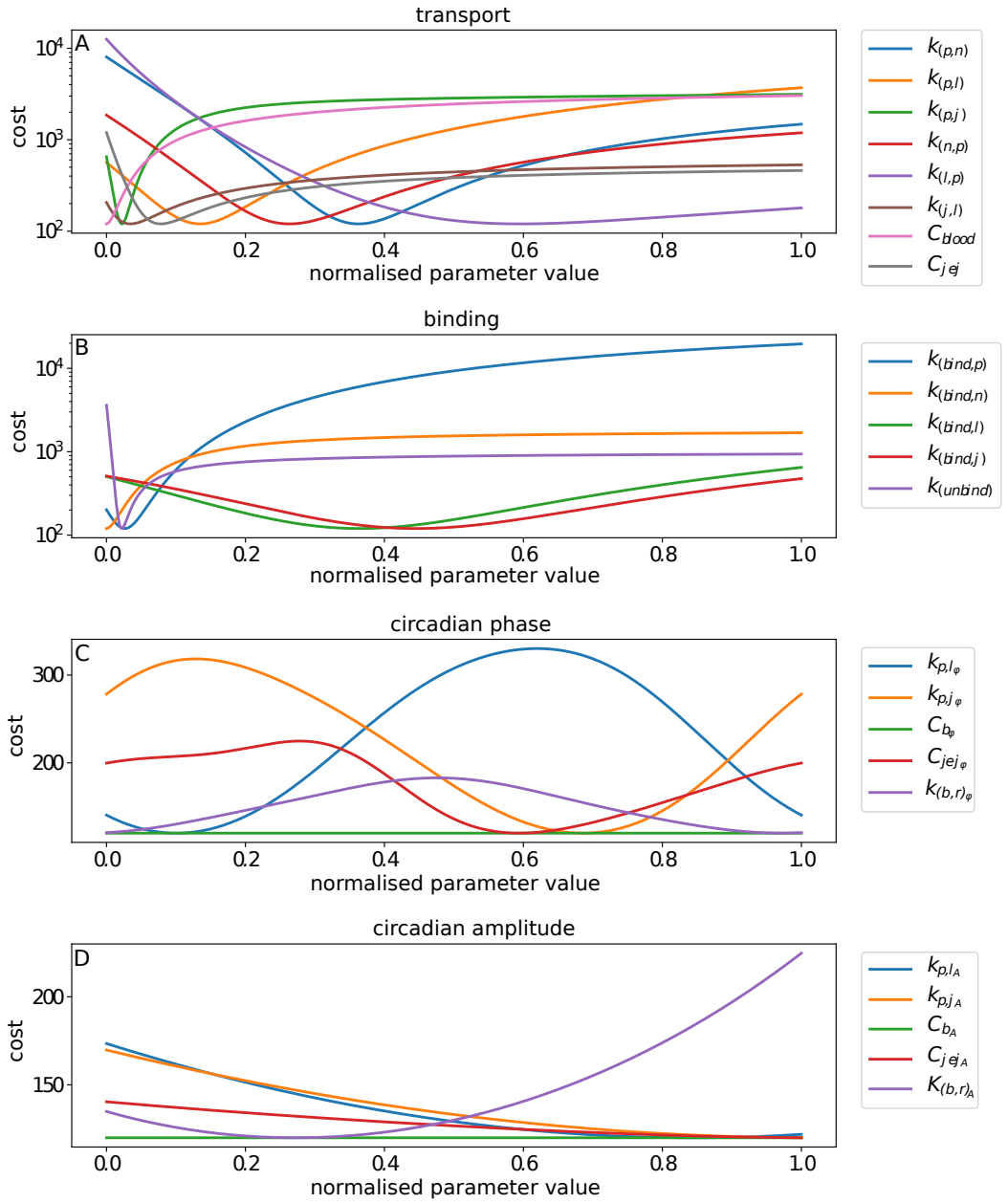

Fig. 4.10 Local sensitivity of parameters for cost function on published data from Boughattas et al 1989 and 1994. Each plot shows how cost varies as the parameter is moved through a range of parameters. The parameters have been split into groups with respect to their process.

4.4.3 Identifiability conclusion

The model has been shown to be structurally globally identifiable assuming availability of both the published data and the future experimental data. This is very good and also a fundamental prerequisite for parameter identifiability [160]. The published data has a large disparity relative to the impact of the parameters on the cost function, shown by both the sobol sensitivity and the local sensitivity, which may

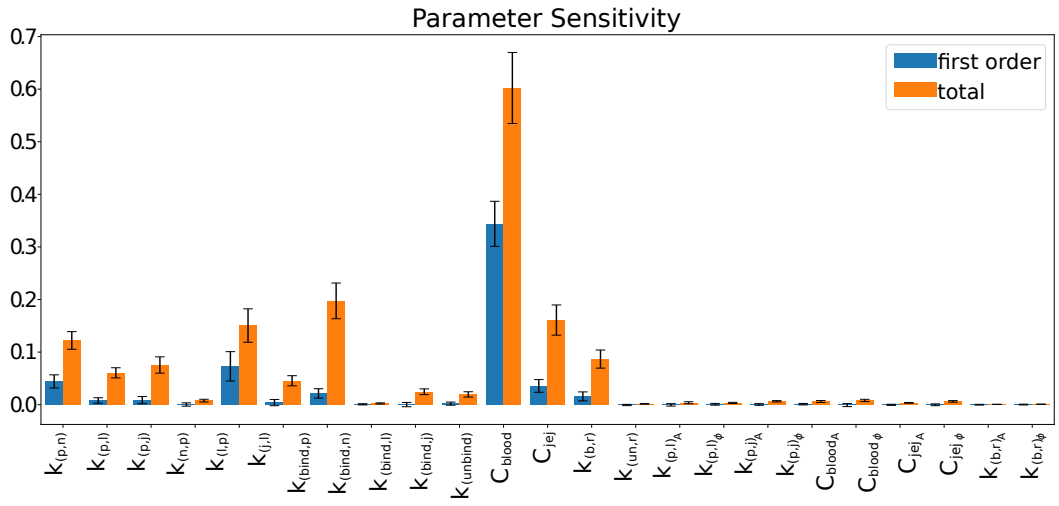

Fig. 4.11 Parameter sensitivity to cost function of the synthetic data for the whole body mouse model. With parameters ranging across full fitting range used in the initial parameter fitting to published data from Boughattas et al 1989 and 1994.

impact reliability of fit of some parameters. Since two parameters are not locally sensitive and others show a monotonically decreasing or increasing change in the cost function, the model is unlikely to be identifiable for this data set. The lack of influence of circadian parameters (amplitude and phase) of the clearance from the blood may be due to the fact that the published data in the blood was taken to be an aggregate of the three different times of administration. This aggregation was done as the blood data showed no significant differences between delivery times.

Global sensitivity of the synthetic data showed very similar profiles to the published data. The local sensitivity analysis showed that for the synthetic data the blood clearance phase and amplitude were not sensitive, which aligns with the model fitted to the published data from Bougattas et al. Local sensitivity also shows that the phase for transport between plasma and the liver has no impact on the cost function.

Overall, sensitivity analysis shows that the majority of parameters are sensitive and this is an encouraging sign for model identifiability, but if real data has the same sensitivity as synthetic data, the model will not be identifiable and some circadian parameters may need to be informed by the literature, removed from the model or extra experimental samples observed.

Once the real experimental data are available, sensitivity analysis will be evaluated on the new data set. To fully evaluate the practical identifiability of the model, the method of likelihood profiles will be used as for Chapter 3. However, due to the large number of parameters and the complexity of the model, an optimised way

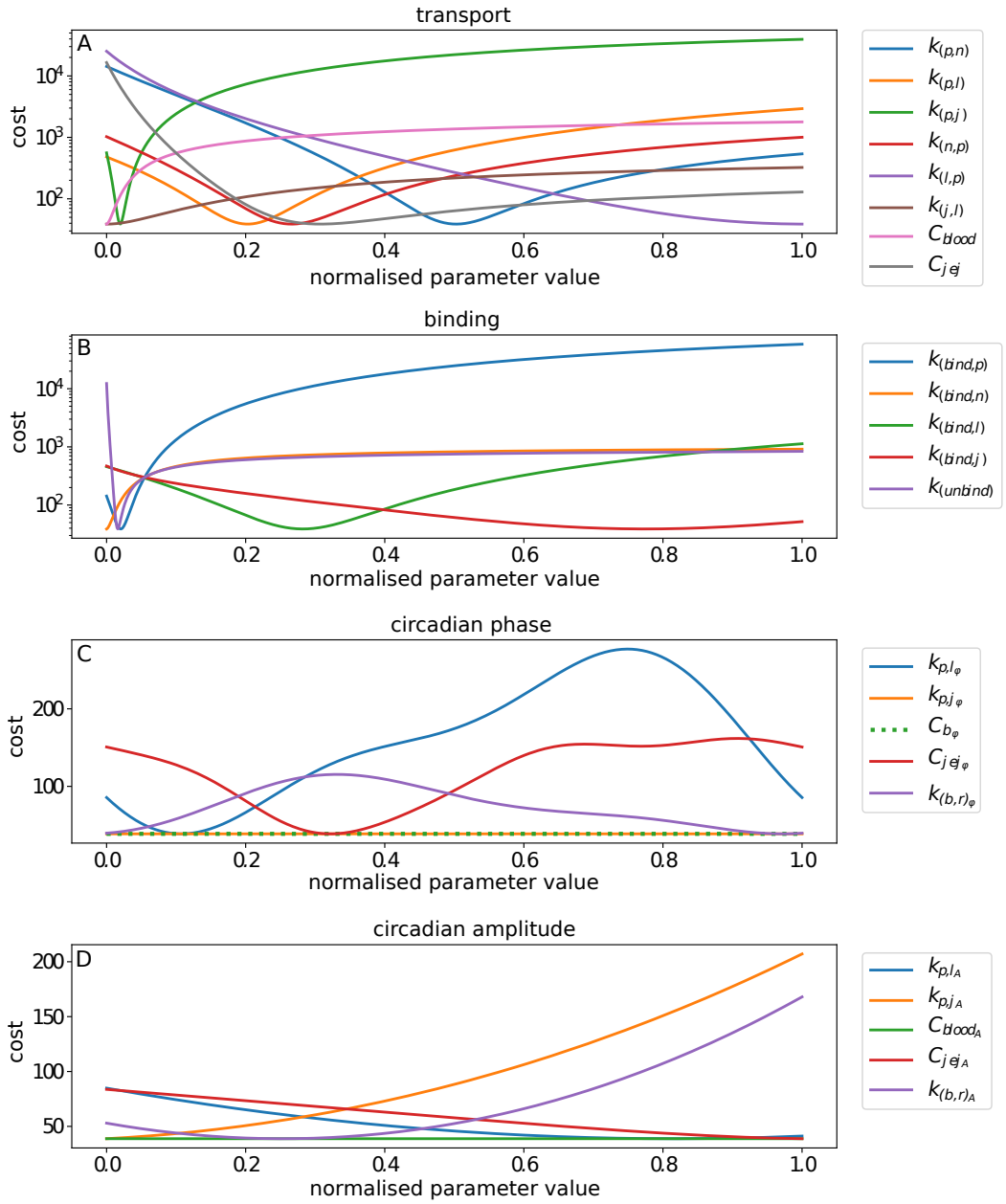

Fig. 4.12 Local sensitivity of parameters for cost function on synthetic data. Each plot shows how cost varies as the parameter is moved through a range of parameters. The parameters have been split into groups with respect to their process.

of simulating the likelihood profile method would be required to allow for reduced simulation time.

4.4.4 Future work

The fitting of the model could be done for males and females separately, using the CMAES algorithm with the distance from model simulation to data points measured

by the least squares approach. Once the fit of the model is satisfactory (R^2 value of over 0.95) the residual errors will be assessed using graphical plots. With an accurate fit to PK in all the compartments, parameter sensitivity analysis can be evaluated. Sensitivity analysis could also be undertaken on the fixed volumes of each compartment to see if inter-patient/specimine variation would have a significant effect on PK outcomes.

The evaluation of sensitivity could be done using the Sobol method discussed in Section 2.3.6 and local sensitivity in a similar fashion to Section 4.4. Parameters would first need to be tested for circadian influence on the jejunum PK since this is where we want the therapeutic effect to take place and where major toxicity is observed. The parameters would also need to be investigated to see which of the non-circadian parameters has the greatest effect on concentrations in the organs of interest. This could be done by looking into sensitivity of a given measurement such as the area under the curve (AUC) relative to the different parameters.

After characterising parameter influence on overall PK, sex specific differences in PK and tolerability have been completed, these results would need to be given biological meaning. To this end, a literature search of proteins and pathways relevant to the most influential parameters would be undertaken to look for evidence of circadian rhythms, previous evidence of the influence on oxaliplatin and potential biomarkers or gene polymorphisms that could impact the efficacy of their processes. If the search was fruitful then these would be suggested as potential biomarkers for treatment personalisation.

Another element which will be added to the model is the effects of oxaliplatin on the bone marrow and haematopoietic system. Bone marrow is the predominant site of blood cell production (haematopoiesis). Since myelosuppression (decreased bone marrow activity) is a possible side effect of the regimes which include oxaliplatin, experiments are currently running at INSERM U935 (Villejuif, France) to evaluate the effect of oxaliplatin treatment in the bone marrow of mice. In order to add these details into the model, the NET compartment would need to be separated into the bone marrow and the rest of NET so as to track the PK. A PD model would also be added to the bone marrow compartment. The bone marrow PD parameters would be fitted to the new data using CMAES and least squares residuals. With a successful fit this could give important information on how to reduce this often dose limiting side effect of oxaliplatin treatment regimes.

Chapter 5

Conclusion

This PhD thesis aimed to design mathematical models to allow for precise and personalised chronotherapeutics against gastrointestinal cancers towards improved treatment outcomes. My initial aim as set out in section 1.6.1, has been achieved in chapter 3 with an improve delivery profile being created and a novel method of patient stratification being outlined, however the method still needs to be verified on a larger patient cohort. The second main aim of this thesis has only been partly achieved due to unforeseen problems with data acquisition. A method of inter-species scaling was devised however needs to be verified with another species to show validity. A whole body model has been developed but has not been able to be fit to real world data and subsequently has not been able to give insight into sex specific differences. The full frame work is, however, ready to be used to complete these goals when data becomes available.

Chapter 3 designed a mathematical framework which allowed for accurate analysis of patient pharmacokinetic data from 11 patients receiving oxaliplatin, irinotecan and 5-fluorouracil via a chronomodulated pump into the hepatic artery. A representative model of the dynamics of the drug solution from the pump to the patient's blood was designed, irrespective of the drug delivery device. This model was used to represent the chronomodulated drug administration via the Mélodie infusion pump used within the study. The model revealed important inconsistencies between the drug profiles intended by clinicians and the simulated profiles patients may have been receiving. The model also allowed for the design of innovative drug infusion profiles which precisely match the desired drug delivery into the patient's blood. The pump-to-patient model was then used in connection with the semi-physiological models of the PK of irinotecan, oxaliplatin and 5-fluorouracil. The overall framework achieved a very good fit to data and gave insights into inter-patient variability in the PK of each drug. Potential clinical biomarkers for the personalisation of treatments were suggested although further investigations in larger cohorts of patients are required to confirm the validity of this work. Overall, the complete framework developed in

this chapter gives insight into drug delivery dynamics and patient-specific PK of irinotecan, oxaliplatin and 5-fluorouracil and could be used as a step towards the precise and personalised administration of these drugs.

Chapter 4 looks into preclinical models to deepen the knowledge of oxaliplatin PK, with a focus on inter-species scaling and a framework which could potentially give insight into sex dimorphism. An in vitro physiologically based model was developed with the intention to be able to scale between species. The model showed a good fit to the rat and human data and is globally structurally identifiable and at least locally practically identifiable. Allometric scaling by itself could not explain the difference in the drug PK between the two different species. However, a single parameter, plasma binding, needed to be fit specifically to each species to fit all data. This work implies that the binding affinity of oxaliplatin to serum proteins of multiple species should be investigated, if a translational model of oxaliplatin were to be created. The model was then used to provide possible predictions for mouse PK and revealed that the proportion of platinum found in each compartment was shown to be highly dependent on this binding parameter. This in vitro model was then used in a multi-scale fashion to inform the whole body model of oxaliplatin PK in mice, thus reducing model parameters and improving identifiability.

Chapter 4 continues by developing a whole body model of oxaliplatin PK in mice. The model has a strong physiological grounding, with all compartmental volumes being taken from literature. As a proof of concept, the model is shown to fit historical data successfully. The model is then fit to synthetic data which takes the form of future data which is currently being gathered. Sensitivity analysis shows the cost function is sensitive to most parameters, although not for the three circadian parameters. Analysis of the whole model showed it is structurally identifiable with the given observation locations which is a fundamental prerequisite to practical identifiability. The framework for future model analysis is then outlined. The model when fitted successfully will be able to give insights into the sex dependent differences in oxaliplatin chronotoxicity and direct biological research as to how oxaliplatin chrono-infusion could be personalised in the future.

As more data become available and the benefit of chronotherapy becomes more apparent, mathematical modelling, as outlined in this thesis, has the potential to become more important. The combination of mathematical models and biological experiments may give a much great quality of information and help progress the personalisation and improvement of treatments for digestive cancers.

References

[1] A. Ballesta, P. F. Innominato, R. Dallmann, D. A. Rand, and F. A. Lévi, "Systems Chronotherapeutics," *Pharmacological Reviews*, vol. 69, no. 2, pp. 161–199, 2017.

[2] N. A. Boughattas, F. Levi, C. Fournier, G. Lemaigre, A. Roulon, B. Hecquet, G. Mathe, and A. Reinberg, "Circadian rhythm in toxicities and tissue uptake of 1,2-diamminocyclohexane(trans-1)oxalatoplatinum(II) in mice," *Cancer Research*, vol. 49, no. 12, pp. 3362–3368, 1989.

[3] X. M. Li, A. Mohammad-Djafari, M. Dumitru, S. Dulong, E. Filipski, S. Siffroi-Fernandez, A. Mteyrek, F. Scaglione, C. Guettier, F. Delaunay, and F. Lévi, "A circadian clock transcription model for the personalization of cancer chronotherapy," *Cancer Research*, vol. 73, no. 24, pp. 7176–7188, 2013.

[4] F. Lévi, A. Altinok, J. Clairambault, and A. Goldbeter, "Implications of circadian clocks for the rhythmic delivery of cancer therapeutics," *Philosophical Transactions of the Royal Society A: Mathematical, Physical and Engineering Sciences*, vol. 366, no. 1880, pp. 3575–3598, 2008.

[5] F. Levi, C. Garufi, A. Karaboué, C. Focan, P. Chollet, X.-M. Li, and P. Innominato, "Sex-related differences in circadian-dependent tolerance of Irinotecan (I) added to chronomodulated (chrono) 5-Fluorouracil (F), Leucovorin (L) and Oxaliplatin (O): Final results from international randomised time-finding study in patients with metast," *Annals of Oncology*, vol. 28, sep 2017.

[6] F. Lévi, A. Karaboué, M.-C. Etienne-Grimaldi, G. Paintaud, C. Focan, P. Innominato, M. Bouchahda, G. Milano, and E. Chatelut, "Pharmacokinetics of Irinotecan, Oxaliplatin and 5-Fluorouracil During Hepatic Artery Chronomodulated Infusion: A Translational European OPTILIV Study," *Clinical Pharmacokinetics*, pp. 1–13, 2016.

[7] F. R. Luo, S. D. Wyrick, and S. G. Chaney, "Biotransformations of oxaliplatin in rat blood in vitro.," *Journal of biochemical and molecular toxicology*, vol. 13, no. 3-4, pp. 159–69, 1999.

[8] N. A. Boughattas, B. Hecquet, C. Fournier, B. Bruguerolle, H. Trabelsi, K. Bouzouita, B. Omrane, and F. Levi, "Comparative pharmacokinetics of oxaliplatin (L-OHP) and carboplatin (CBDCA) in mice with reference to circadian dosing time," *Biopharmaceutics and Drug Disposition*, vol. 15, no. 9, pp. 761–773, 1994.

[9] J. N. Vauthey, E. K. Abdalla, D. A. Doherty, P. Gertsch, M. J. Fenstermacher, E. M. Loyer, J. Lerut, R. Materne, X. Wang, A. Encarnacion, D. Herron, C. Mathey, G. Ferrari, C. Charnsangavej, K. A. Do, and A. Denys, "Body surface area and body weight predict total liver volume in western adults," *Liver Transplantation*, vol. 8, no. 3, pp. 233–240, 2002.

[10] S. B. Nadler, J. U. Hidalgo, and T. Bloch, "Prediction of blood volume in normal human adults," *Surgery*, vol. 51, pp. 224–232, feb 1962.

[11] J. Sendroy and H. A. Collison, "Determination of human body volume from height and weight.," *Journal of Applied Physiology*, vol. 21, no. 1, pp. 167–172, 1966.

[12] R. P. Brown, M. D. Delp, S. L. Lindstedt, L. R. Rhomberg, and R. P. Beliles, "Physiological parameter values for physiologically based pharmacokinetic models," *Toxicology and Industrial Health*, vol. 13, no. 4, pp. 407–484, 1997.

[13] C. River, "Baseline Hematology and Clinical Chemistry Values for Charles River Wistar Rats [Crl:(WI)BR] as a Function of Sex and Age (Spring 1998)," 1998.

[14] I. Udroiu, "Estimation of erythrocyte surface area in mammals," *arXiv preprint arXiv:1403.7660*, pp. 0–7, 2014.

[15] J. Barth and J. K. Rae, "Harmonisation of Reference Intervals President, Association for Clinical Biochemistry," *Pathologyharmony.co.uk*, no. January, 2011.

[16] G. Schlager and R. S. Weibust, "Selection for hematocrit percent in the house mouse," *J Hered*, vol. 67, no. 5, pp. 295–299, 1976.

[17] J. Cafasso and A. Gotter, "Red Blood Cell Count (RBC): Purpose, Procedure, and Preparation," 2017.

[18] a. Besarab, W. K. Bolton, J. K. Browne, J. C. Egrie, a. R. Nissenson, D. M. Okamoto, S. J. Schwab, and D. a. Goodkin, "The effects of normal as compared with low hematocrit values in patients with cardiac disease who are receiving hemodialysis and epoetin.," *The New England journal of medicine*, vol. 339, no. 9, pp. 584–90, 1998.

[19] V. Patel, "Deaths registered in England and Wales 2017," tech. rep., Office of National Statistics, 2018.

[20] M. R. Trusheim, E. R. Berndt, and F. L. Douglas, "Stratified medicine: Strategic and economic implications of combining drugs and clinical biomarkers," *Nature Reviews Drug Discovery*, vol. 6, no. 4, pp. 287–293, 2007.

[21] E. Abrahams, G. S. Ginsburg, and M. Silver, "The Personalized Medicine Coalition Goals and Strategies," *American Journal of Pharmacogenomics*, vol. 5, no. 6, pp. 345–55, 2005.

[22] S. Day, R. C. Coombes, L. McGrath-Lone, C. Schoenborn, and H. Ward, "Stratified, precision or personalised medicine? Cancer services in the 'real world' of a London hospital," *Sociology of Health and Illness*, vol. 39, no. 1, pp. 143–158, 2017.

[23] S. Bates, "Progress towards personalized medicine," *Drug Discovery Today*, vol. 15, no. February, pp. 115–120, 2010.

[24] F. Ciardiello, D. Arnold, P. G. Casali, A. Cervantes, J.-Y. Douillard, A. Eggermont, A. Eniu, K. McGregor, S. Peters, M. Piccart, R. Popescu, E. V. Cutsem, C. Zielinski, and R. Stahel, "Delivering precision medicine in oncol- ogy today and in future—the promise and challenges of personalised cancer medicine: a position paper by the European Society for Medical Oncology (ESMO)," *Annals of Oncology*, vol. 25, no. 9, pp. 1673–1678, 2014.

[25] N. Rahman and and Michael R. Stratton, "The Genetics of Breast Cancer Susceptibility," *Annual Review of Genetics*, vol. 32, no. 1, pp. 95–121, 1998.

[26] S. E. Jackson and J. D. Chester, "Personalised cancer medicine," *International Journal of Cancer*, vol. 137, no. 2, pp. 262–266, 2015.

[27] L. Lostumbo, C. Ne, and J. Wallace, "Prophylactic mastectomy for the prevention of breast cancer (Review)," *Cochrane Database of Systematic Reviews*, no. 11, 2010.

[28] E. Half, D. Bercovich, P. Rozen, E. E. Half, D. Bercovich, and P. Rozen, "Familial adenomatous polyposis," *Orphanet JOurnal of Rare Disesases*, vol. 4, no. 22, pp. 1–23, 2009.

[29] A. Kartheuser, P. Stangherlin, D. Brandt, C. Remue, and C. Sempoux, "Restorative proctocolectomy and ileal pouch-anal anastomosis for familial adenomatous polyposis revisited," *Familial Cancer*, vol. 5, pp. 241–260, 2006.

[30] K. C. S., K.-F. Shirin, J. D. J., O. C. J., T. Dongsheng, T. N. C., S. R. John, C. Haji, S. J. D., R. Sonia, P. T. J., S. Lois, A. Heather-Jane, L. Christiane, M. M. J., and Z. J. R., "K-ras Mutations and Benefit from Cetuximab in Advanced Colorectal Cancer," *New England Journal of Medicine*, vol. 359, no. 17, pp. 1757–1765, 2008.

[31] Q. Yan, "Circadian Biomarkers and Chronotherapy: Implications for Personalized and Systems Medicine," in *Cellular Rhythms and Networks: Implications for Systems Medicine*, pp. 71–81, Cham: Springer International Publishing, 2015.

[32] J. M. Selfridge, T. Gotoh, S. Schiffhauer, and J. Liu, "Chronotherapy : Intuitive , Sound , Founded ... But Not Broadly Applied," *Drugs*, vol. 76, no. 16, pp. 1507–1521, 2016.

[33] A. Stein and D. Arnold, "Oxaliplatin: a review of approved uses," *Expert Opinion on Pharmacotherapy*, vol. 13, pp. 125–137, jan 2012.

[34] Cancer Research UK, "Bowel cancer incidence statistics," 2019.

[35] J. Ferlay, M. Colombet, I. Soerjomataram, T. Dyba, G. Randi, M. Bettio, A. Gavin, O. Visser, and F. Bray, "Cancer incidence and mortality patterns in Europe: Estimates for 40 countries and 25 major cancers in 2018," *European Journal of Cancer*, vol. 103, pp. 356–387, 2018.

[36] Z. Momenimovahed and H. Salehiniya, "Incidence, mortality and risk factors of cervical cancer in the world," *Biomedical Research and Therapy*, vol. 4, no. 12, p. 1795, 2017.

[37] Cancer Research UK, "Bowel cancer incidence statistics," 2016.

[38] Cancer Research UK, "Chemotherapy drugs | Bowel cancer | Cancer Research UK," 2016.

[39] C. R. Culy, D. Clemett, and L. R. Wiseman, "Oxaliplatin: A review of its pharmacological properties and clinical efficacy in metastatic colorectal cancer and its potential in other malignancies," *Drugs*, vol. 60, no. 4, pp. 895–924, 2000.

[40] S. P. Joel, D. Papamichael, F. Richards, T. Davis, V. Aslanis, E. Chatelut, K. Locke, M. L. Slevin, and M. T. Seymour, "Lack of pharmacokinetic interaction between 5-fluorouracil and oxaliplatin," *Clinical Pharmacology & Therapeutics*, vol. 76, no. 1, pp. 45–54, 2004.

[41] R. P. Riechelmann and E. D. Saad, "A systematic review on drug interactions in oncology," *Cancer Investigation*, vol. 24, no. 7, pp. 704–712, 2006.

[42] R. G. Moran and K. Keyomarsi, "Biochemical rationale for the synergism of 5-fluorouracil and folinic acid.," *NCI monographs: a publication of the National Cancer Institute*, no. 5, pp. 159–163, 1987.

[43] L. Yuen, P. Ross, and J. Turner, "FOLFIRINOX protocol," 2014.

[44] E. Raymond, S. G. Chaney, A. Taamma, and E. Cvitkovic, "Oxaliplatin: A review of preclinical and clinical studies," *Annals of Oncology*, vol. 9, pp. 1053–1071, 1998.

[45] F. Lévi, G. Metzger, C. Massari, and G. Milano, "Oxaliplatin: pharmacokinetics and chronopharmacological aspects.," *Clinical pharmacokinetics*, vol. 38, no. 1, pp. 1–21, 2000.

[46] NHS, "Peripheral neuropathy," 2019.

[47] leonard B. Saltz, "Clinical Use of Irinotecan: Current Status and Future Considerations.," *The oncologist*, vol. 2, no. 6, pp. 402–409, 1997.

[48] Cancer.net, "Neutropenia," 2018.

[49] H. M. Pinedo and G. F. Peters, "Flourouracil: Biochemistry and pharmacology," 1988.

[50] A. Shahrokni, M. R. Rajebi, and M. W. Saif, "Toxicity and efficacy of 5-fluorouracil and capecitabine in a patient with TYMS gene polymorphism: A challenge or a dilemma?," *Clinical Colorectal Cancer*, vol. 8, no. 4, pp. 231–234, 2009.

[51] Cancer Research UK, "Bowel cancer mortality statistics," 2016.

[52] C. R. Smittenaar, K. A. Petersen, K. Stewart, and N. Moitt, "Cancer incidence and mortality projections in the UK until 2035," *Nature Publishing Group*, vol. 115, no. 9, pp. 1147–1155, 2016.

[53] M. Ilic and I. Ilic, "Epidemiology of pancreatic cancer," *World Journal of Gastroenterology*, vol. 22, no. 44, pp. 9694–9705, 2016.

[54] I. A. Riddell and S. J. Lippard, "Cisplatin and Oxaliplatin: Our current understanding of their actions," *Metallo-Drugs: Development and Action of Anticancer Agents: Development and Action of Anticancer Agents*, vol. 18, p. 1, 2018.

[55] F. Quenet, B. Nordlinger, M. Rivoire, J. R. Delpero, G. Portier, D. Mery-Mignard, E. Magherini, S. Payrard, and M. Ychou, "Resection of previously unresectable liver metastases from colorectal cancer (LMCRC) after chemotherapy (CT) with CPT-11/L-OHP/LV5FU (Folfirinox): A prospective phase II trial," *Journal of Clinical Oncology*, vol. 22, no. 14_suppl, p. 3613, 2004.

[56] K. D. Ivy and J. H. Kaplan, "A Re-Evaluation of the Role of hCTR1, the Human High-Affinity Copper Transporter, in Platinum-Drug Entry into Human Cells," *Molecular Pharmacology*, vol. 83, no. 6, pp. 1237–1246, 2013.

[57] I. Buß, A. Hamacher, N. Sarin, M. U. Kassack, and G. V. Kalayda, "Relevance of copper transporter 1 and organic cation transporters 1-3 for oxaliplatin uptake and drug resistance in colorectal cancer cells," *Metallomics*, vol. 10, no. 3, pp. 414–425, 2018.

[58] G. Samimi, R. Safaei, K. Katano, A. K. Holzer, M. Rochdi, M. Tomioka, M. Goodman, and S. B. Howell, "Increased expression of the copper efflux transporter ATP7A mediates resistance to cisplatin, carboplatin, and oxaliplatin in ovarian cancer cells," *Clinical Cancer Research*, vol. 10, no. 14, pp. 4661–4669, 2004.

[59] E. Martinez-Balibrea, A. Martínez-Cardús, E. Musulén, A. Ginés, J. L. Manzano, E. Aranda, C. Plasencia, N. Neamati, and A. Abad, "Increased levels of copper efflux transporter ATP7B are associated with poor outcome in colorectal cancer patients receiving oxaliplatin-based chemotherapy," *International Journal of Cancer*, vol. 124, no. 12, pp. 2905–2910, 2009.

[60] M. A. Graham, G. F. Lockwood, D. Greenslade, S. Brienza, M. Bayssas, and E. Gamelin, "Clinical Pharmacokinetics of Oxaliplatin : A Critical Review," *Clinical Cancer Research*, vol. 18, no. 1, pp. 1205–1218, 2000.

[61] S. Uriens and J. P. Tillement, "In vitro binding of oxaliplatin to human serum proteins," *Drug interactions. Debiopharm Study Report No. LPH0022*, 1995.

[62] K. Zhang, P. Mack, and K. P. Wong, "Glutathione-related mechanisms in cellular resistance to anticancer drugs.," *International journal of oncology*, vol. 12, no. 4, pp. 871–953, 1998.

[63] D. Hagrman, J. Goodisman, and A.-K. Souid, "Kinetic study on the reactions of platinum drugs with glutathione.," *The Journal of pharmacology and experimental therapeutics*, vol. 308, no. 2, pp. 658–666, 2004.

[64] T. Alcindor and N. Beauger, "Oxaliplatin: a review in the era of molecularly targeted therapy," *Current Oncology*, vol. 18, no. 1, pp. 18–25, 2011.

[65] P. M. Bruno, Y. Liu, G. Y. Park, J. Murai, C. E. Koch, T. J. Eisen, J. R. Pritchard, Y. Pommier, S. J. Lippard, and M. T. Hemann, "A subset of platinum-containing chemotherapeutic agents kills cells by inducing ribosome biogenesis stress," *Nature Medicine*, vol. 23, no. 4, pp. 461–471, 2017.

[66] L. Golomb, S. Volarevic, and M. Oren, "P53 and ribosome biogenesis stress: The essentials," *FEBS Letters*, vol. 588, no. 16, pp. 2571–2579, 2014.

[67] E. F. Freed, F. Bleichert, L. M. Dutca, and S. J. Baserga, "When ribosomes go bad: Diseases of ribosome biogenesis," *Molecular BioSystems*, vol. 6, no. 3, pp. 481–493, 2010.

[68] K. Kobayashi, B. Bouscarel, Y. Matsuzaki, S. Ceryak, S. Kudoh, and H. Fromm, "pH-dependent uptake of Irinotecan and its active metabolite, SN-38, by intestinal cells," *International Journal of Cancer*, vol. 83, no. 4, pp. 491–496, 1999.

[69] Y. Pommier, P. Pourquier, Y. Urasaki, J. Wu, and G. S. Laco, "Topoisomerase I inhibitors: Selectivity and cellular resistance," *Drug Resistance Updates*, vol. 2, no. 5, pp. 307–318, 1999.

[70] N. F. Smith, W. D. Figg, and A. Sparreboom, "Pharmacogenetics of irinotecan metabolism and transport: An update," *Toxicology in Vitro*, vol. 20, no. 2, pp. 163–175, 2006.

[71] M. L. Rothenberg, "Irinotecan (CPT-11): Recent Developments and Future Directions–Colorectal Cancer and Beyond," *The Oncologist*, vol. 6, pp. 66–80, 2001.

[72] R. H. J. Mathijssen, R. J. V. Alphen, J. Verweij, W. J. Loos, K. Nooter, G. Stoter, and A. Sparreboom, "Clinical Pharmacokinetics and Metabolism of Irinotecan (CPT-11)," *Clinical Cancer Research*, vol. 7, no. August, pp. 2182–2194, 2001.

[73] C. L. Morton, M. Wierdl, L. Oliver, M. K. Ma, M. K. Danks, C. F. Stewart, J. L. Eiseman, and P. M. Potter, "Activation of CPT-11 in mice: Identification and analysis of a highly effective plasma esterase," *Cancer Research*, vol. 60, no. 15, pp. 4206–4210, 2000.

[74] A. Ballesta, S. Dulong, C. Abbara, B. Cohen, A. Okyar, J. Clairambault, and F. Levi, "A combined experimental and mathematical approach for molecular-based optimization of irinotecan circadian delivery," *PLoS Computational Biology*, vol. 7, no. 9, pp. 1–12, 2011.

[75] P. J. Houghton, P. J. Cheshire, J. D. Hallman, L. Lutz, H. S. Friedman, M. K. Danks, and J. A. Houghton, "Efficacy of topoisomerase I inhibitors, topotecan and irinotecan, administered at low dose levels in protracted schedules to mice bearing xenografts of human tumors," *Cancer Chemotherapy and Pharmacology*, vol. 36, no. 5, pp. 393–403, 1995.

[76] Y. Sordet, O.; Khan, Q.A.; Kohn, K.W.; Pommier, "Apoptosis Induced by Topoisomerase Inhibitors," *Current Medicinal Chemistry - Anti-Cancer Agents*, vol. 3, no. 4, 2003.

[77] Y. Pommier, "Topoisomerase I inhibitors: Camptothecins and beyond," *Nature Reviews Cancer*, vol. 6, no. 10, pp. 789–802, 2006.

[78] C. F. Thorn, S. Marsh, M. W. Carrillo, H. L. McLeod, T. E. Klein, and R. B. Altman, "Pharm GKB summary: Fluoropyrimidine pathways," *Pharmacogenetics and Genomics*, vol. 21, no. 4, pp. 237–242, 2011.

[79] Y. Kobayashi, N. Ohshiro, R. Sakai, M. Ohbayashi, N. Kohyama, and T. Yamamoto, " Transport mechanism and substrate specificity of human organic anion transporter 2 (hOat2 [SLC22A7]) ," *Journal of Pharmacy and Pharmacology*, vol. 57, no. 5, pp. 573–578, 2005.

[80] J. H. Yuan, J. Q. Cheng, L. Y. Jiang, W. D. Ji, L. F. Guo, J. J. Liu, X. Y. Xu, J. S. He, X. M. Wang, and Z. X. Zhuang, "Breast cancer resistance protein expression and 5-fluorouracil resistance," *Biomedical and Environmental Sciences*, vol. 21, no. 4, pp. 290–295, 2008.

[81] J. Yuan, H. Lv, B. Peng, C. Wang, Y. Yu, and Z. He, "Role of BCRP as a biomarker for predicting resistance to 5-fluorouracil in breast cancer," *Cancer Chemotherapy and Pharmacology*, vol. 63, no. 6, pp. 1103–1110, 2009.

[82] W. Hagmann, R. Jesnowski, R. Faissner, C. Guo, and J. M. Löhr, "ATP-binding cassette C transporters in human pancreatic carcinoma cell lines," *Pancreatology*, vol. 9, no. 1-2, pp. 136–144, 2009.

[83] D. B. Longley, D. P. Harkin, and P. G. Johnston, "5-Fluorouracil: Mechanisms of Action and Clinical Strategies.," *Nature reviews. Cancer*, vol. 3, no. 5, pp. 330–8, 2003.

[84] G. R. Simon, R. R. Costa, and D. R. Gandara, *Pharmacogenomics in Lung Cancer: Predictive Biomarkers for Chemotherapy.* Elsevier Inc., second edi ed., 2018.

[85] R. B. Diasio and B. E. Harris, "Clinical Pharmacology of 5-Fluorouracil," *Clinical Pharmacokinetics*, vol. 16, pp. 215–237, apr 1989.

[86] B. R. L. Schilsky, "Biochemical and Clinical Pharmacology of 5-Fluorouracil Cellular Determinants of Sensitivity to Fluoropyrimidines," *Oncology*, vol. 12, no. 7, pp. 13–18, 1998.

[87] M. Merrow and Till Roenneberg, "Circadian clocks — the fall and rise of physiology," *MOLECULAR CELL BIOLOGY*, vol. 5837, no. 2007, pp. 965–971, 2009.

[88] L. J. Lorenz, J. C. Hall, and M. Rosbash, "Expression of a Drosophila mRNA is under circadian clock control during pupation.," *Development (Cambridge, England)*, vol. 107, no. 4, pp. 869–880, 1989.

[89] K. Spoelstra, M. Wikelski, S. Daan, A. S. I. Loudon, and M. Hau, "Natural selection against a circadian clock gene mutation in mice," *Proceedings of the National Academy of Sciences*, vol. 113, no. 3, pp. 686–691, 2016.

[90] M. H. Smolensky and N. A. Peppas, "Chronobiology, drug delivery, and chronotherapeutics," *Advanced Drug Delivery Reviews*, vol. 59, no. 9-10, pp. 828–851, 2007.

[91] E. Van Cauter, R. Leproult, and D. J. Kupfer, "Effects of gender and age on the levels and circadian rhythmicity of plasma cortisol.," *The Journal of Clinical Endocrinology & Metabolism*, vol. 81, no. 7, pp. 2468–2473, 1996.

[92] F. Levi and U. Schibler, "Circadian rhythms: mechanisms and therapeutic implications.," *Annual review of pharmacology and toxicology*, vol. 47, pp. 593–628, 2007.

[93] R. Zhang, N. F. Lahens, H. I. Ballance, M. E. Hughes, and J. B. Hogenesch, "A circadian gene expression atlas in mammals: Implications for biology and medicine," *Proceedings of the National Academy of Sciences*, vol. 111, no. 45, pp. 16219–16224, 2014.

[94] L. S. Mure, H. D. Le, G. Benegiamo, M. W. Chang, L. Rios, N. Jillani, M. Ngotho, T. Kariuki, O. Dkhissi-Benyahya, H. M. Cooper, and S. Panda, "Diurnal transcriptome atlas of a primate across major neural and peripheral tissues," *Science*, vol. 359, no. 6381, pp. 1–20, 2018.

[95] I. N. Karatsoreos, S. Bhagat, E. B. Bloss, J. H. Morrison, and B. S. McEwen, "Disruption of circadian clocks has ramifications for metabolism, brain, and behavior," *Proceedings of the National Academy of Sciences*, vol. 108, no. 4, pp. 1657–1662, 2011.

[96] S. Davis and D. K. Mirick, "Circadian disruption, shift work and the risk of cancer: A summary of the evidence and studies in Seattle," *Cancer Causes and Control*, vol. 17, no. 4, pp. 539–545, 2006.

[97] J. Hansen, "Breast Cancer Among Women Who Work at Night," *Epidemiology*, vol. 12, no. 5, pp. 588–589, 2001.

[98] S. Davis, D. Mirick, and R. Stevens, "Shift work, light at night, and the risk of breast cancer.," *Journal of the National Cancer Institute*, vol. 92, no. 20, pp. 1557–1562, 2001.

[99] G. A. Schernhammer, E.S., Laden, F., Speizer, F. E., Willett, W.C., Hunter, D., J., Kawachi, I., Colditz, "Rotating night shifts and risk of breast cancer in women participating in the Nurses' Health Study," *J Natl Cancer Inst*, vol. 93, no. 20, pp. 1563–1568, 2001.

[100] E. S. Schernhammer, F. Laden, F. E. Speizer, W. C. Willet, D. J. Hunter, I. Kawachi, C. S. Fuchs, and G. A. Colditz, "Night-shift work and risk of colorectal cancer in the Nurses' Health Study," *Journal of the National Cancer Institute*, vol. 95, no. 11, pp. 825–828, 2003.

[101] E. Pukkala, A. Auvinen, and G. Wahlberg, "Incidence of cancer among Finnish airline cabin attendants, 1967-92," *British Medical journal*, vol. 311, no. September, pp. 649–652, 1995.

[102] Â. Rafnsson and H. Tulinius, "Risk of breast cancer in female flight attendants : a population-based study (Iceland)," *Cancer Causes and Control*, vol. 12, pp. 95–101, 2001.

[103] T. Tynes, M. Hannevik, A. Andersen, A. I. Vistnes, and T. Haldorsen, "Incidence of breast cancer in Norwegian female radio and telegraph operators," *Cancer Causes and Control*, vol. 7, no. 2, pp. 197–204, 1996.

[104] E. Pukkala, R. Aspholm, A. Auvinen, H. Eliasch, M. Gundestrup, T. Haldorsen, N. Hammar, P. E. Ukkala, A. R. Spholm, A. A. Uvinen, E. H. Liasch, and G. M. Undestrup, "Cancer Incidence Among 10,211 Airline Pilots :," *Aviation Space and Environmental Medicine*, vol. 74, no. 7, pp. 699–706, 2003.

[105] P. A. Demers, H. Checkoway, T. L. Vaughan, N. S. Weiss, N. J. Heyer, and L. Rosenstock, "Cancer incidence among firefighters in Seattle and Tacoma, Washington (United States)," *Cancer Causes & Control*, vol. 5, no. 2, pp. 129–135, 1994.

[106] E. L. Haus and M. H. Smolensky, "Shift work and cancer risk: Potential mechanistic roles of circadian disruption, light at night, and sleep deprivation," *Sleep Medicine Reviews*, vol. 17, no. 4, pp. 273–284, 2013.

[107] D. E. Blask, R. T. Dauchy, G. C. Brainard, and J. P. Hanifin, "Circadian stage-dependent inhibition of human breast cancer metabolism and growth by the nocturnal melatonin signal: Consequences of its disruption by light at night in rats and women," *Integrative Cancer Therapies*, vol. 8, no. 4, pp. 347–353, 2009.

[108] D. E. Blask, S. M. Hill, R. T. Dauchy, S. Xiang, L. Yuan, T. Duplessis, L. Mao, E. Dauchy, and L. A. Sauer, "Circadian Regulation Metabolic Signaling Mechanisms of Human Breast Cancer Growth By the Nocturnal Melatonin Signal and the Consequences," *Journal of Pineal Research*, vol. 51, no. 3, pp. 259–269, 2012.

[109] X. Yang, P. A. Wood, E. Y. Oh, J. Du-Quiton, C. M. Ansell, and W. J. M. Hrushesky, "Down regulation of circadian clock gene Period 2 accelerates breast cancer growth by altering its daily growth rhythm," *Breast Cancer Research and Treatment*, vol. 117, no. 2, pp. 423–431, 2009.

[110] E. Filipski, X. M. Li, and F. Lévi, "Disruption of circadian coordination and malignant growth," *Cancer Causes and Control*, vol. 17, no. 4, pp. 509–514, 2006.

[111] C. Savvidis and M. Koutsilieris, "Circadian Rhythm Disruption in Cancer Biology," *Molecular Medicine*, vol. 18, no. 9, p. 1, 2012.

[112] F. Levi, A. Okyar, S. Dulong, P. F. Innominato, J. Clairambault, and F. Lévi, "Circadian timing in cancer treatments.," *Annual review of pharmacology and toxicology*, vol. 50, no. November, pp. 377–421, 2010.

[113] R. Dallmann, A. Okyar, and F. Lévi, "Dosing-Time Makes the Poison: Circadian Regulation and Pharmacotherapy," *Trends in Molecular Medicine*, vol. 22, no. 5, pp. 430–445, 2016.

[114] M. C. Mormont and F. Levi, "Cancer chronotherapy: Principles, applications, and perspectives," *Cancer*, vol. 97, no. 1, pp. 155–169, 2003.

[115] A. Sancar, L. A. Lindsey-boltz, S. Gaddameedhi, C. P. Selby, R. Ye, Y.-y. Chiou, M. G. Kemp, J. Hu, J. H. Lee, and N. Ozturk, "Circadian Clock, Cancer, and Chemotherapy," *Biochemistry*, vol. 54, pp. 110–123, 2015.

[116] D. Montaigne, X. Marechal, T. Modine, A. Coisne, S. Mouton, G. Fayad, S. Ninni, C. Klein, S. Ortmans, C. Seunes, C. Potelle, A. Berthier, C. Gheeraert, C. Piveteau, R. Deprez, J. Eeckhoute, H. Duez, D. Lacroix, B. Deprez, B. Jegou, M. Koussa, J.-L. Edme, P. Lefebvre, and B. Staels, "Daytime variation of perioperative myocardial injury in cardiac surgery and its prevention by Rev-Erbalpha antagonism: a single-centre propensity-matched cohort study and a randomised study.," *Lancet (London, England)*, vol. 391, no. 10115, pp. 59–69, 2018.

[117] M. H. Smolensky, B. Lemmer, and A. E. Reinberg, "Chronobiology and chronotherapy of allergic rhinitis and bronchial asthma," *Advanced Drug Delivery Reviews*, vol. 59, no. 9-10, pp. 852–882, 2007.

[118] G. L. Sahlem, B. Kalivas, J. B. Fox, K. Lamb, A. Roper, E. N. Williams, N. R. Williams, J. E. Korte, Z. D. Zuschlag, S. El Sabbagh, C. Guille, K. S. Barth, T. W. Uhde, M. S. George, and E. B. Short, "Adjunctive triple chronotherapy (combined total sleep deprivation, sleep phase advance, and bright light therapy) rapidly improves mood and suicidality in suicidal depressed inpatients: An open label pilot study," *Journal of Psychiatric Research*, vol. 59, pp. 101–107, 2014.

[119] Y. L. Tong, W. L. Nelson, R. B. Sothern, and F. Halberg, "Estimation of the orthophase (timing of high values) on a non-sinusoidal rhythm, illustrated by the best timing for experimental cancer chronotherapy," in *XII Int Conf Soc Chronobiol*, pp. 765–769, 1977.

[120] F. Halberg, W. Nelson, G. Cornelissen, E. Haus, L. E. Scheving, and R. A. Good, "On methods for testing and achieving cancer chronotherapy," *Cancer treatment reports*, vol. 63, pp. 1428–1430, aug 1979.

[121] F. Halberg, W. Nelson, F. Levi, D. Culley, A. Bogden, and D. J. Taylor, "Chronotherapy of mammary cancer in rats," *International journal of chronobiology*, vol. 7, no. 2, pp. 85–99, 1980.

[122] U.S. National Library of Medicine, "Home - ClinicalTrials," 2019.

[123] E. R. Burns and S. S. Beland, "Effect of Biological Time on the Determination of the LD50 of 5-Fluorouracil in Mice," *Pharmacology*, vol. 28, no. 5, pp. 296–300, 1984.

[124] G. J. Peters, J. D. Van, J. C. Nadal, C. J. G. Van, J. Lankelma, and H. M. Pinedo, "Diurnal variation in the therapeutic efficacy of 5-fluorouracil against murine colon cancer.," *In vivo*, vol. 1, no. 2, pp. 113–117, 1987.

[125] E. Petit, G. Milano, F. Levi, A. Thyss, F. Bailleul, and M. Schneider, "Circadian Rhythm-varying Plasma Concentration of 5-Fluorouracil during a Five-Day Continuous Venous Infusion at a Constant Rate in Cancer Patients," *Cancer Research*, vol. 48, no. 6, pp. 1676–1679, 1988.

[126] B. Harris, R. Song, S.-J. Soong, and R. Diasio, "Relationship between dihydropyrimidine dehydrogenase activity and plasma 5-fluorouracil levels with evidence for circadian variation of enzyme activity and plasma," *Cancer research*, vol. 50, no. 1, pp. 197–201, 1990.

[127] G. Metzger, C. Massari, M. Etienne, M. Comisso, S. Brienza, Y. Touitou, G. Milano, G. Bastian, J. L. Misset, and F. Lévi, "Spontaneous or imposed circadian changes in plasma concentrations of 5-fluorouracil coadministered with folinic acid and oxaliplatin: Relationship with mucosal toxicity in patients with cancer," *Clinical Pharmacology & Therapeutics*, vol. 56, no. 2, pp. 190–201, 1994.

[128] F. Lévi, J. Misset, S. Brienza, R. Adam, G. Metzger, M. Itzakhi, J. Caussanel, F. Kunstlinger, S. Lecouturier, and A. Descorps-Declère, "A chronopharmacologic phase II clinical trial with 5-fluorouracil, folinic acid, and oxaliplatin using an ambulatory multichannel programmable pump. High antitumor effectiveness against metastatic colorectal cancer," *Cancer*, vol. 69, no. 4, pp. 893–900, 1992.

[129] F. Levi, S. Giacchetti, R. Adam, R. Zidani, G. Metzger, and J. L. Misset, "Chronomodulation of chemotherapy against metastatic colorectal cancer.," *European Journal of Cancer Part A: General Topics*, vol. 31, no. 7-8, pp. 1264–1270, 1995.

[130] C. R. Cederroth, U. Albrecht, J. Bass, S. A. Brown, J. Dyhrfjeld-Johnsen, F. Gachon, C. B. Green, M. H. Hastings, C. Helfrich-Förster, J. B. Hogenesch, F. Lévi, A. Loudon, G. B. Lundkvist, J. H. Meijer, M. Rosbash, J. S. Takahashi, M. Young, and B. Canlon, "Medicine in the Fourth Dimension," *Cell Metabolism*, vol. 30, no. 2, pp. 238–250, 2019.

[131] J.-P. Caussanel, F. Lévi, S. Brienza, J.-L. Misset, M. Itzhaki, R. Adam, G. Milano, B. Hecquet, and G. Mathé, "Phase I Trial of 5-Day Continuous Venous Infusion of Oxaliplatin at Circadian Rhythm-Modulated Rate Compared With Constant Rate," *JNCI: Journal of the National Cancer Institute*, vol. 82, pp. 1046–1050, jun 1990.

[132] F. Levi, A. Soussan, R. Adam, J. P. Caussanel, G. Metzger, C. Jasmin, H. Bismuth, M. Smolensky, and J. L. Misset, "A phase I-II trial of five-day continuous intravenous infusion of 5-fluorouracil delivered at circadian rhythm

modulated rate in patients with metastatic colorectal cancer.," *The Journal of infusional chemotherapy*, vol. 5, no. 3 Suppl 1, pp. 153–158, 1995.

[133] F. Lévi, R. Zidani, and J. L. Misset, "Randomised multicentre trial of chronotherapy with oxaliplatin, fluorouracil, and folinic acid in metastatic colorectal cancer," *Lancet*, vol. 350, no. 9079, pp. 681–686, 1997.

[134] E. Filipski, G. Lemaigre, X. H. Liu, D. Méry-Mignard, M. Mahjoubi, and F. Lévi, "Circadian rhythm of irinotecan tolerability in mice," *Chronobiology International*, vol. 21, no. 4-5, pp. 613–630, 2004.

[135] S. Dulong, A. Ballesta, A. Okyar, and F. Levi, "Identification of Circadian Determinants of Cancer Chronotherapy through In Vitro Chronopharmacology and Mathematical Modeling," *Molecular Cancer Therapeutics*, vol. 14, no. 9, pp. 2154–2164, 2015.

[136] S. Giacchetti, P. A. Dugué, P. F. Innominato, G. A. Bjarnason, C. Focan, C. Garufi, S. Tumolo, B. Coudert, S. Iacobelli, R. Smaaland, M. Tampellini, R. Adam, T. Moreau, and F. Lévi, "Sex moderates circadian chemotherapy effects on survival of patients with metastatic colorectal cancer: A meta-analysis," *Annals of Oncology*, vol. 23, no. 12, pp. 3110–3116, 2012.

[137] F. Lévi, C. Focan, A. Karaboué, V. de la Valette, D. Focan-Henrard, B. Baron, F. Kreutz, and S. Giacchetti, "Implications of circadian clocks for the rhythmic delivery of cancer therapeutics," *Advanced Drug Delivery Reviews*, vol. 59, no. 9-10, pp. 1015–1035, 2007.

[138] P. Innominato, A. Ballesta, Q. Huang, C. Focan, P. Chollet, A. Karaboue, C. Garufi, and Francis Lévi, "Sex-dependent least toxic timing of Irinotecan in combination with chronomodulated 5-Fluorouracil, Leucovorin and Oxaliplatin (chronoIFLO) in patients with metastatic colorectal cancer: a randomized multicentre trial (EORTC 05011)," 2019.

[139] J. Le, "Overview of Pharmacokinetics - Clinical Pharmacology - MSD Manual Professional Edition," 2018.

[140] C. Csajka and D. Verotta, "Pharmacokinetic-pharmacodynamic modelling: History and perspectives," *Journal of Pharmacokinetics and Pharmacodynamics*, vol. 33, no. 3, pp. 227–279, 2006.

[141] L. Aarons, "Physiologically based pharmacokinetic modelling: A sound mechanistic basis is needed," *British Journal of Clinical Pharmacology*, vol. 60, no. 6, pp. 581–583, 2005.

[142] N. Tsamandouras, A. Rostami-Hodjegan, and L. Aarons, "Combining the 'bottom up' and 'top down' approaches in pharmacokinetic modelling: Fitting PBPK models to observed clinical data," *British Journal of Clinical Pharmacology*, vol. 79, no. 1, pp. 48–55, 2015.

[143] M. Rowland, C. Peck, and G. Tucker, "Physiologically-based pharmacokinetics in drug development and regulatory science.," *Annual review of pharmacology and toxicology*, vol. 51, pp. 45–73, 2011.

[144] P. Zhao, L. Zhang, J. A. Grillo, Q. Liu, J. M. Bullock, Y. J. Moon, P. Song, S. S. Brar, R. Madabushi, T. C. Wu, B. P. Booth, N. A. Rahman, K. S. Reynolds, E. Gil Berglund, L. J. Lesko, and S.-M. Huang, "Applications of Physiologically Based Pharmacokinetic (PBPK) Modeling and Simulation During Regulatory

Review," *Clinical Pharmacology & Therapeutics*, vol. 89, no. 2, pp. 259–267, 2011.

[145] H. Yu, N. Steeghs, J. S. Kloth, D. De Wit, J. G. Van Hasselt, N. P. Van Erp, J. H. Beijnen, J. H. Schellens, R. H. Mathijssen, and A. D. Huitema, "Integrated semi-physiological pharmacokinetic model for both sunitinib and its active metabolite SU12662," *British Journal of Clinical Pharmacology*, vol. 79, no. 5, pp. 809–819, 2015.

[146] M. A. Felmlee, M. E. Morris, and D. E. Mager, "Mechanism-based pharmacodynamic modeling," *Methods in molecular biology (Clifton, N.J.)*, vol. 929, pp. 583–600, 2012.

[147] S. Goutelle, M. Maurin, F. Rougier, X. Barbaut, L. Bourguignon, M. Ducher, and P. Maire, "The Hill equation: A review of its capabilities in pharmacological modelling," *Fundamental and Clinical Pharmacology*, vol. 22, no. 6, pp. 633–648, 2008.

[148] C. Mircioiu, V. Voicu, V. Anuta, A. Tudose, C. Celia, D. Paolino, M. Fresta, R. Sandulovici, and I. Mircioiu, "Mathematical Modeling of Release Kinetics from Supramolecular Drug Delivery Systems," *Pharmaceutics*, vol. 11, no. 3, pp. 140–185, 2019.

[149] B. Chopard, J. Borgdorff, and A. G. Hoekstra, "A framework for multi-scale modelling," *Phil. Trans. R. Soc. A*, vol. 372, no. 2021, p. 20130378, 2014.

[150] S. Karabasov, D. Nerukh, A. Hoekstra, B. Chopard, and P. V. Coveney, "Multiscale modelling: Approaches and challenges," *Philosophical Transactions of the Royal Society A: Mathematical, Physical and Engineering Sciences*, vol. 372, no. 2021, pp. 2–4, 2014.

[151] C. Li and T.-W. Chou, "Multiscale Modeling of Carbon Nanotube Reinforced Polymer Composites," *Journal of Nanoscience and Nanotechnology*, vol. 3, no. 5, pp. 423–430, 2003.

[152] E. Cristiani, B. Piccoli, and A. Tosin, "Multiscale Modeling of Granular Flows with Applications to Crowd Dynamics," *Multiscale Modeling & Simulation*, vol. 9, no. 1, pp. 155–182, 2011.

[153] Z. Qu, A. Garfinkel, J. N. Weiss, and M. Nivala, "Multi-scale modeling in biology: How to bridge the gaps between scales?," *Progress in Biophysics and Molecular Biology*, vol. 107, no. 1, pp. 21–31, 2011.

[154] A. Stéphanou, E. Fanchon, P. F. Innominato, and A. Ballesta, "Systems biology, systems medicine, systems pharmacology: The what and the why," *Acta Biotheoretica*, vol. 66, no. 4, pp. 345–365, 2018.

[155] X. L. Li, W. O. Oduola, L. Qian, and E. R. Dougherty, "Integrating multiscale modeling with drug effects for cancer treatment," *Cancer Informatics*, vol. 15, pp. 21–31, 2016.

[156] O. Wolkenhauer, C. Auffray, O. Brass, J. Clairambault, A. Deutsch, D. Drasdo, F. Gervasio, L. Preziosi, P. Maini, A. Marciniak-Czochra, C. Kossow, L. Kuepfer, K. Rateitschak, I. Ramis-Conde, B. Ribba, A. Schuppert, R. Smallwood, G. Stamatakos, F. Winter, and H. Byrne, "Enabling multiscale modeling in systems medicine," *Genome Medicine*, vol. 6, no. 3, pp. 4–6, 2014.

[157] A. F. Villaverde, "Observability and Structural Identifiability of Nonlinear Biological Systems," *Complexity*, vol. 2019, 2019.

[158] N. D. Evans, H. A. Moyse, D. Lowe, D. Briggs, R. Higgins, D. Mitchell, D. Zehnder, and M. J. Chappell, "Structural identifiability of surface binding reactions involving heterogeneous analyte: Application to surface plasmon resonance experiments," *Automatica*, vol. 49, no. 1, pp. 48–57, 2013.

[159] A. F. Villaverde, N. D. Evans, M. J. Chappell, and J. R. Banga, "Input-dependent structural identifiability of nonlinear systems," *IEEE Control Systems Letters*, vol. 3, no. 2, pp. 272–277, 2019.

[160] G. Bellu, M. P. Saccomani, S. Audoly, and L. D'Angiò, "DAISY: A new software tool to test global identifiability of biological and physiological systems," *Computer Methods and Programs in Biomedicine*, vol. 88, no. 1, pp. 52–61, 2007.

[161] O. Chiş, J. R. Banga, and E. Balsa-Canto, "GenSSI: A software toolbox for structural identifiability analysis of biological models," *Bioinformatics*, vol. 27, no. 18, pp. 2610–2611, 2011.

[162] N. Meshkat, C. Er-zhen Kuo, and J. DiStefano, "On finding and using identifiable parameter combinations in nonlinear dynamic systems biology models and combos: A novel web implementation," *PLoS ONE*, vol. 9, no. 10, 2014.

[163] A. M. Legendre, *Nouvelles méthodes pour la détermination des orbites des comètes*. F. Didot, 1805.

[164] J. Cao, L. Wang, J. Xu, and A. Science, "Robust Estimation for Ordinary Differential Equation Models," *Biometrics*, vol. 67, no. December, pp. 1305–1313, 2011.

[165] N. Hansen, "The CMA Evolution Strategy: A Comparing Review BT - Towards a New Evolutionary Computation: Advances in the Estimation of Distribution Algorithms," in *Towards a New Evolutionary Computation* (J. A. Lozano, P. Larrañaga, I. Inza, and E. Bengoetxea, eds.), pp. 75–102, Berlin, Heidelberg: Springer Berlin Heidelberg, 2006.

[166] B. Sendhoff, "Covariance Matrix Adaptation Revisited – the CMSA Evolution Strategy –," *International Conference on Parallel Problem Solving from Nature*, vol. 3242, no. Conference Paper · September 2008, 2008.

[167] C. G. Moles, P. Mendes, and J. R. Banga, "Parameter estimation in biochemical pathways: A comparison of global optimization methods," *Genome Research*, vol. 13, no. 11, pp. 2467–2474, 2003.

[168] N. Hansen, "CMA-ES: Evolution Strategy with Covariance Matrix Adaptation for nonlinear function minimization.."

[169] N. Hansen, Y. Akimoto, and P. Baudis, "CMA-ES/pycma on Github." Zenodo, DOI:10.5281/zenodo.2559634, feb 2019.

[170] A. Raue, C. Kreutz, T. Maiwald, J. Bachmann, U. Klingmüller, M. Schilling, and J. Timmer, "Structural and practical identifiability analysis of partially observed dynamical models by exploiting the profile likelihood," *Bioinformatics*, vol. 25, no. 15, pp. 1923–1929, 2009.

[171] C. Kreutz, A. Raue, D. Kaschek, and J. Timmer, "Profile likelihood in systems biology," *FEBS Journal*, vol. 280, no. 11, pp. 2564–2571, 2013.

[172] X.-y. Zhang, M. N. Trame, L. J. Lesko, and S. Schmidt, "Sobol Sensitivity Analysis : A Tool to Guide the Development and Evaluation of Systems Pharmacology Models," *CPT: pharmacometrics & systems pharmacology*, vol. 4, pp. 69–79, 2015.

[173] H. Stryhn and J. Christensen, "Confidence intervals by the profile likelihood method, with applications in veterinary epidemiology," *Proceedings of the 10th International Symposium on Veterinary Epidemiology and Economics, Vina del Mar*, vol. 45, no. Supplement, pp. S–102, 2003.

[174] CASyM, "CASyM and the road to Systems Medicine," 2015.

[175] B. R. Iyengar, R. B. Altman, O. G. Troyanskaya, and G. A. Fitzgerald, "Experimentation Can Enable Precision Medicine," *Science*, vol. 350, no. 6258, pp. 282–283, 2015.

[176] A. R. A. Anderson and V. Quaranta, "Integrative mathematical oncology," *Nature Reviews Cancer*, vol. 8, no. 3, pp. 227–234, 2008.

[177] Z. Agur, M. Elishmereni, and Y. Kheifetz, "Personalizing oncology treatments by predicting drug efficacy, side-effects, and improved therapy: Mathematics, statistics, and their integration," *Wiley Interdisciplinary Reviews: Systems Biology and Medicine*, vol. 6, no. 3, pp. 239–253, 2014.

[178] J. P. Boissel, C. Auffray, D. Noble, L. Hood, and F. H. Boissel, "Bridging systems medicine and patient needs," *CPT: Pharmacometrics and Systems Pharmacology*, vol. 4, no. 3, pp. 135–145, 2015.

[179] K. K. Giuliano and C. Niemi, "The urgent need for innovation in I.V. infusion devices," *Nursing*, vol. 46, no. 4, pp. 66–68, 2016.

[180] D. L. Hertz and J. Rae, "Pharmacogenetics of Cancer Drugs," *Annual Review of Medicine*, vol. 66, no. 1, pp. 65–81, 2015.

[181] A. Paci, G. Veal, C. Bardin, D. Levêque, N. Widmer, J. Beijnen, A. Astier, and E. Chatelut, "Review of therapeutic drug monitoring of anticancer drugs part 1 - Cytotoxics," *European Journal of Cancer*, vol. 50, no. 12, pp. 2010–2019, 2014.

[182] P. F. Innominato, F. A. Lévi, and G. A. Bjarnason, "Chronotherapy and the molecular clock: Clinical implications in oncology," *Advanced Drug Delivery Reviews*, vol. 62, no. 9-10, pp. 979–1001, 2010.

[183] E. Ortiz-Tudela, P. F. Innominato, M. A. Rol, F. Lévi, and J. A. Madrid, "Relevance of internal time and circadian robustness for cancer patients," *BMC Cancer*, vol. 16, no. 1, 2016.

[184] F. A. Lévi, V. Boige, M. Hebbar, D. Smith, C. Lepère, C. Focan, A. Karaboué, R. Guimbaud, C. Carvalho, S. Tumolo, P. Innominato, Y. Ajavon, S. Truant, D. Castaing, T. D. Baere, F. Kunstlinger, M. Bouchahda, M. Afshar, P. Rougier, R. Adam, and M. Ducreux, "Conversion to resection of liver metastases from colorectal cancer with hepatic artery infusion of combined chemotherapy and systemic cetuximab in multicenter trial OPTILIV," *Annals ofOncology*, vol. 27, no. November 2015, pp. 267–274, 2016.

[185] F. Lévi, A. Karaboué, R. Saffroy, C. Desterke, V. Boige, D. Smith, M. Hebbar, P. Innominato, J. Taieb, C. Carvalho, R. Guimbaud, C. Focan, M. Bouchahda, R. Adam, M. Ducreux, G. Milano, and A. Lemoine, "Pharmacogenetic determinants of outcomes on triplet hepatic artery infusion and intravenous cetuximab for liver metastases from colorectal cancer (European trial OPTILIV, NCT00852228)," *British Journal of Cancer*, vol. 117, no. 7, pp. 965–973, 2017.

[186] E. Jones, T. Oliphant, P. Peterson, and Others, "{SciPy}: Open source scientific tools for {Python}," 2001.

[187] S. Basu, M. Zeng, T. Yin, S. Gao, and M. Hu, "Development and validation of an UPLC-MS/MS method for the quantification of irinotecan, SN-38 and SN-38 glucuronide in plasma, urine, feces, liver and kidney: Application to a pharmacokinetic study of irinotecan in rats," *Journal of Chromatography B: Analytical Technologies in the Biomedical and Life Sciences*, vol. 1015-1016, pp. 34–41, 2016.

[188] B. N. Matos, P. M. D. Oliveira, T. A. Reis, T. Gratieri, M. Cunha-Filho, and G. M. Gelfuso, "Development and Validation of a Simple and Selective Analytical HPLC Method for the Quantification of Oxaliplatin," *Journal of Chemistry*, vol. 2015, 2015.

[189] M. Munawar Hayat, M. Sohail, and M. Ashraf, "Spectrophotometric determination of cisplatin, carboplatin and oxaliplatin in pure and injectable dosage forms," *Biomedical Research*, vol. 30, no. 4, pp. 557–562, 2019.

[190] D. Kang, J. B. Schwartz, and D. Verotta, "Sample Size Computations for PK / PD Population Models," *Journal of Pharmacokinetics and Pharmacodynamics*, vol. 32, no. 5-6, pp. 685–701, 2005.

[191] K. Ogungbenro, L. Aarons, K. Ogungbenro, and L. Aarons, "Sample Size / Power Calculations for Population Pharmacodynamic Experiments Involving Repeated-Count Measurements," *Journal of Biopharmaceutical Statistics ISSN:*, vol. 20, no. 5, pp. 1026–1042, 2010.

[192] Y. Fukuyama, "A new method of choosing the number of clusters for the fuzzy c-mean method," in *Proc. 5th Fuzzy Syst. Symp., 1989*, pp. 247–250, 1989.

[193] F. Pedregosa, G. Varoquaux, A. Gramfort, V. Michel, B. Thirion, O. Grisel, M. Blondel, P. Prettenhofer, R. Weiss, V. Dubourg, J. Vanderplas, A. Passos, D. Cournapeau, M. Brucher, M. Perrot, and E. Duchesnay, "Scikit-learn: Machine Learning in {P}ython," *Journal of Machine Learning Research*, vol. 12, pp. 2825—-2830, 2011.

[194] N. Jaworska and A. C. Anastasova, "A Review of Multidimensional Scaling (MDS) and its Utility in Various Psychological Domains," *Tutorials in Quantitative Methods for Psychology*, vol. 5, no. 1, 2009.

[195] L. C. Evans and A. M. Society, *Partial Differential Equations*. Graduate studies in mathematics, American Mathematical Society, 1998.

[196] J. G. Slatter, L. J. Schaaf, J. P. Sams, K. L. Feenstra, M. G. Johnson, P. A. Bombardt, K. S. Cathcart, M. T. Verburg, L. K. Pearson, L. D. Compton, L. L. Miller, D. S. Baker, and C. V. Pesheck, "Pharmacokinetics, Metabolism, and Excretion of Irinotecan (Cpt-11) following I. V. Infusion of [14C]Cpt-11 in Cancer Patients," *Drug Metabolism and Disposition*, vol. 28, no. 4, pp. 423–433, 2000.

[197] . Ron H. J. Mathijssen, . Robbert J. van Alphen, Jaap Verweij, Walter J. Loos, Kees Nooter, Gerrit Stoter, and A. Sparreboom, "Clinical pharmacokinetics and metabolism of Irinotecan (CPT-11) Ron," *Clinical Cancer Research*, vol. 7, no. 1-2, pp. 2182–2194, 2001.

[198] H. . DOUGLASS, M. JR, and M. A. MITTELMAN, "METABOLIC STUDIES OF 5-FLUOROURACIL-11. INFLUENCE OF THE ROUTE OF ADMINISTRATION ON THE DYNAMICS OF DISTRIBUTION IN MAN," *Cancer*, vol. 34, pp. 1878–1881, 1974.

[199] M. S. Roberts, B. M. Magnusson, F. J. Burczynski, and M. Weiss, "Enterohepatic circulation: Physiological, pharmacokinetic and clinical implications," *Clinical Pharmacokinetics*, vol. 41, no. 10, pp. 751–790, 2002.

[200] L. P. Rivory, M. R. Bowles, J. Robert, and S. M. Pond, "Conversion of irinotecan (CPT-11) to its active metabolite, 7-ethyl-10-hydroxycamptothecin (SN-38) by human liver carboxylesterase," *Biochemical Pharmacology*, vol. 52, no. 7, pp. 1103–1111, 1996.

[201] D. Wang, L. Zou, Q. Jin, J. Hou, G. Ge, and L. Yang, "Human carboxylesterases: a comprehensive review," *Acta Pharmaceutica Sinica B*, vol. 8, no. 5, pp. 699–712, 2018.

[202] A. Ahluwalia, "Allometric scaling in-vitro," *Scientific Reports*, vol. 7, p. 42113, feb 2017.

[203] Y. Tsukamoto, Y. Kato, M. Ura, I. Horii, H. Ishitsuka, H. Kusuhara, and Y. Sugiyama, "A physiologically based pharmacokinetic analysis of capecitabine, a triple prodrug of 5-FU, in humans: The mechanism for tumor-selective accumulation of 5-FU," *Pharmaceutical Research*, vol. 18, no. 8, pp. 1190–1202, 2001.

[204] O. Combes, J. Barré, J. C. Duché, L. Vernillet, Y. Archimbaud, M. P. Marietta, J. P. Tillement, and S. Urien, "In vitro binding and partitioning of irinotecan (CPT-11) and its metabolite, SN-38, in human blood," *Investigational New Drugs*, vol. 18, no. 1, pp. 1–5, 2000.

[205] C. Bertucci, G. Ascoli, G. Uccello-Barretta, L. Di Bari, and P. Salvadori, "The binding of 5-fluorouracil to native and modified human serum albumin: UV, CD, and 1H and 19F NMR investigation.," *Journal of pharmaceutical and biomedical analysis*, vol. 13, no. 9, pp. 1087–93, 1995.

[206] Pfizer, "CAMPTOSAR (Irinotecan) HIGHLIGHTS OF PRESCRIBING INFORMATION," tech. rep., Pfizer, 2014.

[207] W. Wang and Y. Zhang, "On fuzzy cluster validity indices," *Fuzzy Sets and Systems*, vol. 158, no. 19, pp. 2095–2117, 2007.

[208] L. Deyme, D. Barbolosi, and F. Gattacceca, "Population pharmacokinetics of FOLFIRINOX : a review of studies and parameters," *Cancer Chemotherapy and Pharmacology*, vol. 83, no. 1, pp. 27–42, 2019.

[209] H. van de Waterbeemd and E. Gifford, "ADMET in silico modelling: Towards prediction paradise?," *Nature Reviews Drug Discovery*, vol. 2, no. 3, pp. 192–204, 2003.

[210] H. Olson, G. Betton, D. Robinson, K. Thomas, A. Monro, G. Kolaja, P. Lilly, J. Sanders, G. Sipes, W. Bracken, M. Dorato, K. Van Deun, P. Smith, B. Berger, and A. Heller, "Concordance of the toxicity of pharmaceuticals in humans and in animals," *Regulatory Toxicology and Pharmacology*, vol. 32, no. 1, pp. 56–67, 2000.

[211] C. H. I. H. Wong, K. W. E. I. Siah, and A. W. Lo, "Estimation of clinical trial success rates and related," *Biostatistics*, vol. 20, no. 2, pp. 273–286, 2019.

[212] I. W. Y. Mak, N. Evaniew, and M. Ghert, "Lost in translation : animal models and clinical trials in cancer treatment," *American journal of translational research*, vol. 6, no. 2, pp. 114–118, 2014.

[213] M. Viceconti, A. Henney, and E. Morley-Fletcher, "in silico Clinical Trials: How Computer Simulation will Transform the Biomedical Industry.," 2016.

[214] K. Yoshida, N. Budha, and J. Y. Jin, "Impact of physiologically based pharmacokinetic models on regulatory reviews and product labels: Frequent utilization in the field of oncology," *Clinical Pharmacology and Therapeutics*, vol. 101, no. 5, pp. 597–602, 2017.

[215] G. Helmlinger, N. Al-Huniti, S. Aksenov, K. Peskov, K. M. Hallow, L. Chu, D. Boulton, U. Eriksson, B. Hamrén, C. Lambert, E. Masson, H. Tomkinson, and D. Stanski, "Drug-disease modeling in the pharmaceutical industry - where mechanistic systems pharmacology and statistical pharmacometrics meet," *European Journal of Pharmaceutical Sciences*, vol. 109, no. May, pp. S39–S46, 2017.

[216] K. Gadkar, D. Kirouac, N. Parrott, and S. Ramanujan, "Quantitative systems pharmacology: a promising approach for translational pharmacology," *Drug Discovery Today: Technologies*, vol. 21-22, no. Ldl, pp. 57–65, 2016.

[217] K. Venkatakrishnan, L. E. Friberg, D. Ouellet, J. T. Mettetal, A. Stein, I. F. Trocóniz, R. Bruno, N. Mehrotra, J. Gobburu, and D. R. Mould, "Optimizing oncology therapeutics through quantitative translational and clinical pharmacology: challenges and opportunities," *Clinical Pharmacology & Therapeutics*, vol. 97, no. 1, pp. 37–54, 2015.

[218] W. Ritschel, N. Vachharajani, R. Johnson, and A. Hussain, "The allometric approach for interspecies scaling of pharmacokinetic parameters," *Comparative Biochemistry and Physiology*, vol. 103c, no. 2, pp. 249–253, 1992.

[219] L. P. Bonate, , and J.-L. Steimer, *Pharmacokinetic- Pharmacodynamic Modeling and Simulation*. New York: Springer, 2011.

[220] H. M. Jones, M. Dickins, K. Youdim, J. R. Gosset, N. J. Attkins, T. L. Hay, I. K. Gurrell, Y. R. Logan, P. J. Bungay, B. C. Jones, and I. B. Gardner, "Application of PBPK modelling in drug discovery and development at Pfizer," *Xenobiotica*, vol. 42, no. 1, pp. 94–106, 2012.

[221] G. Manley, "ITC Recommendations for Transporter Kinetic Parameter Estimation and Translational Modeling of Transport-Mediated PK and DDIs in Humans," *Clinical Pharmacology & Therapeutics*, vol. 71, no. 2, pp. 233–236, 2013.

[222] H.-Y. Chang, S. Wu, G. Meno-Tetang, and D. K. Shah, "A translational platform PBPK model for antibody disposition in the brain," *Journal of Pharmacokinetics and Pharmacodynamics*, vol. 8, 2019.

[223] M. Krauss, U. Hofmann, C. Schafmayer, S. Igel, J. Schlender, C. Mueller, M. Brosch, W. von Schoenfels, W. Erhart, A. Schuppert, M. Block, E. Schaeffeler, G. Boehmer, L. Goerlitz, J. Hoecker, J. Lippert, R. Kerb, J. Hampe, L. Kuepfer, and M. Schwab, "Translational learning from clinical studies predicts drug pharmacokinetics across patient populations," *npj Systems Biology and Applications*, vol. 3, no. 1, pp. 1–10, 2017.

[224] M. G. Feasel, R. J. Lawrence, R. L. Kristovich, A. Wohlfarth, and M. A. Huestis, "Translational Human Health Assessment of Carfentanil Using an Experimentally Refined PBPK Model," tech. rep., U.S. Army Research, Development and Engineering Command, Baltimore, 2018.

[225] C. Wagner, P. Zhao, Y. Pan, V. Hsu, J. Grillo, S. M. Huang, and V. Sinha, "Application of physiologically based pharmacokinetic (PBPK) modeling to support dose selection: Report of an FDA public workshop on PBPK," *CPT: Pharmacometrics and Systems Pharmacology*, vol. 4, no. 4, pp. 226–230, 2015.

[226] A. Ballesta, Q. Zhou, X. Zhang, H. Lv, and J. M. Gallo, "Multiscale Design of Cell-Type–Specific Pharmacokinetic/Pharmacodynamic Models for Personalized Medicine: Application to Temozolomide in Brain Tumors," *CPT Pharmacometrics Syst. Pharmacol.*, vol. 3, no. 4, p. e112, 2014.

[227] B. P. Espósito and R. Najjar, "Interactions of antitumoral platinum-group metallodrugs with albumin," *Coordination Chemistry Reviews*, vol. 232, no. 1-2, pp. 137–149, 2002.

[228] C. Thiel, S. Schneckener, M. Krauss, A. Ghallab, U. Hofmann, T. Kanacher, S. Zellmer, R. Gebhardt, J. G. Hengstler, and L. Kuepfer, "A systematic evaluation of the use of physiologically based pharmacokinetic modeling for cross-species extrapolation," *Journal of Pharmaceutical Sciences*, vol. 104, no. 1, pp. 191–206, 2015.

[229] L. Pendyala and P. J. Creaven, "In Vitro Cytotoxicity , Protein Binding , Red Blood Cell Partitioning , and Biotransformation of Oxaliplatin.," *Cancer Research*, no. ll, pp. 5970–5976, 1993.

[230] MATLAB, "MATLAB : 2018b," 2018.

[231] Yarpiz, "CMA-ES in Matlab," 2015.

[232] A. H. Bryk and J. R. Wiśniewski, "Quantitative Analysis of Human Red Blood Cell Proteome," *Journal of Proteome Research*, vol. 16, no. 8, pp. 2752–2761, 2017.

[233] Charles River, "C57BL/6 Mouse Hematology," Tech. Rep. December, Charles River, 2008.

[234] S. P. Gavan, A. J. Thompson, and K. Payne, "The economic case for precision medicine," *Expert Review of Precision Medicine and Drug Development*, vol. 3, no. 1, pp. 1–9, 2018.

[235] G. Vernon, "The chronotherapy of hypertension: or the benefit of taking blood pressure tablets at bedtime," *British Journal of General Practice*, vol. 67, no. 657, p. 171, 2017.

[236] P. F. Innominato, S. Komarzynski, O. G. Palesh, R. Dallmann, G. A. Bjarnason, S. Giacchetti, A. Ulusakarya, M. Bouchahda, M. Haydar, A. Ballesta, A. Karaboué, N. I. Wreglesworth, D. Spiegel, and F. A. Lévi, "Circadian rest-activity rhythm as an objective biomarker of patient-reported outcomes in patients with advanced cancer," *Cancer Medicine*, vol. 7, no. 9, pp. 4396–4405, 2018.

[237] G. Wu, M. D. Ruben, R. E. Schmidt, L. J. Francey, D. F. Smith, R. C. Anafi, J. J. Hughey, R. Tasseff, J. D. Sherrill, J. E. Oblong, K. J. Mills, and J. B. Hogenesch, "Population-level rhythms in human skin with implications for circadian medicine," *Proceedings of the National Academy of Sciences*, vol. 115, no. 48, pp. 12313–12318, 2018.

[238] C. Ober, D. A. Loisel, and Y. Gilad, "Sex-specific genetic architecture of human disease," *Nature Reviews Genetics*, vol. 9, no. 12, pp. 911–922, 2008.

[239] O. P. Soldin, S. H. Chung, and D. R. Mattison, "Sex differences in drug disposition," *Journal of Biomedicine and Biotechnology*, vol. 2011, pp. 7–9, 2011.

[240] M. Bailey and R. Silver, "Sex differences in circadian timing systems: Implications for disease," *Frontiers in Neuroendocrinology*, vol. 35, no. 1, pp. 111–139, 2014.

[241] A. N. Edginton, F.-P. Theil, W. Schmitt, and S. Willmann, "Whole body physiologically-based pharmacokinetic models: their use in clinical drug development," *Expert Opinion on Drug Metabolism & Toxicology*, vol. 4, pp. 1143–1152, sep 2008.

[242] Ivan Nestorov, "Whole body pharmacokinetic models," *Clinical Pharmacokinetics*, vol. 42, no. 10, pp. 883–908, 2003.

[243] M. Riihimaki, A. Hemminki, J. Sundquist, and K. Hemminki, "Patterns of metastasis in colon and rectal cancer," *Scientific Reports*, vol. 6, pp. 1–9, 2016.

[244] J. K. Aronson, M. J. Chappell, K. R. Godfrey, and M. K. Yew, "Modelling circadian variation in the pharmacokinetics of non-steroidal anti-inflammatory drugs," *European Journal of Clinical Pharmacology*, vol. 45, no. 4, pp. 357–361, 1993.

[245] J. Y. Noh, D. H. Han, J. A. Yoon, M. H. Kim, S. E. Kim, I. G. Ko, K. H. Kim, C. J. Kim, and S. Cho, "Circadian rhythms in urinary functions: Possible roles of circadian clocks?," *International Neurourology Journal*, vol. 15, no. 2, pp. 64–73, 2011.

[246] W. A. Hoogerwerf, V. B. Shahinian, G. Cornélissen, F. Halberg, J. Bostwick, J. Timm, P. A. Bartell, and V. M. Cassone, "Rhythmic changes in colonic motility are regulated by period genes," *American Journal of Physiology-Gastrointestinal and Liver Physiology*, vol. 298, no. 2, pp. G143–G150, 2009.

Appendix A

Appendix

Chapter 4: DAISY input in vitro model

```
WRITE "MOD CPT11"$

% B_ is a reserved name used to indicate the vector input,
output and state variables
B_:={y1,y2,y3,P_f,P_b,R_f,R_b}$

% Define the components of vector B_ as time-depending
variables
FOR EACH EL_ IN B_ DO DEPEND EL_,T$

% B1_ is a reserved name used to indiate the vector of
unknown parameters
B1_:={p1,p2,p3,p4,p5,p6}$

% NX_ and NY_ are reserved to indicate the numbers of
states, outputs and inputs respectively
NX_:=4$
NY_:=3$
NU_:=0$
% C_is a reserved variable name used to indicate the
system of differential polynomials that describe the model
C_:={df(P_f,t)=-p1*P_f + p2*P_b - p3*P_f + p4*R_f,
df(P_b,t)=p1*P_f - p2*P_b,
df(R_f,t)=-p4*R_f + p3*P_f -p5*R_f + p6*R_b,
df(R_b,t)=p5*R_f - p6*R_b,
y1=P_f,
```

```
y2=P_b,
y3=R_f+R_b}$
flag_:=1$
% Invoke the procedure that calculates the
characteristic set
SEED_:=25$
DAISY()$
IC_:={P_f=100,P_b=0,R_f=0,R_b=0}$
%ICUNK_:={x10=x1u}$
CONDINIZ()$
END$
```

Chapter 4: DAISY input whole body model

```
WRITE "MOD whole body pk"$

% B_ is a reserved name used to indicate the vector input,
output and state variables
B_:={y1,y2,y3,y4,y5,y6,y7,y8,P_f,P_b,R_f,R_b,M_f,M_b,N_f,
N_b,L_f,L_b,J_f,J_b}$

% Define the components of vector B_ as time-depending
variables
FOR EACH EL_ IN B_ DO DEPEND EL_,T$

% B1_ is a reserved name used to indiate the vector of
unknown parameters
B1_:={k_p_r,k_p_m,k_p_n,k_p_l,k_p_j,k_r_p,k_m_p,k_n_p,
k_l_p,k_j_l,k_b_p,k_b_r,k_b_m,k_b_n,k_b_l,k_b_j,k_un,
Clear_b,Clear_l,Clear_j}$

% NX_ and NY_ are reserved to indicate the numbers of
states, outputs and inputs respectively
NX_:=12$
NY_:=8$
NU_:=0$
% C_is a reserved variable name used to indicate the
system of differential polynomials that describe the model
C_:={df(P_f,t)=((k_un*P_b + k_r_p*R_f + k_n_p*N_f +
k_m_p*M_f + k_l_p*L_f) - (k_b_p + k_p_r + k_p_n +
k_p_m + k_p_l + k_p_j + Clear_b)*P_f)/V_p,
```

```
df(P_b,t)=(k_b_p*P_f - k_un*P_b)/V_p,
df(R_f,t)=((k_p_r*P_f + k_un*R_b) -
(k_b_r + k_r_p)*R_f)/V_r,
df(R_b,t)=(k_b_r*R_f - k_un*R_b)/V_r,
df(M_f,t)=((k_p_m*P_f + k_un*M_b) -
(k_b_m + k_m_p)*M_f)/V_m,
df(M_b,t)=(k_b_m*M_f - k_un*M_b)/V_M,
df(N_f,t)=((k_p_n*P_f + k_un*N_b) -
(k_b_n + k_n_p)*N_f)/V_n,
df(N_b,t)=(k_b_n*N_f - k_un*N_b)/V_n,
df(L_f,t)=((k_p_l*P_f + k_un*L_b + k_j_l*J_f) -
(k_b_l + k_l_p + Clear_l)*L_f)/V_l,
df(L_b,t)=(k_b_l*L_f - k_un*L_b)/V_l,
df(J_f,t)=((k_p_j*P_f + k_un*J_b) -
(k_b_j + k_j_l + Clear_j)*J_f)/V_j,
df(J_b,t)=(k_b_j*J_f - k_un*J_b)/V_j,
y1=P_f,
y2=P_b,
y3=R_f,
y4=R_b,
y5=L_f,
y6=L_b,
y7=J_f,
y8=J_b}$

%let k_b_n = k_n_b$

% Invoke the procedure that calculates the
characteristic set
SEED_:=60$
DAISY()$

IC_:={p_f=50,p_b=0,r_f=0,r_b=0,n_f=0,n_b=0,
m_f=0,m_b=0,l_f=0,l_b=0,j_f=0,j_b=0}$
CONDINIZ()$
END$
```

Chapter 4: DAISY output in vitro model

```
MOD IN VITRO MODEL$
```

```
seed_ := 25$

NUMBER OF EQUATIONS$

n_ := 7$

VARIABLES VECTOR$

b_ := {y1,
y2,
y3,
p_f,
p_b,
r_f,
r_b}$

UNKNOWN PARAMETER(S) VECTOR$

b1_ := {p1,
p2,
p3,
p4,
p5,
p6}$

RANKING AMONG THE VARIABLES$

bb_ := {y1,
y2,
y3,
df(y1,t),
df(y2,t),
df(y3,t),
df(y1,t,2),
df(y2,t,2),
df(y3,t,2),
df(y1,t,3),
df(y2,t,3),
df(y3,t,3),
```

```
df(y1,t,4),
df(y2,t,4),
df(y3,t,4),
p_f,
p_b,
r_f,
r_b,
df(p_f,t),
df(p_b,t),
df(r_f,t),
df(r_b,t)}$

NUMBER OF INPUT(S)$

nu_ := 0$

NUMBER OF OUTPUT(S)$

ny_ := 3$

NUMBER OF STATE(S) $

nx_ := 4$

MODEL EQUATION(S)$

c_ := {df(p_f,t)= - (p3*p_f - p4*r_f - p2*p_b) - p1*p_f,
df(p_b,t)=p1*p_f - p2*p_b,
df(r_f,t)= - (p5*r_f - p6*r_b + p4*r_f) + p3*p_f,
df(r_b,t)=p5*r_f - p6*r_b,
y1=p_f,
y2=p_b,
y3=r_b + r_f}$

CHARACTERISTIC SET$

aa_(1) :=  - df(y2,t) + y1*p1 - y2*p2$

aa_(2) :=  - df(y1,t)*p4**3 - df(y3,t)*p4**3 - y1*p1*p4**3
+ y2*p2*p4**3$
```

```
aa_(3) :=  - df(y1,t,2)*p4**4
- df(y1,t)*p4**4*(p1 + p3 + p4 + p5 + p6)
+ y1*p4**4*(p1*p2 - p1*p4 - p1*p5 - p1*p6 - p3*
p5 - p3*p6) + y2*p2*p4**4*( - p2 + p4 + p5 + p6)
+ y3*p4**5*p6$

aa_(4) :=  - p_f + y1$

aa_(5) :=  - p_b + y2$

aa_(6) :=  - df(y1,t) + r_f*p4 - y1*(p1 + p3) + y2*p2$

aa_(7) :=  - df(y1,t) - r_b*p4 - y1*(p1 + p3) + y2*p2 + y3*p4$
```

MODEL ALGEBRAICALLY OBSERVABLE$

NORMALIZED INPUT /OUTPUT RELATION(S) $

```
aan_(1) :=  - df(y2,t) + y1*p1 - y2*p2$

aan_(2) := df(y1,t) + df(y3,t) + y1*p1 - y2*p2$

aan_(3) := df(y1,t,2) + df(y1,t)*(p1 + p3 + p4 + p5 + p6)
+ y1*( - p1*p2 + p1*p4 + p1*p5 + p1*p6 + p3*p5 + p3*p6) + y2*
p2*(p2 - p4 - p5 - p6) - y3*p4*p6$
```

RANDOMLY CHOSEN NUMERICAL PARAMETER(S) VECTOR$

```
b2_ := {p1=5,p2=10,p3=24,p4=22,p5=16,p6=17}$
```

EXHAUSTIVE SUMMARY $

```
flist_ := {p1 - 5,
 - p2 + 10,
p1 - 5,
 - p2 + 10,
 - p4*p6 + 374,
p2**2 - p2*p4 - p2*p5 - p2*p6 + 450,
p1 + p3 + p4 + p5 + p6 - 84,
```

```
 - p1*p2 + p1*p4 + p1*p5 + p1*p6 + p3*p5 + p3*p6 - 1017}$

MODEL PARAMETER SOLUTION(S)$

 G_:=GROESOLVE(FLIST_,B1_) $

g_ := {{p3=24,p4=22,p5=16,p6=17,p1=5,p2=10}}$

MODEL GLOBALLY IDENTIFIABLE$

INITIAL CONDITION(S)  NOT NECESSARY$
```

Chapter 4: DAISY output whole body model

```
MOD whole body pk$

seed_ := 60$

NUMBER OF EQUATIONS$

n_ := 18$

VARIABLES VECTOR$

b_ := {y1,
y2,
y3,
y4,
y5,
y6,
y7,
y8,
p_f,
p_b,
r_f,
r_b,
n_f,
n_b,
l_f,
l_b,
```

```
j_f,
j_b}$

UNKNOWN PARAMETER(S) VECTOR$

b1_ := {k_p_r,
k_p_n,
k_p_l,
k_p_j,
k_r_p,
k_n_p,
k_l_p,
k_j_l,
k_b_p,
k_b_r,
k_b_n,
k_b_l,
k_b_j,
k_un,
clear_b,
clear_l,
clear_j}$

RANKING AMONG THE VARIABLES$

bb_ := {y1,
y2,
y3,
y4,
y5,
y6,
y7,
y8,
df(y1,t),
df(y2,t),
df(y3,t),
df(y4,t),
df(y5,t),
df(y6,t),
df(y7,t),
```

```
df(y8,t),
df(y1,t,2),
df(y2,t,2),
df(y3,t,2),
df(y4,t,2),
df(y5,t,2),
df(y6,t,2),
df(y7,t,2),
df(y8,t,2),
df(y1,t,3),
df(y2,t,3),
df(y3,t,3),
df(y4,t,3),
df(y5,t,3),
df(y6,t,3),
df(y7,t,3),
df(y8,t,3),
df(y1,t,4),
df(y2,t,4),
df(y3,t,4),
df(y4,t,4),
df(y5,t,4),
df(y6,t,4),
df(y7,t,4),
df(y8,t,4),
df(y1,t,5),
df(y2,t,5),
df(y3,t,5),
df(y4,t,5),
df(y5,t,5),
df(y6,t,5),
df(y7,t,5),
df(y8,t,5),
df(y1,t,6),
df(y2,t,6),
df(y3,t,6),
df(y4,t,6),
df(y5,t,6),
df(y6,t,6),
df(y7,t,6),
```

```
df(y8,t,6),
df(y1,t,7),
df(y2,t,7),
df(y3,t,7),
df(y4,t,7),
df(y5,t,7),
df(y6,t,7),
df(y7,t,7),
df(y8,t,7),
df(y1,t,8),
df(y2,t,8),
df(y3,t,8),
df(y4,t,8),
df(y5,t,8),
df(y6,t,8),
df(y7,t,8),
df(y8,t,8),
df(y1,t,9),
df(y2,t,9),
df(y3,t,9),
df(y4,t,9),
df(y5,t,9),
df(y6,t,9),
df(y7,t,9),
df(y8,t,9),
df(y1,t,10),
df(y2,t,10),
df(y3,t,10),
df(y4,t,10),
df(y5,t,10),
df(y6,t,10),
df(y7,t,10),
df(y8,t,10),
p_f,
p_b,
r_f,
r_b,
n_f,
n_b,
l_f,
```

```
l_b,
j_f,
j_b,
df(p_f,t),
df(p_b,t),
df(r_f,t),
df(r_b,t),
df(n_f,t),
df(n_b,t),
df(l_f,t),
df(l_b,t),
df(j_f,t),
df(j_b,t)}$

NUMBER OF INPUT(S)$

nu_ := 0$

NUMBER OF OUTPUT(S)$

ny_ := 8$

NUMBER OF STATE(S) $

nx_ := 10$

MODEL EQUATION(S)$

c_ := {df(p_f,t)=(k_r_p*r_f + k_un*p_b - k_p_r*p_f
- k_p_n*p_f - k_p_m*p_f - k_p_l*p_f - k_p_j*p_f
+ k_n_p*n_f + k_m_p*
m_f + k_l_p*l_f - k_b_p*p_f - clear_b*p_f)/v_p,
df(p_b,t)=(k_b_p*p_f - k_un*p_b)/v_p,
df(r_f,t)=( - (k_r_p*r_f - k_un*r_b - k_p_r*p_f)
- k_b_r*r_f)/v_r,
df(r_b,t)=(k_b_r*r_f - k_un*r_b)/v_r,
df(n_f,t)=(k_p_n*p_f + k_un*n_b - k_n_p*n_f
- k_b_n*n_f)/v_n,
df(n_b,t)=(k_b_n*n_f - k_un*n_b)/v_n,
df(l_f,t)=(k_p_l*p_f + k_un*l_b - k_l_p*l_f - k_b_l*l_f
```

```
+ j_f*k_j_l - clear_l*l_f)/v_l,
df(l_b,t)=(k_b_l*l_f - k_un*l_b)/v_l,
df(j_f,t)=( - ((k_b_j + k_j_l)*j_f - k_p_j*p_f - j_b*k_un)
- clear_j*j_f)/v_j,
df(j_b,t)=( - j_b*k_un + j_f*k_b_j)/v_j,
y1=p_f,
y2=p_b,
y3=r_f,
y4=r_b,
y5=l_f,
y6=l_b,
y7=j_f,
y8=j_b}$
```

CHARACTERISTIC SET$

```
aa_(1) :=  - df(y2,t)*v_p + y1*k_b_p - y2*k_un$

aa_(2) := df(y3,t)*v_r - y1*k_p_r + y3*(k_b_r + k_r_p)
- y4*k_un$

aa_(3) :=  - df(y4,t)*v_r + y3*k_b_r - y4*k_un$

aa_(4) :=  - df(y5,t)*v_l + y1*k_p_l
- y5*(clear_l + k_b_l + k_l_p) + y6*k_un + y7*k_j_l$

aa_(5) :=  - df(y6,t)*v_l + y5*k_b_l - y6*k_un$

aa_(6) := df(y7,t)*v_j - y1*k_p_j
+ y7*(clear_j + k_b_j + k_j_l) - y8*k_un$

aa_(7) :=  - df(y8,t)*v_j + y7*k_b_j - y8*k_un$

aa_(8) := df(y1,t,3)*k_n_p**4*k_un*v_j*v_l**4*v_n**2*v_p
**4*v_r**4
+ df(y1,t,2)*k_n_p**4*k_un*v_j*v_l**4*v_n*v_p**3*v_r
**4*(clear_b*v_n + k_b_n*v_p + k_b_p*v_n + k_n_p*v_p
+ k_p_j*v_n+ k_p_l*v_n+ k_p_m*v_n + k_p_n*v_n + k_p_r*v_n
+ k_un*v_p)
+ df(y1,t)*k_n_p**4*k_un*v_j*v_l**3*v_p**2*v_r**3*(
```

```
clear_b*k_b_n*v_l*v_n*v_p*v_r + clear_b*k_n_p*v_l*v_n*v_p*v_r
+ clear_b*k_un*v_l*v_n*v_p*v_r + k_b_n*k_b_p*v_l*v_n*v_p*v_r
+ k_b_n*k_p_j*v_l*v_n*v_p*v_r + k_b_n*k_p_l*v_l*v_n*v_p*v_r
+ k_b_n*k_p_m*v_l*v_n*v_p*v_r + k_b_n*k_p_n*v_l*v_n*v_p*v_r
+ k_b_n*k_p_r*v_l*v_n*v_p*v_r + k_b_p*k_n_p*v_l*v_n*v_p*v_r
- k_b_p*k_un*v_l*v_n**2*v_r + k_b_p*k_un*v_l*v_n*v_p*v_r
- k_l_p*k_p_l*v_n**2*v_p*v_r + k_n_p*k_p_j*v_l*v_n*v_p*v_r +
k_n_p*k_p_l*v_l*v_n*v_p*v_r + k_n_p*k_p_m*v_l*v_n*v_p*v_r +
k_n_p*k_p_r*v_l*v_n*v_p*v_r + k_n_p*k_un*v_l*v_p**2*v_r +
k_p_j*k_un*v_l*v_n*v_p*v_r + k_p_l*k_un*v_l*v_n*v_p*v_r
+ k_p_m*k_un*v_l*v_n*v_p*v_r + k_p_n*k_un*v_l*v_n*v_p*v_r -
k_p_r*k_r_p*v_l*v_n**2*v_p + k_p_r*k_un*v_l*v_n*v_p*v_r)
+ y1*k_n_p**4*k_un*v_l**2*v_p*v_r**2*(clear_b*k_n_p*k_un*v_j*
v_l**2*v_p**2*v_r**2
+ clear_l*k_l_p*k_p_l*v_j*v_n**2*v_p**2*v_r**2
+ k_b_l*k_l_p*k_p_l*v_j*v_n**2*v_p**2*v_r**2
- k_b_n*k_b_p*k_un*v_j*v_l**2*v_n*v_p*v_r**2
- k_b_n*k_l_p*k_p_l*v_j*v_l*v_n*v_p**2*v_r**2
- k_b_n*k_p_r*k_r_p*v_j*v_l**2*v_n*
v_p**2*v_r - k_b_p*k_n_p*k_un*v_j*v_l**2*v_n*v_p*v_r**2
+ k_b_p*k_n_p*k_un*v_j*v_l**2*v_p**2*v_r**2
+ k_b_p*k_un**2*v_j*v_l**2*v_n**2*v_r**2
- k_b_p*k_un**2*v_j*v_l**2*v_n*v_p*v_r**2
+ k_b_r*k_p_r*k_r_p*v_j*v_l**2*v_n**2*v_p**2
- k_j_l*k_l_p*k_p_j*v_l*v_n**2*v_p**2*v_r**2
+ k_l_p**2*k_p_l*v_j*v_n**2*v_p**2*v_r**2
- k_l_p*k_n_p*k_p_l*v_j*v_l*v_n*v_p**2*v_r**2
- k_l_p*k_p_l*k_un*v_j*v_l*v_n*v_p**2*v_r**2
+ k_n_p*k_p_j*k_un*v_j*v_l**2*v_p**2*v_r**2
+ k_n_p*k_p_l*k_un*v_j*v_l**2*v_p**2*v_r**2
+ k_n_p*k_p_m*k_un*v_j*v_l**2*v_p**2*v_r**2
- k_n_p*k_p_r*k_r_p*v_j*v_l**2*v_n*v_p**2*v_r
+ k_n_p*k_p_r*k_un*v_j*v_l**2*v_p**2*v_r**2
+ k_p_r*k_r_p**2*v_j*v_l**2*v_n**2*v_p**2
- k_p_r*k_r_p*k_un*v_j*v_l**2*v_n*v_p**2*v_r)
+ y2*k_n_p**4*k_un**3*v_j*v_l**4*v_p*v_r**4*(
k_b_n*v_n*v_p + k_n_p*v_n*v_p
- k_n_p*v_p**2 - k_un*v_n**2 + k_un*v_n*
v_p) + y3*k_n_p**4*k_r_p*k_un*v_j*v_l**4*v_p**3*v_r**2*(
k_b_n*k_b_r*v_n*v_r + k_b_n*k_r_p*v_n*v_r - k_b_r**2*v_n**2
```

```
+ k_b_r*k_n_p*v_n*v_r - 2*k_b_r*k_r_p*v_n**2
- k_b_r*k_un*v_n**2 + k_b_r*k_un*v_n*v_r
+ k_n_p*k_r_p*v_n*v_r - k_n_p*k_un*
v_r**2 - k_r_p**2*v_n**2 + k_r_p*k_un*v_n*v_r)
+ y4*k_n_p**4*k_r_p*k_un**2*v_j*v_l**4*v_n*v_p**3*v_r**2*(
- k_b_n*v_r + k_b_r*v_n - k_n_p*v_r + k_r_p*v_n
+ k_un*v_n - k_un*v_r)
+ y5*k_l_p*k_n_p**4*k_un*v_j*v_l**2*v_p**3*v_r**4*(
- clear_l**2*v_n**2 - 2*clear_l*k_b_l*v_n**2
+ clear_l*k_b_n*v_l*v_n- 2*clear_l*k_l_p*v_n**2
+ clear_l*k_n_p*v_l*v_n+ clear_l*k_un*v_l*v_n
- k_b_l**2*v_n**2+ k_b_l*k_b_n*v_l*v_n
- 2*k_b_l*k_l_p*v_n**2+ k_b_l*k_n_p*v_l*v_n
+ k_b_l*k_un*v_l*v_n- k_b_l*k_un*v_n**2
+ k_b_n*k_l_p*v_l*v_n- k_l_p**2*v_n**2
+ k_l_p*k_n_p*v_l*v_n+ k_l_p*k_un*v_l*v_n
- k_n_p*k_un*v_l**2)
+ y6*k_l_p*k_n_p**4*k_un**2*v_j*v_l**2*v_n*v_p**3*v_r**4*(
clear_l*v_n + k_b_l*v_n - k_b_n*v_l + k_l_p*v_n - k_n_p*v_l
 - k_un*v_l + k_un*v_n)
+ y7*k_j_l*k_l_p*k_n_p**4*k_un*v_l**2*v_n*v_p**3*v_r**4*(
clear_j*v_l*v_n + clear_l*v_j*v_n + k_b_j*v_l*v_n
+ k_b_l*v_j*v_n - k_b_n*v_j*v_l + k_j_l*v_l*v_n
+ k_l_p*v_j*v_n - k_n_p*v_j*v_l - k_un*v_j*v_l)
- y8*k_j_l*k_l_p*k_n_p**4*k_un**2*v_l**3*v_n**2*v_p**3*v_r**4
- k_m_p*k_n_p**5*k_un**2*m_f*v_j*v_l**4*v_p**3*v_r**4$

aa_(9) :=  - p_f + y1$

aa_(10) :=  - p_b + y2$

aa_(11) :=  - r_f + y3$

aa_(12) :=  - r_b + y4$

aa_(13) :=  - df(y1,t)*v_p + n_f*k_n_p
- y1*(clear_b + k_b_p + k_p_j+ k_p_l + k_p_m
+ k_p_n + k_p_r) + y2*k_un
+ y3*k_r_p + y5*k_l_p + k_m_p*m_f$
```

```
aa_(14) :=  - df(y1,t,2)*k_n_p*v_l*v_n*v_p**2*v_r -
df(y1,t)*k_n_p*v_l*v_p*v_r*(clear_b*v_n + k_b_n*v_p
+ k_b_p*v_n+ k_n_p*v_p + k_p_j*v_n + k_p_l*v_n
+ k_p_m*v_n + k_p_n*v_n + k_p_r*v_n)
+ n_b*k_n_p**2*k_un*v_l*v_p*v_r
+ y1*k_n_p*( - clear_b*k_b_n*v_l*v_p*v_r
- clear_b*k_n_p*v_l*v_p*v_r - k_b_n*k_b_p*v_l*v_p*v_r
- k_b_n*k_p_j*v_l*v_p*v_r - k_b_n*k_p_l*v_l*v_p*v_r
- k_b_n*k_p_m*v_l*v_p*v_r - k_b_n*k_p_n*v_l*v_p*v_r
- k_b_n*k_p_r*v_l*v_p*v_r - k_b_p*k_n_p*v_l*v_p*v_r +
k_b_p*k_un*v_l*v_n*v_r + k_l_p*k_p_l*v_n*v_p*v_r
- k_n_p*k_p_j*v_l*v_p*v_r - k_n_p*k_p_l*v_l*v_p*v_r
- k_n_p*k_p_m*v_l*
v_p*v_r - k_n_p*k_p_r*v_l*v_p*v_r + k_p_r*k_r_p*v_l*v_n*v_p)
+ y2*k_n_p*k_un*v_l*v_r*(k_b_n*v_p + k_n_p*v_p - k_un*v_n)
+ y3*k_n_p*k_r_p*v_l*v_p*(k_b_n*v_r - k_b_r*v_n
+ k_n_p*v_r - k_r_p*v_n)
+ y4*k_n_p*k_r_p*k_un*v_l*v_n*v_p + y5*k_l_p*k_n_p*v_p*v_r*(
- clear_l*v_n - k_b_l*v_n + k_b_n*v_l - k_l_p*v_n + k_n_p*v_l)
+ y6*k_l_p*k_n_p*k_un*v_n*v_p*v_r + y7*
k_j_l*k_l_p*k_n_p*v_n*v_p*v_r
+ k_m_p*k_n_p*m_f*v_l*v_p*v_r*(k_b_n + k_n_p)$

aa_(15) :=  - l_f + y5$

aa_(16) :=  - l_b + y6$

aa_(17) :=  - j_f + y7$

aa_(18) :=  - j_b + y8$

MODEL ALGEBRAICALLY OBSERVABLE$

NORMALIZED  INPUT /OUTPUT RELATION(S) $

aan_(1) :=  - df(y2,t)*v_p + y1*k_b_p - y2*k_un$

aan_(2) := df(y3,t)*v_r - y1*k_p_r
+ y3*(k_b_r + k_r_p) - y4*k_un$
```

```
aan_(3) :=  - df(y4,t)*v_r + y3*k_b_r - y4*k_un$

aan_(4) :=  - df(y5,t)*v_l + y1*k_p_l
- y5*(clear_l + k_b_l + k_l_p) + y6*k_un + y7*k_j_l$

aan_(5) :=  - df(y6,t)*v_l + y5*k_b_l - y6*k_un$

aan_(6) := df(y7,t)*v_j - y1*k_p_j
+ y7*(clear_j + k_b_j + k_j_l) - y8*k_un$

aan_(7) :=  - df(y8,t)*v_j + y7*k_b_j - y8*k_un$

aan_(8) := (df(y1,t,3)*v_j*v_l**2*v_n**2*v_p**3*v_r**2
+ df(y1,t,2)*v_j*v_l**2*v_n*v_p**2*v_r**2*(clear_b*v_n
+ k_b_n*
v_p + k_b_p*v_n + k_n_p*v_p + k_p_j*v_n + k_p_l*v_n
+ k_p_m*v_n + k_p_n*v_n + k_p_r*v_n + k_un*v_p) +
df(y1,t)*v_j*v_l*v_p*v_r*(clear_b*k_b_n*v_l*v_n*v_p*v_r
+ clear_b*k_n_p*v_l*v_n*v_p*v_r
+ clear_b*k_un*v_l*v_n*v_p*v_r + k_b_n*k_b_p*v_l*v_n*v_p*v_r
+ k_b_n*k_p_j*v_l*v_n*v_p*v_r + k_b_n*k_p_l*v_l*v_n*v_p*v_r
+ k_b_n*k_p_m*v_l*v_n*v_p*v_r + k_b_n*k_p_n*v_l*
v_n*v_p*v_r + k_b_n*k_p_r*v_l*v_n*v_p*v_r
+ k_b_p*k_n_p*v_l*v_n*v_p*v_r - k_b_p*k_un*v_l*v_n**2*v_r
+ k_b_p*k_un*v_l*v_n*v_p*v_r - k_l_p*k_p_l*v_n**2*v_p*v_r
+ k_n_p*k_p_j*v_l*v_n*v_p*v_r + k_n_p*k_p_l*v_l*v_n*v_p*v_r
+ k_n_p*k_p_m*v_l*v_n*v_p*v_r + k_n_p*k_p_r*v_l*v_n*v_p*v_r
+ k_n_p*k_un*v_l*v_p**2*v_r + k_p_j*k_un*v_l*v_n*v_p*v_r
+ k_p_l*k_un*v_l*v_n*v_p*v_r + k_p_m*k_un*v_l*v_n*v_p*v_r
+ k_p_n*k_un*v_l*v_n*v_p*v_r - k_p_r*k_r_p*v_l*v_n**2*v_p
+ k_p_r*k_un*v_l*v_n*v_p*v_r)
 + y1*(clear_b*k_n_p*k_un*v_j*v_l**2*v_p**2*v_r**2
+ clear_l*k_l_p*k_p_l*v_j*v_n**2*v_p**2*v_r**2
+ k_b_l*k_l_p*k_p_l*v_j*v_n**2*v_p**2*v_r**2
- k_b_n*k_b_p*k_un*v_j*v_l**2*v_n*v_p*v_r**2
- k_b_n*k_l_p*k_p_l*v_j*v_l*v_n*v_p**2*v_r**2
- k_b_n*k_p_r*k_r_p*v_j*v_l**2*v_n*v_p**2*v_r
- k_b_p*k_n_p*k_un*v_j*v_l**2*v_n*v_p*v_r**2
+ k_b_p*k_n_p*k_un*v_j*v_l**2*v_p**2*v_r**2
+ k_b_p*k_un**2*v_j*v_l**2*v_n**2*v_r**2
```

```
- k_b_p*k_un**2*v_j*v_l**2*v_n*v_p*v_r**2
+ k_b_r*k_p_r*k_r_p*v_j*v_l**2*v_n**2*v_p**2
- k_j_l*k_l_p*k_p_j*v_l*v_n**2*v_p**2*v_r**2
+ k_l_p**2*k_p_l*v_j*v_n**2*v_p**2*v_r**2
- k_l_p*k_n_p*k_p_l*v_j*v_l*v_n*v_p**2*v_r**2
- k_l_p*k_p_l*k_un*v_j*v_l*v_n*v_p**2*v_r**2
+ k_n_p*k_p_j*k_un*v_j*v_l**2*v_p**2*v_r**2
+ k_n_p*k_p_l*k_un*v_j*v_l**2*v_p**2*v_r**2
+ k_n_p*k_p_m*k_un*v_j*v_l**2*v_p**2*v_r**2
- k_n_p*k_p_r*k_r_p*v_j*v_l**2*v_n*v_p**2*v_r
+ k_n_p*k_p_r*k_un*v_j*v_l**2*v_p**2*v_r**2
+ k_p_r*k_r_p**2*v_j*v_l**2*v_n**2*v_p**2
- k_p_r*k_r_p*k_un*v_j*v_l**2*v_n*v_p**2*v_r)
+ y2*k_un**2*v_j*v_l**2*v_r**2*(k_b_n*v_n*v_p
+ k_n_p*v_n*v_p - k_n_p*v_p**2 - k_un*v_n**2 + k_un*v_n*v_p)
+ y3*k_r_p*v_j*v_l**2*v_p**2*(k_b_n*k_b_r*v_n*v_r
+ k_b_n*k_r_p*v_n*v_r- k_b_r**2*v_n**2
+ k_b_r*k_n_p*v_n*v_r - 2*k_b_r*k_r_p*v_n**2
- k_b_r*k_un*v_n**2 + k_b_r*k_un*v_n*v_r
+ k_n_p*k_r_p*v_n*v_r - k_n_p*k_un*v_r**2
- k_r_p**2*v_n**2 + k_r_p*k_un*v_n*v_r)
+ y4*k_r_p*k_un*v_j*v_l**2*v_n*v_p**2*( - k_b_n*v_r
+ k_b_r*v_n - k_n_p*v_r + k_r_p*v_n + k_un*v_n - k_un*v_r)
+ y5*k_l_p*v_j*v_p**2*v_r**2*( - clear_l**2*v_n**2
- 2*clear_l*k_b_l*v_n**2 + clear_l*k_b_n*v_l*v_n
- 2*clear_l*k_l_p*v_n**2 + clear_l*k_n_p*v_l*v_n
+ clear_l*k_un*v_l*v_n - k_b_l**2*v_n**2
+ k_b_l*k_b_n*v_l*v_n - 2*k_b_l*k_l_p*v_n**2
+ k_b_l*k_n_p*v_l*v_n + k_b_l*k_un*v_l*v_n
- k_b_l*k_un*v_n**2 + k_b_n*k_l_p*v_l*v_n
- k_l_p**2*v_n**2 + k_l_p*k_n_p*v_l*v_n
+ k_l_p*k_un*v_l*v_n - k_n_p*k_un*v_l**2)
+ y6*k_l_p*k_un*v_j*v_n*v_p**2*v_r
**2*(clear_l*v_n + k_b_l*v_n - k_b_n*v_l
+ k_l_p*v_n - k_n_p*v_l - k_un*v_l + k_un*v_n)
+ y7*k_j_l*k_l_p*v_n*v_p**2*v_r
**2*(clear_j*v_l*v_n + clear_l*v_j*v_n + k_b_j*v_l*v_n
+ k_b_l*v_j*v_n - k_b_n*v_j*v_l + k_j_l*v_l*v_n + k_l_p*v_j*v_n
- k_n_p*v_j*v_l - k_un*v_j*v_l)
- y8*k_j_l*k_l_p*k_un*v_l*v_n**2*v_p**2*v_r**2
```

```
- k_m_p*k_n_p*k_un*m_f*v_j*v_l**2*v_p**2*
v_r**2)/(v_j*v_l**2*v_n**2*v_p**3*v_r**2)$
```

RANDOMLY CHOSEN NUMERICAL PARAMETER(S) VECTOR$

```
b2_ := {k_p_r=54,
k_p_n=7,
k_p_l=9,
k_p_j=15,
k_r_p=52,
k_n_p=18,
k_l_p=17,
k_j_l=23,
k_b_p=5,
k_b_r=22,
k_b_n=38,
k_b_l=41,
k_b_j=6,
k_un=20,
clear_b=3,
clear_l=59,
clear_j=57}$
```

EXHAUSTIVE SUMMARY $

```
flist_ := {k_b_p - 5,
 - k_un + 20,
 - k_p_r + 54,
 - k_un + 20,
k_b_r - 22,
 - k_un + 20,
k_p_l - 9,
k_un - 20,
k_j_l - 23,
k_b_l - 41,
 - k_un + 20,
 - k_p_j + 15,
 - k_un + 20,
k_b_j - 6,
 - k_un + 20,
```

```
k_b_r + k_r_p - 74,
( - k_j_l*k_l_p*k_un + 7820)/(v_j*v_l*v_p),
(k_m_p*m_f*( - k_n_p*k_un + 360))/(v_n**2*v_p),
 - clear_l - k_b_l - k_l_p + 117,
clear_j + k_b_j + k_j_l - 86,
(k_b_n*k_un**2*v_n*v_p + k_n_p*k_un**2*v_n*v_p
- k_n_p*k_un**2*v_p**2 - k_un**3*v_n**2
+ k_un**3*v_n*v_p + 8000*v_n**2 -
 30400*v_n*v_p + 7200*v_p**2)/(v_n**2*v_p**3),
( - k_b_n*k_r_p*k_un*v_r + k_b_r*k_r_p*k_un*v_n
- k_n_p*k_r_p*k_un*v_r + k_r_p**2*k_un*v_n
+ k_r_p*k_un**2*v_n - k_r_p*k_un**2*v_r
- 97760*v_n + 79040*v_r)/(v_n*v_p*v_r**2),
(clear_l*k_l_p*k_un*v_n + k_b_l*k_l_p*k_un*v_n
- k_b_n*k_l_p*k_un*v_l + k_l_p**2*k_un*v_n
- k_l_p*k_n_p*k_un*v_l - k_l_p*k_un**2*v_l
+ k_l_p*k_un**2*v_n + 25840*v_l
- 46580*v_n)/(v_l**2*v_n*v_p),
(clear_b*v_n + k_b_n*v_p + k_b_p*v_n + k_n_p*v_p
+ k_p_j*v_n + k_p_l*v_n + k_p_n*v_n + k_p_r*v_n
+ k_un*v_p - 93*v_n - 76*v_p)/(v_n*v_p),
(clear_j*k_j_l*k_l_p*v_l*v_n
+ clear_l*k_j_l*k_l_p*v_j*v_n +
k_b_j*k_j_l*k_l_p*v_l*v_n + k_b_l*k_j_l*k_l_p*v_j*v_n
- k_b_n*k_j_l*k_l_p*v_j*v_l + k_j_l**2*k_l_p*v_l*v_n
+ k_j_l*k_l_p**2*v_j*v_n - k_j_l*k_l_p*k_n_p*v_j*v_l
- k_j_l*k_l_p*k_un*v_j*v_l + 29716*v_j*v_l
- 45747*v_j*v_n - 33626*v_l*v_n)/(v_j*v_l**2*v_n*v_p),
(k_b_n*k_b_r*k_r_p*v_n*v_r + k_b_n*k_r_p**2*v_n*v_r
- k_b_r**2*k_r_p*v_n**2 + k_b_r*k_n_p*k_r_p*v_n*v_r
- 2*k_b_r*k_r_p**2*v_n**2 - k_b_r*k_r_p*k_un*v_n**2
+ k_b_r*k_r_p*k_un*v_n*v_r + k_n_p*k_r_p**2*v_n*v_r
- k_n_p*k_r_p*k_un*v_r**2 - k_r_p**3*v_n**2
+ k_r_p**2*k_un*v_n*v_r + 307632*v_n**2
- 292448*v_n*v_r + 18720*v_r**2)/(v_n**2*v_p*v_r**2),
( - clear_l**2*k_l_p*v_n**2 - 2*clear_l*k_b_l*k_l_p*v_n**2
+ clear_l*k_b_n*k_l_p*v_l*v_n - 2*clear_l*k_l_p**2*v_n**2
+clear_l*k_l_p*k_n_p*v_l*v_n + clear_l*k_l_p*k_un*v_l*v_n
- k_b_l**2*k_l_p*v_n**2 + k_b_l*k_b_n*k_l_p*v_l*v_n
- 2*k_b_l*k_l_p**2*v_n**2 + k_b_l*k_l_p*k_n_p*v_l*v_n
```

```
+ k_b_l*k_l_p*k_un*v_l*v_n - k_b_l*k_l_p*k_un*v_n**2
+ k_b_n*k_l_p**2*v_l*v_n - k_l_p**3*v_n**2
+ k_l_p**2*k_n_p*v_l*v_n + k_l_p**2*k_un*v_l*v_n
- k_l_p*k_n_p*k_un*v_l**2 + 6120*v_l**2 - 151164*
v_l*v_n + 246653*v_n**2)/(v_l**2*v_n**2*v_p),
(clear_b*k_b_n*v_l*v_n*v_p*v_r +
clear_b*k_n_p*v_l*v_n*v_p*v_r +
clear_b*k_un*v_l*v_n*v_p*v_r + k_b_n*k_b_p*v_l*v_n*v_p*
v_r + k_b_n*k_p_j*v_l*v_n*v_p*v_r +
k_b_n*k_p_l*v_l*v_n*v_p*v_r +
k_b_n*k_p_m*v_l*v_n*v_p*v_r + k_b_n*k_p_n*v_l*v_n*v_p*
v_r + k_b_n*k_p_r*v_l*v_n*v_p*v_r
+ k_b_p*k_n_p*v_l*v_n*v_p*v_r -
k_b_p*k_un*v_l*v_n**2*v_r + k_b_p*k_un*v_l*v_n*v_p*v_r
- k_l_p*k_p_l*v_n**2*v_p*v_r + k_n_p*k_p_j*v_l*v_n*v_p*v_r
+ k_n_p*k_p_l*v_l*v_n*v_p*v_r + k_n_p*k_p_m*v_l*v_n*v_p*v_r
+ k_n_p*k_p_r*v_l*v_n*v_p*v_r +
k_n_p*k_un*v_l*v_p**2*v_r + k_p_j*k_un*v_l*v_n*v_p*v_r
+ k_p_l*k_un*v_l*v_n*v_p*v_r +
k_p_m*k_un*v_l*v_n*v_p*v_r - 76*k_p_m*v_l*v_n*v_p*v_r
+ k_p_n*k_un*v_l*v_n*v_p*v_r - k_p_r*k_r_p*v_l*v_n**2*v_p
+ k_p_r*k_un*v_l*v_n*v_p*v_r + 2808*v_l*v_n**2*v_p
+ 100*v_l*v_n**2*v_r - 6942*v_l*v_n*v_p*v_r
- 360*v_l*v_p**2*v_r + 153*v_n**2
*v_p*v_r)/(v_l*v_n**2*v_p**2*v_r),
(clear_b*k_n_p*k_un*v_j*v_l**2*v_p**2*v_r**2
+ clear_l*k_l_p*k_p_l*v_j*v_n**2*v_p**2*v_r**2
+ k_b_l*k_l_p*k_p_l*v_j*v_n
**2*v_p**2*v_r**2
- k_b_n*k_b_p*k_un*v_j*v_l**2*v_n*v_p*v_r**2
- k_b_n*k_l_p*k_p_l*v_j*v_l*v_n*v_p**2*v_r**2
- k_b_n*k_p_r*k_r_p*v_j*v_l**2*v_n*v_p**2*v_r
- k_b_p*k_n_p*k_un*v_j*v_l**2*v_n*v_p*v_r**2
+ k_b_p*k_n_p*k_un*v_j*v_l**2*v_p**2*v_r**2
+ k_b_p*k_un**2*v_j*v_l**2*v_n**2*v_r**2
- k_b_p*k_un**2*v_j*v_l**2*v_n*v_p*v_r**2
+ k_b_r*k_p_r*k_r_p*v_j*v_l**2*v_n**2*v_p**2
- k_j_l*k_l_p*k_p_j*v_l*v_n**2*v_p**2*v_r**2
+ k_l_p**2*k_p_l*v_j*v_n**2*v_p**2*v_r**2
- k_l_p*k_n_p*k_p_l*v_j*v_l*v_n*v_p**2*v_r**2
```

```
- k_l_p*k_p_l*k_un*v_j*v_l*v_n*v_p**2*v_r**2
+ k_n_p*k_p_j*k_un*v_j*v_l**2*v_p**2*v_r**2
 + k_n_p*k_p_l*k_un*v_j*v_l**2*v_p**2*v_r**2
+ k_n_p*k_p_m*k_un*v_j*v_l**2*v_p**2*v_r**2
- k_n_p*k_p_r*k_r_p*v_j*v_l**2*v_n*v_p**2*v_r
+ k_n_p*k_p_r*k_un*v_j*v_l**2*v_p**2*v_r**2
- 360*k_p_m*v_j*v_l**2*v_p**2*v_r**2
+ k_p_r*k_r_p**2*v_j*v_l**2*v_n**2*v_p**2
- k_p_r*k_r_p*k_un*v_j*v_l**2*v_n*v_p**2*v_r
- 207792*v_j*v_l**2*v_n**2*v_p**2
- 2000*v_j*v_l**2*v_n**2*v_r**2
+ 213408*v_j*v_l**2*v_n*v_p**2*v_r
+ 7600*v_j*v_l**2*v_n*v_p*v_r**2
- 30960*v_j*v_l**2*v_p**2*v_r**2
+ 11628*v_j*v_l*v_n*v_p**2*v_r**2
- 17901*v_j*v_n**2*v_p**2*v_r**2
+ 5865*v_l*v_n**2*v_p**2*v_r**2)/(
v_j*v_l**2*v_n**2*v_p**3*v_r**2)}$
```

```
MODEL PARAMETER SOLUTION(S)$
```

```
 G_:=GROESOLVE(FLIST_,B1_) $
```

```
g_ := {{k_p_n=7,
clear_j=57,
k_b_j=6,
k_p_r=54,
clear_b=3,
k_p_j=15,
k_b_p=5,
k_p_l=9,
k_b_n=38,
k_n_p=18,
k_b_r=22,
k_j_l=23,
k_b_l=41,
clear_l=59,
k_r_p=52,
k_l_p=17,
k_un=20}}$
```

MODEL GLOBALLY IDENTIFIABLE$

INITIAL CONDITION(S) NOT NECESSARY$